UNIVERSIDAD MICHOACANA DE SAN NICOLÁS DE HIDALGO

FACULTAD DE INGENIERÍA ELÉCTRICA
DIVISIÓN DE ESTUDIOS DE POSGRADO

"Shunt Filtering Techniques for Steady-State and Dynamic Harmonic Mitigation and Reactive Power Compensation in Power Systems"

TESIS

Que para obtener el Grado de:
DOCTOR EN CIENCIAS EN INGENIERÍA ELÉCTRICA

Presenta:
HUGO ANTONIO RAMOS CARRANZA

Director de Tesis:
DR. J. AURELIO MEDINA RÍOS

Morelia, Michoacán Agosto de 2010

SHUNT FILTERING TECHNIQUES FOR STEADY-STATE AND DYNAMIC HARMONIC MITIGATION AND REACTIVE POWER COMPENSATION IN POWER SYSTEMS

Los Miembros del Jurado de Examen de Grado aprueban
la **Tesis de Doctorado en Ciencias en Ingeniería Eléctrica** de *Hugo Antonio Ramos Carranza*

Dr. Edmundo Barrera Cardiel
Presidente

Dr. J. Aurelio Medina Ríos
Director de Tesis

Dr. Félix Calderón Solorio
Vocal

Dra. Elisa Espinosa Juárez
Vocal

Dr. Manuel Madrigal Martínez
Revisor Externo
Instituto Tecnológico de Morelia

Dr. J. Aurelio Medina Ríos
Jefe de la División de Estudios de Posgrado
En Ingeniería Eléctrica.

UNIVERSIDAD MICHOACANA DE SAN NICOLÁS DE HIDALGO
Agosto 2010

Agradecimientos

Gracias a Dios.

Gracias a mi esposa por su apoyo incondicional durante la realización de este trabajo y durante todo este tiempo. Este trabajo también es de ella.

Gracias a mis padres por darme el apoyo siempre que lo necesite y más.

Gracias a mis hermanos, los tres son un ejemplo para mí.

Gracias a mi asesor y Director de Tesis, Dr. J. Aurelio Medina Ríos por todo su apoyo, enseñanza y dedicación durante la realización de este trabajo de investigación.

Gracias a mis profesores, Dr. Manuel Madrigal, Dr. Félix Calderón.

De manera muy especial, Gracias al Dr. Gary W. Chang. La estancia de investigación en Taiwan R.O.C. formó una parte muy importante en la realización de esta investigación. De la misma manera gracias a todos los compañeros en el PQ LAB de National Chung Cheng University.

Gracias a la mesa sinodal formada por el Dr. Edmundo Barrera Cardiel, Dr. J. Aurelio Medina Ríos, Dr. Félix Calderón Solorio, Dra. Elisa Espinosa Juárez, Dr. Manuel Madrigal Martínez. Sus contribuciones han enriquecido el trabajo presentado en esta tesis.

Mi agradecimiento también para todos los compañeros y amigos del programa de Posgrado en Ingeniería Eléctrica de la Universidad Michoacana de San Nicolás de Hidalgo.

Gracias también a la Sra. Yolanda por su ayuda con los trámites administrativos.

También un profundo agradecimiento para el Ing. Ricardo Prince Aldrete, gracias por su apoyo durante la etapa final y culminación de esta tesis, así como durante el proceso de titulación.

Abstract

The research work presented in this thesis is focused in the shunt filtering techniques to mitigate harmonic distortion and compensate reactive power in electric systems. Among the different alternatives and devices available, the attention is centered in the shunt Active Power Filter, Shunt Hybrid Filter and the Active Power Line Conditioner for compensation of reactive power and/or mitigation of harmonic currents in electric systems.

The Active Power Filter has proved to be an efficient alternative due to its well known capabilities to perform harmonic distortion and reactive power compensation. Nevertheless, the research field is very active in the development of control algorithms for determining the reference signals of compensation. In this thesis, a control algorithm in phase coordinates, able to handle steady-state and dynamic compensation, has been developed and implemented in Matlab/Simulink®.

In order to validate a future physical implementation of the compensation device, the control algorithm to determine the reference signals, as well as the complete model of the shunt APF, has been tested with Real-Time simulations to validate the feasibility of the control algorithm affordable computational demand. The real-time simulations include both steady-state and dynamic compensation of nonlinear loads.

Following the aim of taking into account practical considerations of the compensation scheme, the Shunt Hybrid Filter is presented by adding a shunt capacitor to the compensation scheme. The shunt capacitor is placed to compensate reactive power, which reduces the necessary rating of the more expensive active power filter device, and can be used as a high-pass filter for draining-out the ripple current of commutation. To achieve this goal properly, a Linear Quadratic Regulator switching current controller has been designed to avoid undesirable/possible parallel resonance effects.

Finally, for the case of harmonic control in distribution power systems, a novel alternative in the Active Power Line Conditioner planning has been fully developed. The proposed alternative is formulated by considering the Individual Harmonic Distortion and Total Harmonic Distortion indices at all buses of the distribution power system. This new proposal in the Active Power Line Conditioner planning has the aim of reducing the necessary control demand. Since each one of the considered Active Power Line Conditioners are injecting only a single harmonic frequency as a corrective measure, the optimization based method to determine the injection currents is found to have a lower computational demand. In addition, the best location for the single-harmonic Active Power Line Conditioners is determined by using a sensitivity analysis, and the injection currents are determined by solving a convex optimization problem. The proposed single harmonic

Active Power Conditioner planning is tested using the IEEE 30-bus test system. Obtained results show the effectiveness of this novel methodology.

Resumen

El trabajo de investigación en esta tesis está enfocado en técnicas de filtrado en paralelo para mitigar distorsión armónica y compensar potencia reactiva en sistemas eléctricos de potencia. De entre las diferentes alternativas y dispositivos disponibles, la atención es centrada en el Filtro Activo de Potencia en paralelo, el Filtro Hibrido en Paralelo y el Acondicionador de Línea de Potencia Activo para compensación de potencia reactive y la mitigación de corrientes armónicas en sistemas eléctricos.

El Filtro de Potencia Activo ha probado ser una alternativa eficiente debido a sus capacidades bien conocidas para la compensación de distorsión armónica y potencia reactiva. No obstante, el campo de investigación es muy activo en el desarrollo de algoritmos de control para determinar las señales de referencia de compensación. En esta tesis, un algoritmo de control en coordenadas de fase, capaz de manejar compensación en estado estacionario y dinámica, ha sido desarrollada e implementada en Matlab/Simulink®.

Con el fin de validar una futura implementación física del dispositivo, el algoritmo de control para determinar las señales de referencia, así como también el modelo completo del FAP, ha sido probado con simulaciones en tiempo real para validar la factibilidad de la demanda computacional asequible del algoritmo de control. Las simulaciones en tiempo real incluyen compensación en estado estacionario y dinámica de cargas no lineales.

Siguiendo con el objetivo de tomar en cuenta consideraciones practicas del esquema de compensación, el Filtro Hibrido en Paralelo es presentado añadiendo un capacitor en derivación al esquema de compensación. El capacitor en derivación es colocado para compensar potencia reactiva, lo cual reduce la tasación necesaria del dispositivo Filtro Activo de Potencia más costoso, y puede ser usado como filtro pasa-altas para drenar la corriente de rizado de conmutación. Para lograr esta meta apropiadamente, un controlador conmutador de corriente Regulador Cuadrático Lineal ha sido diseñado para evitar indeseables/posibles efectos de resonancia en paralelo.

Finalmente, para el caso de control armónico en sistemas de potencia de distribución, una alternativa novedosa en la planeación de Acondicionadores de Línea de Potencia Activos ha sido completamente desarrollada. La alternativa propuesta está formulada considerando los índices de Distorsión Armónica Individual y Distorsión Armónica Total en todos los nodos del sistema de potencia de distribución. Esta nueva propuesta en la planeación de los Acondicionadores de Línea de Potencia Activos, tiene el objetivo de reducir la demanda de control necesaria. Desde que cada uno de los Acondicionadores de Potencia de Línea Activos está inyectando solamente una frecuencia armónica como medida correctiva, en el método basado en optimización para determinar las corrientes de inyección se comprueba

una demanda computacional menor. Además, la mejor ubicación para los Acondicionadores de Potencia de Línea Activos de único armónico, está determinada utilizado un análisis de sensitividad y las inyecciones de corriente son determinadas mediante la solución de un problema de optimización convexo. La planeación de los Acondicionadores de Potencia de Línea Activos de único armónico es probada utilizando el sistema de prueba IEEE-30 nodos. Los resultados obtenidos muestran la efectividad de esta novedosa metodología.

Table of Contents

a	Complex operator $a=e^{j2\pi/3}$
α	Individual harmonic distortion imposed limit. It could be accompanied of a subscript indicating the limit imposed on a voltage or current. As well as, it could be accompanied by a superscript indicating the harmonic order.
β	Total harmonic distortion imposed limit. It could be accompanied of a subscript indicating the limit imposed on a voltage or current.
C_f	Capacitance of the capacitor bank per phase
$diag$	Stands for diagonal matrix
Δ_i	Delta window for the hysteresis-band current controller
f_{obj}	Objective function
hys	Hysteresis-band current controller function
h	Harmonic order
$i_{ck}(t)$	Current through the capacitor at phase $k= a, b, c$
$i^*_{fk}(t)$	Reference filtering current at phase $k= a, b, c$
$i_{fk}(t)$	Filtering current at phase $k=a, b, c$
$i_{k\_residual}(t)$	Non-active component of the load current
$i_{lk}(t)$	Load current a phase $k= a, b, c$
i_N	Neutral current
I_{SC}	Short circuit current
$i^*_{sk}(t)$	Reference source current at phase $k= a, b, c$
$i_{sk}(t)$	Source current at phase $k= a, b, c$
I_L	Nominal fundamental current

I_{m_ABC}	Amplitude of the desired source currents after compensation with the proposed method in phase coordinates.
I_{m_SCD}	Amplitude of the desired source currents after compensation with the SCD method
J	Performance index
$j,\ i$	Imaginary number
K	Feedback gain matrix
L_{eq}	Equivalent inductance
L_f	Energy link inductance between the VSI and the electric system
L_k	Load inductance at phase $k=a, b, c$
L_S	Source inductance
λ	Power Factor
$\underline{\lambda}$	Minimum power factor permissible
P_F	Active power supplied by the shunt APF
P_k	Real power delivered to the load at phase $k=a, b, c$
P_S	Active power supplied from the source
P_T	Total real power delivered to the load
P_{loss}	Power losses caused switching and capacitor voltage variations
φ_{a1}	Angle of the fundamental component of source voltage at phase a
Q	Hermitian matrix
Q_C	Three-phase reactive power supplied by the shunt capacitor
$Q_{3\phi}$	Three-phase reactive power consumed by the load
Q_F	Reactive power supplied by the shunt APF
Q_S	Reactive power supplied from the source

R_{eq}	Equivalent resistance
R_f	Energy link Resistance between the VSI and the electric system
R_k	Load resistance at phase k =*a, b, c*
rms	Root mean square
R_{SC}	Short circuit ratio
u	Optimal control law
$v_{ck}(t)$	Voltage at the capacitor terminals for phase k= *a, b, c*
$v_k(t)$	Source voltages or voltages at the point of common coupling
$v_k^*(t)$	Reference source voltages
$U^{h,(0)}$	Zero sequence unbalance index for harmonic *h*
$U^{h,(-)}$	Negative sequence unbalance index for harmonic *h*
V_{LL}	Line-to-line *rms* voltage
V_{mk}	Source voltage amplitude at phase k= *a, b, c*
V_{mT}	Addition of source voltage amplitudes
V_{mk1}	Source voltage amplitude at fundamental frequency for phase *k*
V_{dc}	*dc* voltage at the *dc* side of the VSI
V_{dc}^*	Reference *dc* voltage at the *dc* side of the VSI
V_S	Source voltage
T	Time
T_s	Sample Time
ω	Angular frequency
$w,\ x$	State vector
w_{ref}	Reference state vector

X_C	Capacitive reactance per phase
$X_{Yk}^{h,r}$	Real component of X for the harmonic h at phase k= a, b, c. Here, X could be a voltage, a current or impedance. And Y indicates that this electric quantity X belongs to the source, load, the capacitor, etc.
$X_{Yk}^{h,i}$	Imaginary component of X for the harmonic h at phase k= a, b, c. Here, X could be a voltage, a current or impedance. And Y indicates that this electric quantity X belongs to the source, load, the capacitor, etc.
$X_Y^{h,(0,-,+)}$	Zero, negative or positive sequence component of X for the harmonic h. Here, X could be a voltage or current. And Y indicates that this electric quantity X belongs to the source, load, the capacitor, etc.
γ^0	Zero sequence unbalance limit
γ^-	Negative sequence unbalance limit
Z_k	Impedance at phase k=a, b, c
$\lvert X_k \rvert$	Magnitude of the phasor X at phase k=a, b, c

ANSI	American National Standards Institute
APF	Active Power Filter
APLC	Active Power Line Conditioner
BS	British Standards
CAD	Computer Aided Design
CEA	Canadian Electrical Association
CPU	Central Processing Unit
CSI	Current Source Inverter
DFT	Discrete Fourier Transform
dc	Stands for direct current or continuous current
EN	European Norms
FFT	Fast Fourier Transform

HDC	Harmonic Distortion Circle
IEC	International Electrotechnical Commission
IEEE	Institute of Electrical and Electronic Engineers
IHD	Individual Harmonic Distortion
KVL	Kirchhoff's Voltage Law
LQR	Linear Quadratic Regulator
ODE4	Ordinary Differential Equation of forth order. A numerical integration solver provided by Matlab/Simulink®
PC	Personal Computer
PCC	Point of Common Coupling
PLT	Phase-Locked Technique
PLL	Phase-Locked Loop
RTW	Real-Time Workshop
RTWT	Real-Time Windows Target
SCD	Synchronous Detection Method
SHAPLC	Single-Harmonic Active Power Line Conditioner
SHF	Shunt Hybrid Filter
SFFT	Short Fast Fourier Transform
THD	Total Harmonic Distortion
VCO	Voltage Controller Oscillator
VSI	Voltage Source Inverter
VAR	Volt-Ampere Reactive
TBFW	Three-Bridge Four-Wire
TLFB	Three-Leg Full Bridge
TLSC	Three-Leg Split-Capacitor

List of Figures

List of Tables

1. **An Active Power Filter in Phase Coordinates for Harmonic Mitigation**. IEEE Transactions on Power Delivery, Vol. 22, No. 3, July 2007, A. Medina, H. A. Ramos-Carranza.
2. **Real-Time Shunt Active Power Filter Compensation**. IEEE Transactions on Power Delivery, Vol. 23, No. 4, October 2008, Hugo. A. Ramos-Carranza, Aurelio Medina, Gary W. Chang.
3. **Optimization Based Method for Shunt Hybrid Compensation in Non-Stiff Systems**, International Journal of Circuit Theory and Applications. Accepted for further publication. Hugo Ramos-Carranza, Aurelio Medina.
4. **Solving Resonance Parallel Problems Associated to the Shunt Active Power Filter Compensation**. Electric Power System and Components. To be submitted. H. A. Ramos-Carranza, Aurelio Medina, J. Segundo, M. Madrigal.
5. **Single Harmonic Active Power Line Conditioner for Harmonic Planning Mitigation in Distribution Power Systems**. International Journal of Circuit Theory and Applications. Under review. Hugo Ramos-Carranza, Aurelio Medina.
6. **Real-Time Application of Shunt Active Power Filter Dynamic Compensation Using Real-Time Windows Target**. European Transactions on Electrical Power. Under review. H. A. Ramos-Carranza, A. Medina, G. W. Chang.

Chapter 1. Introduction

Power system harmonics are defined as sinusoidal voltage and currents of frequencies that are integer multiples of the main generated (or fundamental) frequency and they constitute the major distorting problems of the mains voltage and load current waveforms [Arrillaga and Watson 2003]. Recently, power system harmonics has becoming more notorious in the electric engineering field. But, the fact that power system harmonics is now an important subject of interest between the electric engineers and researchers, it does not mean that it was not important and existed in the past. Reducing voltage and current waveform distortion to acceptable levels has been a problem in power system design from the early days of alternating current. Since then, the harmonic current distortion exists, at more or less extent, in every power system. Electric generation is produced at a constant frequency of 50 or 60 Hz and the waveform can be considered practically sinusoidal. Nevertheless, when a source of sinusoidal voltage is applied to a nonlinear device or load, the resulting current is not perfectly sinusoidal. Even more, with the presence of system impedance this distorted (non-sinusoidal) current causes a distorted (non-sinusoidal) voltage drop and produces voltage distortion at the load terminals. Recent growing concern results from the increasing use of power electronic devices and waveform-sensitive load equipment. However, on the assumption of reasonable periods of steady-state behavior, the distorted voltage and currents comply with the requirements of allowing Fourier analysis, and can be expressed in terms of harmonic components.

In general, current harmonics should be controlled when they cause serious problems on the performance and reliability of the different components of the electric system. Then, the designing and planning of harmonic compensation equipment at the installation terminals has to be taken into account in order to control the harmonic contamination in the voltage and current waveforms. One solution to this problem is to install harmonic filters according to the characteristics of the nonlinear load connected to the electric system. There are different types of harmonic filters including passive, active, and hybrid filters. This thesis is focused in the analysis of the shunt active power filter for harmonic current mitigation and reactive power compensation. Due to practical considerations, special attention is also dedicated to the shunt hybrid filter compensation.

During the past few decades the number and types of nonlinear loads have tremendously increased [Fuchs and Masoum 2008]. This has motivated the utilities and consumers of electric power to implement different harmonic filters. Harmonic filters are capable of compensating harmonics of nonlinear loads through current-based compensation. They are designed to provide a bypass for the harmonic currents to block them from entering the power system, which is the case for passive filters, or to compensate them by locally supplying harmonic currents and/or voltages as is the case for active filters.

Even though, the focus of this work in centered in the performance and operation characteristics of the shunt active filter, it is important to give a brief insight of the passive filters, being that, the active filter in practice should be accompanied of passive elements, as it will be shown in Chapter 4.

Passive filters may be installed to prevent the harmonic currents from being injected into the system and they are less expensive compared to other mitigating devices, e.g. the shunt Active Power Filter. They are composed of only passive elements (inductances, capacitances, and resistances) tuned to the harmonic frequencies of the currents or voltages that must be attenuated. The resonant frequency of the power system must be carefully placed far from any significant harmonic distortion caused by a nonlinear load. For this reason, passive filters should be tuned slightly lower than the harmonic to be attenuated [Acha and Madrigal 2001], [Fuchs and Masoum 2008]. This will provide a margin of safety for the case when there is some change in the system parameters. Otherwise, variations in either filter capacitance and/or filter inductance (e.g., with temperature or failure) might shift resonance conditions such that harmonics can cause increased problems in the power system [Acha and Madrigal 2001]. There are various types of passive filters for single phase and three-phase power systems in shunt and series configurations. Shunt passive filters are the most common type of filters in use. They provide low-impedance paths for the flow of harmonic currents and they will have a lower rating than a series-connected passive filter that must carry the full load current. Consequently, shunt filters are attractive due to their low cost and fine capability to supply reactive power at fundamental frequency. The chosen structure for implementation depends on the type of the dominant harmonic source and the required compensation function (e.g., harmonic current or voltage, and reactive power), as well as the frequency spectrum and the nature of the distortion. The tuning methodologies and criteria design, as well as the potentials and limitations for passive filters planning are well documented [Arrillaga and Watson 2003], [Acha and Madrigal 2001], [Fuchs and Masoum 2008]. Some other references [Chang *et al*. 2004] and [Chang *et al*. 2006], [IEEE-519 1992] offer interesting options for passive filter planning in distribution and industrial power systems. Nevertheless, the passive filter planning is a

continuously active research area and a complete analysis on this field is beyond the scope of this thesis.

Back to the subject of this work, the active filters are feasible alternatives for applications where the system configuration and/or the harmonic spectrum of nonlinear loads change, and can be used instead of passive filters to provide dynamic compensation. The structure of an active filter may be that of series or parallel architectures. The proper structure for implementation depends on the types of harmonic sources in the power system and the effects that different solutions would cause to the overall system performance.

Shunt active filters rely on active power conditioning to compensate undesirable harmonic currents replacing a portion or complete distorting current wave stemming from the nonlinear load. This is achieved by producing harmonic components of equal magnitude but opposite phase angles, which cancel the injected harmonic components of the nonlinear loads. The main performance advantage of the active filters over the passive ones is their fine response to changing loads and harmonic variations.

1.1 State of the Art

The increase in the incorporation of power converters and controllers for industrial processes and drives, and other types of nonlinear loads connected to the power system is consistently growing, as well as they are the undesirable associated effects, such as the harmonic distortion of current and voltage waveforms. In particular, the shunt Active Power Filter (APF) has been demonstrated to be an appropriated tool for the mitigation of harmonic currents and reactive power compensation.

The shunt APF can be modeled as a controlled current source that supplies a compensation current in parallel with the nonlinear load. There are four main components that allow the correct performance of the shunt active power compensation and have brought a wide attention between the electric engineers and researches, these are:

a) The control stage for determining the reference injection current.
b) The power converter.
c) The power converter controller.
d) The *dc* passive element for energy storage.

The control stage computes the reference currents to be injected into the system. So far, different control strategies have been reported for this purpose [Chang and Shee 2002], [Chang and Shee 2004], [Aredes *et al*. 1997]. The appropriate performance of the shunt APF depends at a large extent on the applied control strategy to calculate the reference currents to be injected into the system. The control strategies must take into account the no consumption/supply of average real power by the APF, since the APF does not require of active supply sources, such as batteries for its compensation mechanism [Chang and Shee 2004].

In a shunt APF, the static converter is the element responsible of the current injection into the electric network. In this type of applications, in order to minimize the stress in the transistors, the use of advanced topologies, such as multilevel converters [Rodríguez *et al*. 2002], cascade converters [Chiasson *et al*. 2003] or resonant structures [Kurokawa *et al*. 2000] has been reported. Generally, those topologies with less capacity of current injection need a control commutation technique simpler in counterpart with the topologies with high capacity of current injection, which need a more sophisticated control in the commutation technique. The balance between the desired capabilities of the converter and its control complexity necessary for the implementation makes that the manufacturers of active filters use different topologies in the design of the static converter [ABB 2010], [MGEUPS 2010].

The static converter will always be companied with a commutation technique that ensures that the injected current tracks-down as close as possible the signal current provided as reference. The characteristics of the commutation technique used in the shunt APF are vital for the compensation process. The dynamic response in following the signal references is crucial, which brings the intuition that the current controllers that work directly over the reference signal present a better behavior [Buso *et al*. 1998].

The passive element for energy storage is a capacitor, in the case of Voltage Source Inverter (VSI) or an inductor in the case of Current Source Inverter (CSI). The CSI results to be more robust and it is more expensive to implement [Hayashi *et al*. 1991], [Fukuda and Endoh 1995]. On the other hand, the VSI represents less internal losses and it is cheaper to implement [Akagi 1994]. In this thesis it has been opted to work with the VSI, which represents the commercial trend in most of the available equipment from researches and manufacturers [Akagi 1995], [ABB web site], [MGEUPS web site].

The performance characteristics of the control strategy to calculate the reference signals for the shunt active power filter is described and developed in detail in Chapter 2. This investigation is mainly focused in the control strategy to obtain the reference signal (Chapter 2, 4 and 5), as well as, the control switching pattern of the VSI under the hybrid filtering compensation scheme (Chapter 5). Important consideration has been taken into

account for a future practical/physical implementation of the compensation device (Chapter 3 and 5).

1.2 Harmonic Standards

Many documents for control of power quality have been generated by different organizations and institutes. These documents come in three levels of applicability and validity: guidelines, recommendations, and standards [Fuchs and Mosoum 2008]:

- Power quality guidelines are illustrations and illustrated procedures that contain typical parameters and representative solutions to commonly encountered power quality problems;
- Power quality recommended practices recognize that there are many solutions to power quality problems and recommend certain solutions over others. Any operating limits that are indicated by recommendations are not required but should be target for design; and
- Power quality standards are formal agreements between industry, users, and the government as to the proper procedure, test, measure, manufacture, and consume electric power. In all jurisdictions, violation of standards could be used as evidence in courts of law for litigation purposes.

The main reasons for setting guidelines, recommendations and standards in power systems with no sinusoidal voltages or currents are to keep disturbances to user equipment within permissible limits, to provide uniform terminology and test procedures for power quality problems, and to provide a common basis on which a wide range of engineering is referenced.

There are many standards and related documents that deal with power quality issues. Some of the mostly adopted documents are [Fuchs and Masoum 2008]:

- The North American Standards adopted by many countries of North and South America

  - Institute of Electrical and Electronic Engineers (IEEE). Among others, IEEE-519, Recommended practice for harmonic control and reactive compensation of static converters.

  - American National Standards Institute. Among others, IEEE/ANSI C57.110 Recommended practice for establishing transformer capability when supplying nonsinusoidal load currents.

- Military Specifications (MIL-Specs) published by the U.S. Department of Defense and Canadian Electric Association (CEA). The MIL-Std-1339 (Navy) Interface standard for shipboard systems, also define acceptable levels of harmonic current generation.

- British Standards (BS). BS 54061 Control harmonic emissions for small domestic equipment. (Based on IEC 555 part 2)
- European (Standards) Norms (EN). EN 50160 Voltage characteristics of electricity supplied by public distribution systems.
- International Electrotechnical Commission (IEC). Among others, IEC 1000-3-2 Electric compatibility Part 3: Limits section 2: Limits for harmonic current emissions (Equipment absorbed current <= 16 A per phase), and IEC 1000-3-6 Electromagnetic compatibility Part 3: Limits section 6: Emission limits evaluation for perturbing loads connected to MV and HV networks.

The IEEE-519 Standard [IEEE-519 Std. 1992] is the IEEE recommended practices and requirements for harmonic control in electric power systems. It is one of the well-known documents for power quality limits. IEEE-519 sets limits on the voltage and current harmonics distortion at the Point of Common Coupling (PCC, usually the secondary of the supply transformer). There are two criteria that are used in IEEE-519 to evaluate harmonic distortion:

- Limitation of the harmonic current that a user can transmit/inject into the utility system; and
- Limitation of the voltage distortion that the utility must furnish the user.

The interrelationship of these two criteria shows that the harmonic problem is a system problem, not just tied to the individual load that generates the harmonic current.

Table 1.1 and Table 1.2 list the harmonic current and voltage limits based on the size of the user with respect to the size of the power system to which the user is connected [IEEE-519 1992]. The short circuit current ratio (R_{SC}) is defined as the ratio of the short-circuit current (available at the PCC) to the nominal fundamental current, e.g., I_{SC}/I_L. Thus, the size of the permissible nonlinear user load increases with the size of the system, the stronger the system, the larger the percentage of harmonic current the user is allowed to inject into the utility system.

Table 1.1 IEEE-519 Harmonic current limits.

Maximum harmonic current distortion at PCC (% of fundamental)						
	Harmonic order (odd harmonics)[a]					
I_{SC}/I_L	$h<11$	$11 \le h \le 17$	$17 \le h \le 23$	$23 \le h \le 35$	$h>35$	THD_i
$<20^b$	4.0	2.0	1.5	0.6	0.3	5.0
20-50	7.0	3.5	2.5	1.0	0.5	8.0
50-100	10.0	4.5	4.0	1.5	0.7	12.0
100-1000	12.0	5.5	5.0	2.0	1.0	15.0
>1000	15.0	7.0	6.0	2.5	1.4	20.0

[a] Even harmonics are limited to 25% of the odd harmonic limits above.

[b] All power generation equipment is limited to these values of current distortion, regardless of the actual I_{SC}/I_L.

Here I_{SC} = maximum short circuit current at PCC.

For PCCs from 69 to 138 kV, the limits are 50% of the limits above. A case-by-case evaluation is required for PCCs of 138 kV and above.

Table 1.2 IEEE-519 Harmonic Voltage Limits.

Harmonic voltage distortion (% at PCC)			
	2.3 to 69 kV	69 to 138 kV	>138 kV
IHD_v	3.0	1.5	1.0
THD_v	5.0	2.5	1.5

To meet the power quality values of Tables 1.1 and 1.2, cooperation among all users and the utility is needed to ensure that no one deteriorates the power quality beyond these limits.

1.3 Motivation and Justification

The continuous increase in the incorporation of power-electronic converters and controllers for industrial processes and drives, among other types of nonlinear loads connected to the

power system, has come together with different associated power quality problems, such as harmonic distortion of current and voltage waveforms, which in turn has become an important problem to take into consideration and mainly to solve.

In particular, the shunt active power filter (APF) has demonstrated to be an appropriated tool for the mitigation of harmonic currents and reactive power compensation. The APF includes a main control stage which computes the reference current to be injected into the system. So far, different compensation strategies can be used for this purpose, and the appropriate operation of a shunt APF depends at a large extent on the applied control strategy to calculate the reference filtering currents. To properly achieve its function, the APF requires of an effective control strategy for the computation of the reference filtering currents in order to be able to eliminate the harmonic distortion in the source currents and to provide reactive power compensation to the electric system, keeping other important characteristics on its performance, such as, the no consumption of average real power and feasibility of physical implementation, which implies the affordable computational demand required by its control algorithm.

In addition, with the growing importance of power quality (PQ) problems to electric utilities and customers, there is an increasing interest on the search of new techniques for accurate analysis and resolution of such problems. The real-time simulation techniques are used for several studies of power systems containing nonlinear loads. Available literature details several techniques developed and implemented to perform real-time simulations in power system analysis. These aspects, to mention a few, have encouraged and dictated the directions on the investigation realized and presented in this thesis.

1.4 Objectives of the Work

The objectives of the work are associated in providing the basis for the future/possible implementation of a shunt APF and/or a shunt compensation scheme capable of compensate reactive power and mitigate harmonic currents. Their performance characteristics, as well as, some considerations related to practical applications of the compensation device and implementation should be also incorporated in the analysis. In general, the main objectives of this investigation can be listed as follows:

- Develop a complete digital model in Matlab/Simulink® of the Shunt APF in phase coordinates for harmonic mitigation, full mitigation or partial mitigation under permissible levels, and reactive power compensation of nonlinear loads and devices. The main area of interest will be the control strategy for determining the reference

filtering currents for the shunt APF compensation device, being that, the success in the performance of the shunt APF is highly associated to this matter.

- Provide digital computer-based simulations of the shunt APF model and other shunt compensation schemes, including steady-state and dynamic compensation of nonlinear loads. Here we will be focused in the convenience of using different shunt compensation schemes, taking into account their performance characteristics under certain situations, such as the resonance phenomenon that would be present in practical applications. In particular, for the shunt hybrid filter structure presented in this thesis, a Linear Quadratic Regulator switching controller is to be designed and incorporated in the Matlab/Simulink® digital model.
- Determine the best location and/or the optimal size of the active filters in electric systems. The active devices for compensation in electric systems are more expensive than the passive ones. Regardless their advantage in performance and control, for practical applications their cost is a major drawback. Therefore, reducing the rating of the active devices of compensation is of great interest in the research field. We will focus on minimize the power rating of the compensation device for reactive power compensation and/or harmonic mitigation in electric systems.
- Provide the required basis/guidelines, and directions to proceed with the physical implementation of the shunt APF.

1.5 Methodology

Many strategies have been developed for calculating the reference filtering currents for shunt APF applications. The objective of waveform compensation is to achieve a sinusoidal supply current. There are many signal-processing techniques that can be used to decompose the distorted waveform into its fundamental (to be retained) and harmonic components (to be cancelled). In general, there are two main categories referred for calculating the reference filtering currents, these categories can be identified by the characteristics of their algorithms as time-domain waveform compensation and frequency-domain waveform compensation.

In the time-domain strategies, to facilitate the separation of fundamental and harmonic components of the signal, the algorithms rely on transformation techniques to transfer the signal from the conventional three-phase *abc* reference frame to orthogonal representations. Whereas, the time-domain frequencies with different transformation between frameworks have an instantaneous response to the identification of the reference signals, due there is no

need of a post-process of the measured data (load current or voltage), the main disadvantage for these techniques is their poor performance when the source voltage waveforms are harmonic distorted and/or unbalanced. On the other hand, the frequency-domain strategies require Discrete or Fast Fourier Transform on a section of the signal that contains at least one cycle of the lowest frequency of interest. The main advantage of the flittering in the frequency-domain is the direct identification of fundamental and/or harmonic components. If the FFT window is properly synchronized to the fundamental signal then the phase and magnitude of the component can be accurately determined. The main disadvantage is that the filtering process is not very suitable for real-time filters and sufficient time is required for sampling the signal and performing the transformation. In addition, the signals must be steady-state and periodic because FFT implicitly assumes periodicity of the sample waveform.

The proposed strategy control to determine the reference filtering currents in this thesis is looking for a time-frequency approach to determine the fundamental component. The amount of computational demand effort is to be justified by the correct performance of the technique and proved to be affordable with real-time applications. In particular, the Sliding-Window FFT is incorporated in the control strategy for determining the reference filtering currents. Available literature, details several techniques developed to perform Real-Time simulations on the power systems analysis. This thesis will focus on the following technique: RTWT (Real-Time Windows Target) using Matlab/Simulink®. The main goal is to obtain simulation conditions that are close to the real-time environment under study using only a single computer. RTWT allows the Real-Time application using the same computer as a host and as a target, giving accurate results with a relatively low cost hardware.

Due to their high ratings and cost considerations, the acceptability of active filters has been limited in practical applications. In response to these factors, different structures of hybrid filters have evolved as a cost-effective solution for the compensation of nonlinear loads. The hybrid filter structure in this thesis is developed to be more effective in providing compensation in nonlinear loads. In particular, for the shunt hybrid filter structure presented in this thesis, a Linear Quadratic Regulator switching current controller is to be designed and incorporated in a Matlab/Simulink digital model. The optimization toolbox of Matlab is used to solve the LQR problem taking full capabilities of its linkage with Simulink®. In addition, and following with the intention of reducing the active power filter rating, an optimization based method is to be designed to mitigate harmonic distortion and achieve reactive power compensation in industrial power systems. The optimization toolbox of Matlab is also used for solving the optimization-based approach of the problem. The

flexibility of the optimization-based method allows the search of a partial compensation of the industrial power system, which is intended for a reduction in the necessary *rms* injection current.

In a similar manner, a optimization-based method is to be designed to control the harmonic distortion in distribution power systems. The optimization-based method is programmed and adequate to be solved using the optimization toolbox of Matlab. In particular, desired characteristics for harmonic control are taken into account in the compensation approach. Such characteristics include the control of Individual Harmonic Distortion and Total Harmonic Distortion indices in the entire distribution power system.

1.6 Structure of the Thesis

This chapter gives a background of the presence of the harmonics in the electric system and the possible devices to mitigate them is provided, as well as, it is described the motivation and justification of this investigation and the main objectives and goals have been stated. In addition, a brief description of the Standard IEEE-519, on the section referent to the permissible levels of harmonic distortion in the power system, is given.

Chapter 2 gives the basis of the shunt active power filter working principle. Explains in detail the control strategy in the *abc* frame to obtain the reference currents to be able to apply the shunt APF (steady-state and dynamic) compensation of nonlinear loads.

Chapter 3 shows the application of the proposed control strategy of Chapter 2 and its performance is tested with real-time simulations to validate the control algorithm and its affordable computational demand.

In order to continue the path of a future/possible physical implementation of the compensation device, Chapter 4 raises a solution to the associated resonance problems that could be present in practice. The solution to this problem is based in a particular design of a Linear Quadratic Regulator-(LQR) switching current technique. The designed current controller contributes to the feasibility in the reduction of the kVA rating of the active filter, allowing the incorporation of a passive element to either provide reactive compensation and/or working as a high-pass passive filter.

Chapter 5 formulates a novel alternative in the active power line conditioner (APLC) planning stage. The procedure is focused in determining the size and location of the APLC to mitigate harmonic distortion in electric systems.

Chapter 6 offers the main conclusions of this investigation and gives alternative paths to proceed in the same field of research.

Chapter 2. Operation of the Shunt Active Power Filter

2.1 Introduction

In this chapter an extended description of the main elements that allow the application of the shunt APF compensation is given. The control strategy to derive the reference signals (reference injection current) is obtained in phase coordinates to perform steady-state and is able to perform dynamic compensation of nonlinear loads in three-phase three-wire and four-wire systems. The control strategy could be easily reduced to be implemented in single-phase systems.

2.2 Operation Principle of the Shunt APF.

The shunt active power filter (APF) has demonstrated to be an appropriated tool for the mitigation of harmonic currents and reactive power compensation [Chang and Shee 2004]. The APF includes a control stage which computes the reference current to be injected into the system. So far, different compensation strategies can be used for this purpose [Grady *et al*. 1990], [Chang and Shee-2002], [Chang and Shee 2004], [Aredes *et al*. 1997], [Chen *et al*. 1993] and the appropriate operation of a shunt APF depends at a large extent on the applied control strategy to calculate the reference filtering currents since a characteristic of a shunt APF is the no consumption/supply of average power, as it does not require of active supply sources, such as batteries, for its compensation mechanism [Chang and Shee 2004]. To properly achieve this function, an effective control strategy for the computation of the reference filtering currents is required by the APF, in order to be able to eliminate the harmonic distortion in the source currents, and to provide reactive power compensation to the electric system, keeping other important characteristics on its performance, such as the no consumption of average power and feasibility of physical implementation, which implies the affordable computational demand required by its algorithm.

2.3 Control Strategy for Derivation of the Reference Signal Currents

The compensation strategy of the shunt APF should be efficient. Once the shunt APF is in operation, the source currents should be balanced, without distortion, and it should compensate reactive power. The proposed APF-*abc* compensation strategy for the calculation of the reference filtering currents is a variant of the Synchronous Current Detection (SCD) method [Chen *et al*. 1993], which in order to compute the reference filtering currents, works as a sinusoidal source current method; calculating the desired source currents and subtracting them from the load currents in order to obtain the reference filtering currents

$$i_{fk}^{*}(t) = i_{lk}(t) - i_{sk}^{*}(t) \qquad k = a,b,c \tag{2.1}$$

where $i_{fk}^{*}(t)$ are the reference filtering currents, $i_{lk}(t)$ are the load currents, and $i_{sk}^{*}(t)$ are the desired source currents after compensation. Reference [Chen et al. 1993] proposed the SCD method to maintain ideal three-phase desired source currents when there is a presence of amplitude-unbalanced source voltages. The strategy is based in two main assumptions:

First; the amplitude of the source currents after compensation should be the same, i.e.

$$I_{m\_SCD} = I_{ma} = I_{mb} = I_{mc} \tag{2.2}$$

Second; the source currents after compensation should be in phase with the source voltages at each phase respectively, i.e.

$$\theta_{i_{sk\_SCD}} = \theta_{v_{sk\_SCD}} \qquad (k = a,b,c) \tag{2.3}$$

In addition, after these two assumptions, the total average power delivered to the load should be supplied from the source with equally contribution by the three phases *a*, *b*, *c*. The average power, supplied to the load from the source, after compensation can be expressed according to Equations (2.4) and (2.5).

$$P_T = \frac{1}{T}\int_0^T \left(v_a(t) i^*_{sa\_SCD}(t) + v_b(t) i^*_{sb\_SCD}(t) + v_c(t) i^*_{sc\_SCD}(t) \right) dt \tag{2.4}$$

$$P_T = \frac{V_{ma} I_{ma\_SCD}}{2} + \frac{V_{mb} I_{mb\_SCD}}{2} + \frac{V_{mc} I_{mc\_SCD}}{2} \tag{2.5}$$

Where V_{mk} and I_{mk_SCD} are the amplitudes of the instantaneous source voltages and the desired source currents after compensation for *k= a, b, c*. According with Equation (2.2), the total power delivered to the load in Equation (2.5) now can be expressed as,

$$P_T = \frac{\left(V_{ma} + V_{mb} + V_{mc}\right)\left(I_{m\_SCD}\right)}{2} \tag{2.6}$$

Solving Equation (2.6) for I_{m_SCD} we have that the amplitude of the source currents after compensation is given by,

$$I_{m\_SCD} = \frac{2P_T}{V_{mT}} \tag{2.7}$$

where $V_{mT} = V_{ma} + V_{mb} + V_{mc}$. Finally, a unitary signal of reference, derived from the source voltage, is included to the source currents amplitude. Then, the desired source currents after compensation are calculated as,

$$i^*_{sk\_SCD}(t) = \frac{2P_T}{V_{mT}} \left(\frac{v_k(t)}{V_{mk}} \right) \quad k = a, b, c \tag{2.8}$$

where $P_T = P_a + P_b + P_c$ is the total average power in watts delivered to the load and $v_k(t)$ are the instantaneous source voltage for *k=a,b,c.* The term inside the parenthesis on the right-side term of Equation (2.8) is the instantaneous unitary vector derived from the source voltages at each phase, that allows the source currents after compensation to be in phase with the source voltages.

In (2.8), the instantaneous source voltages are assumed to be free of distortion and phase-balanced. When the SCD method is applied for shunt APF compensation in the presence of harmonic distortion and/or phase-unbalance in the source voltages, it shows a poor performance in the calculation of the desired source currents and consequently in the determination of the reference filtering currents [Chang and Shee 2004]. The proposed variant to the SCD method is based on assuming that the source voltages may be harmonic distorted and/or unbalanced, so that under any condition present in the source voltages, an adequate performance in the calculation of the desired source currents and reference filtering currents must be achieved.

To address the above mentioned problem, which is taking place during the calculation of the reference filtering currents under the presence of harmonic distortion and/or unbalance in the source voltages, a two-step procedure which consists in a post-process of the measured source voltages, to form a reference signal voltage, $v_k^*(t)$, to be used in (2.8) is proposed. The first step is to extract the fundamental component of the harmonic distorted source voltages to avoid harmonic content in the resulting desired source currents; the second step of the procedure is to ensure symmetry in the resulting desired source currents no matter a "possible" phase-unbalance present in the fundamental component of the source voltages previously obtained in the first step of this post-process.

2.3.1 Fundametal Component Extraction

Diverse applications and studies require the determination of the phase and amplitude of the voltage at fundamental frequency. These variables are needed for the determination of the reference signal for the active filtering, the detection of peak voltages for VAR compensation and for the extraction of power at fundamental frequency for the transient stability evaluation [Bollen and Gu 2006]. To obtain the fundamental frequency of the source voltages, the measured data could be treated according with the techniques described as follows.

2.3.1.1 Least-squares Fitting

This curve fitting method uses least squares error estimation to find the amplitude and the angle of the fundamental component. Curve fitting selects the best fit of a curve to a waveform and measures the discrete residual values between the waveform and the fitted curve. The size of these residuals is measured by the addition of their squared values. This

is then minimized to obtain the least square error; and the amplitude and phase of the best fitted curve are calculated.

In particular, this method has been reported as an appropriated alternative for a real-time monitoring and analysis of harmonic variations incorporating the use of neural nets (NNs) for the improvement of computational demand and efficiency [Lai *et al*. 1999], [Lin 2004], [Arrillaga *et al*. 2001].

2.3.1.2 The Fourier Transform

Fourier analysis is used to convert time-domain waveforms into their component frequencies and vice-versa. In practice, data are often available in the form of sample time function, represented by a time series of variable amplitude, separated by fixed time intervals of limited duration. Discrete Fourier Transform (DFT) or its variant the Fast Fourier Transform (FFT), are usually used for this purpose.

The frequency components provided by the DFT or FFT are time independent; in fact, for stationary signals these components remain the same over time. However, this is very different if the voltage waveforms are non-stationary, where the use of a Fourier transform alone becomes inadequate [Bollen and Gu 2006]. A suitable way to extract such information is to apply an innerly related time-frequency signal decomposition. Therefore, for the shunt APF_*abc* compensation presented in this thesis, a discrete Short-Time Fourier Transform (SFFT) [Bollen and Gu 2006], often referred to as the sliding-window DFT, is used for the time-frequency decomposition of non-stationary signals, e.g the extraction of the fundamental component of the source voltages. It is important to mention that any other technique for the extraction of the fundamental source voltage component, which represents a viable option, could be incorporated for this purpose.

Once the fundamental frequency source voltages are obtained, a Phase-Locked Technique (PLT) is proposed to ensure symmetry in the calculated source currents. Phase-Locked Loops (PLLs) are generally built from a phase detector, with a low pass filter and voltage controller oscillator (VCO) placed in a negative feedback closed-loop configuration. In the PLT described next, the phase angle of one of the phases is only required. At this stage, the fundamental frequency source voltages information has been already obtained with any of the techniques described before, particularly with the sliding-window DFT.

2.3.2 Proposed Phase-Locked Technique

If asymmetry is present in the obtained source voltages at fundamental frequency, and the shunt APF is placed to compensate harmonic currents and reactive power in a three-phase four-wire electric system, it will result in the presence of a relatively high neutral current. To avoid this problem, once the fundamental frequency source voltage information is obtained, a 120° positive sequence phase shift to be applied over the reference signal voltages is proposed. This is achieved by detecting the phase angle of the phase selected as the reference, e.g. phase *a*, and adding or subtracting 120° to the other two phases. At the end of the two-step procedure described above, the signal reference voltages to be used for the calculation of the desired source currents are now given as

$$v_a^*(t) = V_{ma1}\sin(\omega t + \phi_{a1}) \tag{2.9}$$

$$v_b^*(t) = V_{mb1}\sin(\omega t + \phi_{a1} - 2\pi/3) \tag{2.10}$$

$$v_c^*(t) = V_{mc1}\sin(\omega t + \phi_{a1} + 2\pi/3) \tag{2.11}$$

where $v_k^*(t)$ are the reference signal voltages, V_{mk1} are the amplitudes of the source voltages at fundamental frequency, and φ_{a1} is the angle of the fundamental component of the source voltage at phase *a*. The substitution of (2.9)-(2.11) into (2.8) gives the proposed formulation to find the desired source currents after shunt APF compensation, i.e.,

$$i_{sa\_APF\_abc}^*(t) = \frac{2P_T V_{ma1}\sin(\omega t + \phi_{a1})}{V_T V_{ma1}} \tag{2.12}$$

$$i_{sb\_APF\_abc}^*(t) = \frac{2P_T V_{mb1}\sin(\omega t + \phi_{a1} - 2\pi/3)}{V_T V_{mb1}} \tag{2.13}$$

$$i^{*}_{sc\_APF\_abc}(t) = \frac{2P_T V_{mc1} \sin(\omega t + \phi_{a1} + 2\pi/3)}{V_T V_{mc1}} \tag{2.14}$$

where $V_T = V_{ma1} + V_{mb1} + V_{mc1}$. Since the power losses caused by switching and capacitor voltage variations must be supplied by the source, a power signal P_{loss} is added to the power delivered to the load. Thus, taking the above into consideration and by observing (2.12)-(2.14) the amplitude of the desired source currents including power losses is given by,

$$I_{m\_ABC} = \frac{2(P_T + P_{loss})}{V_T} \tag{2.15}$$

where I_{m_ABC} is the amplitude of the desired source currents after shunt APF compensation including power losses. Therefore, the reference filtering currents for phases *a*,*b* and *c* are found by the arrangement of (2.15) into (2.12)-(2.14) and then using (2.1),

$$i^{*}_{fa}(t) = i_{la}(t) - I_{m\_ABC} \sin(\omega t + \phi_{a1}) \tag{2.16}$$

$$i^{*}_{fb}(t) = i_{lb}(t) - I_{m\_ABC} \sin(\omega t + \phi_{a1} - 2\pi/3) \tag{2.17}$$

$$i^{*}_{fc}(t) = i_{lc}(t) - I_{m\_ABC} \sin(\omega t + \phi_{a1} + 2\pi/3) \tag{2.18}$$

Under sinusoidal supply voltages, the desired source currents of (2.12)-(2.14) can be regarded as a three-phase generalization of the active current definition proposed by Fryze for a single phase system [Arrillaga *et al*. 2001]. The source currents also agree with the definition proposed by Czarnecki via orthogonal current decomposition for the three-phase system [Czarnecki 1998], where the load current can be decomposed into active and residual components, i.e.,

$$i_{lk}(t) = i^{*}_{sk\_APF\_abc}(t) + i_{k\_residual}(t) \tag{2.19}$$

In (2.19), $i^{*}_{sk\_APF\_abc}(t)$ is the minimum effective source current associated with the transfer of real power from the source to the load and the residual component is the non active

component. Thus, the residual component will be equal to the reference filtering currents allowing the no consumption/supply of real power by the APF.

2.4 Shunt APF implementation model in Matlab/Simulink®

Since Matlab/Simulink provides the full capabilities required for accurate simulations for the development of the test studies presented in this thesis, it is adopted as the simulation tool to be used. Figure 2.1 shows the main elements of the shunt APF model. The measurements of the load currents and source voltages are inputted to the calculator of the reference signal currents (reference filtering currents), which are calculated employing the strategy control explained in Section 2.3. Once the reference currents are determined they are input to a hysteresis-band current controller to produce the control switching pattern of the Voltage Source Inverter (VSI) which in turn injects into the system the actual filtering current with the same waveform of those calculated as the reference. The dc capacitor is placed for energy storage and a PI control is implemented to ensure that the dc voltage variations, due to the switching action of the commutation devices and losses, be controlled under certain limits of operation allowing the correct performance of the filter. The reference filtering currents are calculated as detailed in Section 2.3. In the subsections to follow, the implementation of each one of the main elements forming the shunt APF, illustrated as subsystems in Figure 2.1, are described in detail.

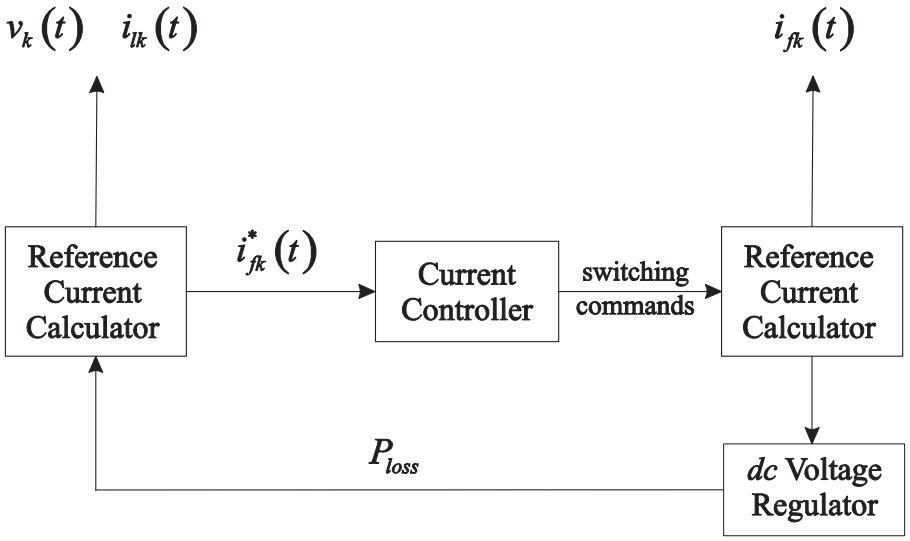

Figure 2.1 Shunt APF model in Matlab/Simulink®

2.4.1 Reference current calculator

Simulink® is an environment for multi-domain simulation and Model-Based Design for dynamic and embedded systems. It provides an interactive graphical environment and a customizable set of block libraries that let us design, simulate, implement, and test a variety of systems, including communications, controls, signal processing, video processing, and image processing. With this simulation package it is possible to quickly create, model, and maintain a detailed block diagram of our system using a comprehensive set of predefined blocks. It provides tools for hierarchical modeling, data management, and subsystem customization, making easy to create concise, accurate representations, regardless the complexity of the system.

The models can be built by dragging and dropping blocks from the library browser, e.g. SimPowerSystems™, into the graphical editor and connecting them with lines that establish mathematical relationships between the blocks. The arrangement of any particular model is achieved by using graphical editing functions. The parameters and/or coefficients that help us define the dynamics and behavior of the system can be easily incorporated. Figure 2.2 shows the implementation of the reference current calculator using the control strategy described and proposed in Section 2.3.

Figure 2.3 andFigure 2.4 show the parameters associated to the blocks of the SimpPowerSystems™ library used for implementing the control strategy to derive the reference signals of the shunt APF. For the case of the Clock block illustrated in Figure 2.2 no parameters are needed since this block only provides as an output the current simulation time. Though Simulink® allows the construction of algorithms and functions defined by the user as needed, we have opted for using the embedded functions and blocks that the SimPowerSystems™ library has already incorporated. This decision is based on taking full advantage of the Matlab/Simulink® capabilities, and for the statement that optimized C code that can be generated by the Real-Time Workshop [RTW 2007] for all the embedded functions included in the library browser.

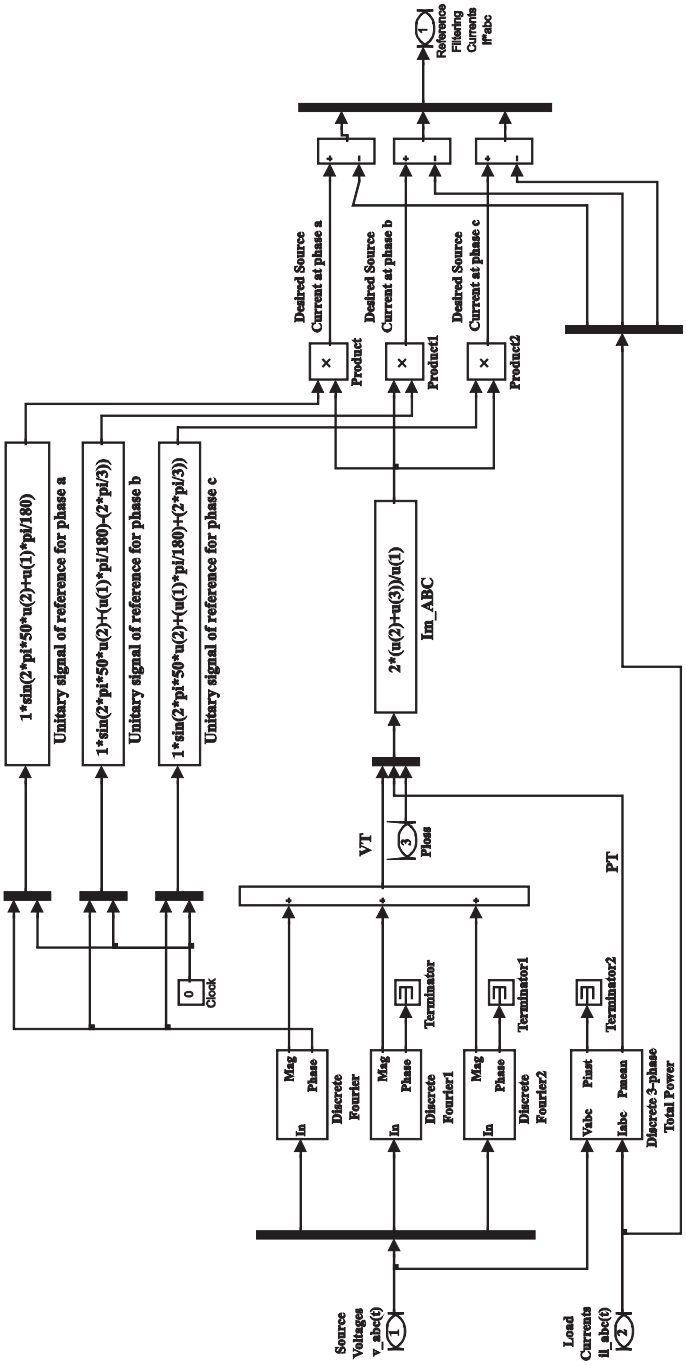

Figure 2.2 Reference current calculator in Matlab/Simulink®.

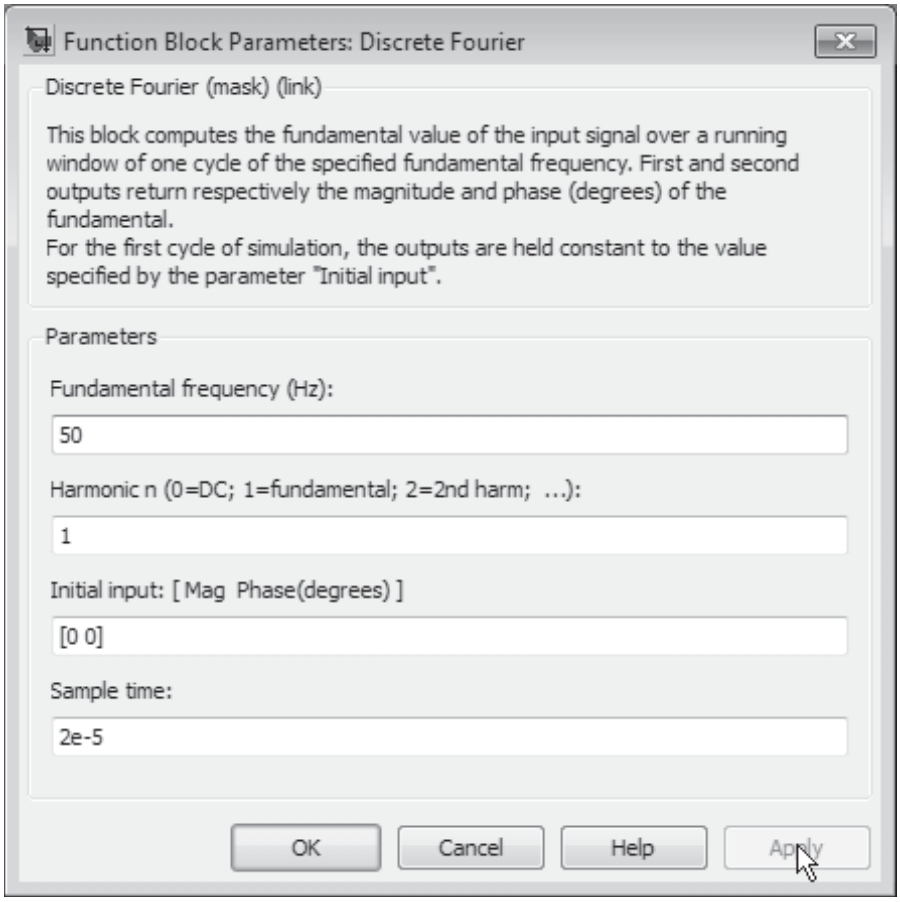

Figure 2.3 Function parameters for the Discrete Fourier block.

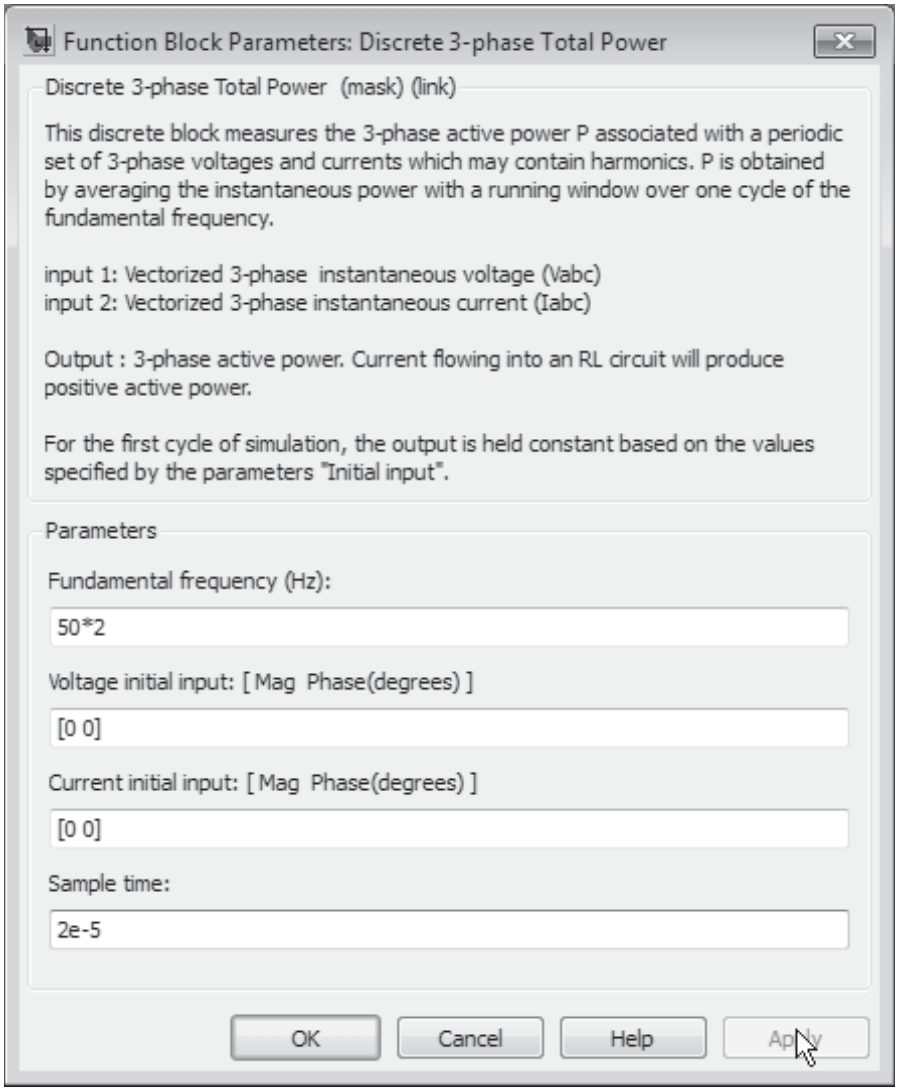

Figure 2.4 Function parameters for the 3-Phase Total Power block.

2.4.2 Hysteresis band current controller

The basic implementation of the hysteresis band current controller derives the switching signals from the comparison of the current error with a fixed hysteresis band [Buso *et al*. 1998], .The control method is simple to implement, and due to its excellent dynamic response it has been widely used in shunt APF applications [Buso *et al*. 1998].

In the basic version of this current controller, the actual injected current is compared with the reference current, and the resulting error is to be applied to a hysteresis fixed band comparator, obtaining in this manner the commutation signals to keep the error in the injected current within the hysteresis band [Buso *et al*. 1998]. Due to its inherent non linearity, and the absence of delays, this current controller is capable of achieving the fastest response possible. The control results stable and robust to load variations and other types of dynamic disturbances [Buso *et al*. 1998].

The main disadvantage is that the hysteresis current controller produces a variable commutation frequency for the power converter. In particular, this situation could lead to some problems, from the difficulty in designing the passive filter at the end connection of the active filter to the excitation of resonance phenomenon as it will be illustrated in Chapter 4. Figure 2.5 shows the basic implementation of the hysteresis band current controller in Matlab/Simulink®. The value parameters for the hysteresis window can be inputted as needed by the user, see Figure 2.6.

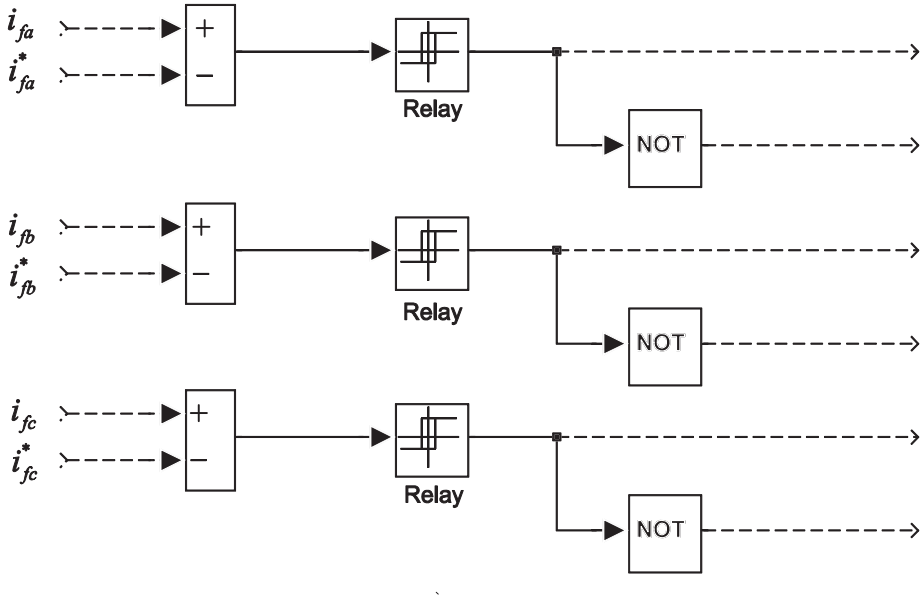

Figure 2.5 Hysteresis-band current controller in Matlab/Simulink®.

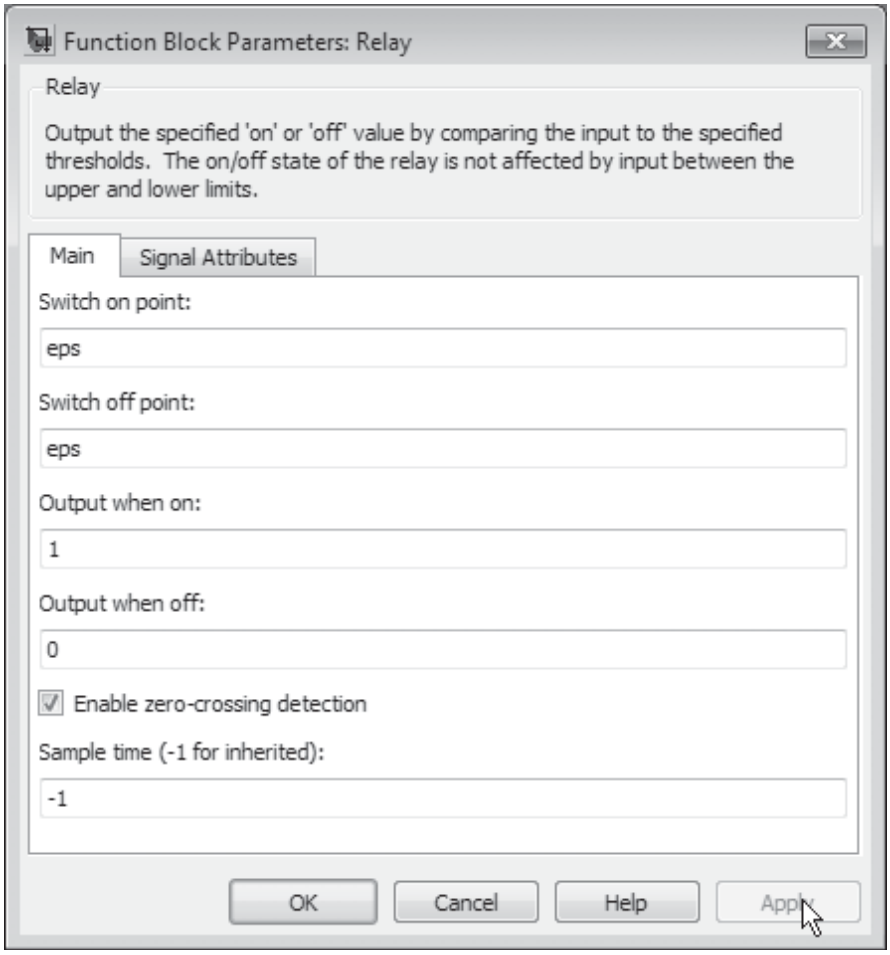

Figure 2.6 Relay block parameters.

Many improvements to the original control structure have been suggested by industrial applications [Kawamura and Hoft 1984], [Chiarelli *et al*. 1993], [Malesani and Tenti 1990]. Among the improvements of the current control technique, a fixed modulation frequency has been achieved by a variable with of the hysteresis band as function of the instantaneous output voltage [Malesani and Tenti 1990], [Yao and Holmes 1993], [Malesani *et al*. 1996]

Independently of the current controller chosen and assuming that there is no passive filter to drain the high frequency components, a ripple current is going to be present in the injected current into the system. In Chapter 4 this situation is taken into consideration by designing a second order modulation technique.

2.4.3 Voltage Source Inverter

In general, the static converter of the shunt APF can be implemented with a Voltage Source Inverter (VSI) or a Current Source Inverter (CSI). The CSI results to be more robust and in turn is more expensive to implement [Hayashi *et. al*. 1991], [Fukuda and Endoh 1995]. On the other hand, the VSI present fewer losses and is cheaper to implement [Akagi 1994]. In this thesis the VSI will be used in the shunt APF model, which agrees with the trend in most of the compensation devices available in the market [Akagi 1995].

The inverter shown in Figure 2.7 receives the name of Three-Leg Full Bridge (TLFB) and its application in the shunt active power filter compensation scheme in three-phase three-wire systems was introduced by Akagi in 1984 [Akagi *et al*. 1984], and it has become widely used in this kind of applications, motivating since then new contributions to the field [Qiao *et al*. 2004], [Nuñez-Zuñiga and Pomillo 2001], [Mattavelli 2002]. It is important to mention that with the TLFB results impossible to inject zero-sequence currents to the electric system, thus this topology is only to be used in three-phase three-wire systems.

On the other hand, for the case of low power three-phase four-wire systems, is very common the existence of single-phase phase loads connected between a phase and neutral wire. For these cases, it is necessary the use of a different converter topology. In particular, the simplest solution consists in the topology shown in Figure 2.8, namely Three-Leg Split-Capacitor (TLSC). The TLSC permits each of the three-legs to be controlled independently, and allows the zero-sequence injection currents. However, all the zero-sequence currents flow through the dc-bus capacitors. This current could lead to imbalance in the capacitors voltage sharing, forcing to increase the capacitors rating to ensure that capacitor voltages have a sufficiently high absolute value.

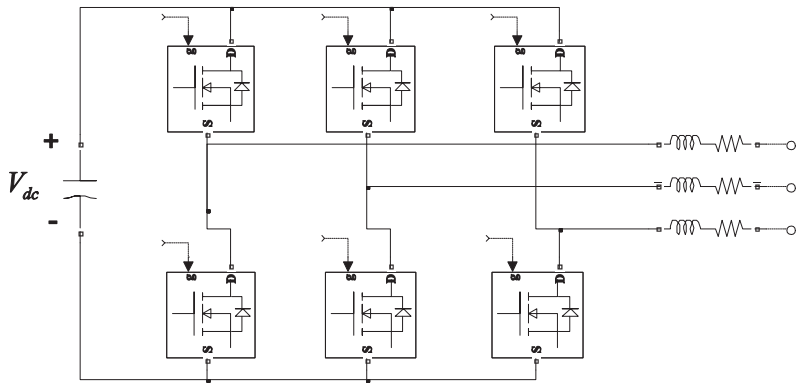

Figure 2.7 Three-Leg Full-Bridge voltage source inverter.

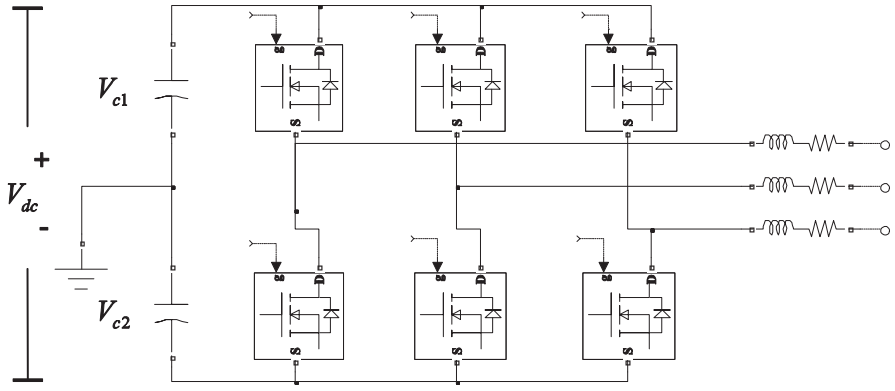

Figure 2.8 Three-Leg Split-Capacitor voltage source inverter.

Finally, in high power systems the topology shown in Figure 2.9, namely Three-Bridge Four-Wire (TBFW), is commonly used. The TBFW voltage source inverter has a high functionality in high power systems due to the coupling transformers. This topology can be seen as three independent single-phase inverters, one per phase, giving a higher capacity of current injection. The single-phase inverters have the power rate capacity, and each one of the single-phase inverters is able to inject zero, negative and positive sequence currents. The control of the commutation sequences is simple and it allows the feasibility in high power applications by reducing the commutation frequency and minimizing the ripple current injected into the network.

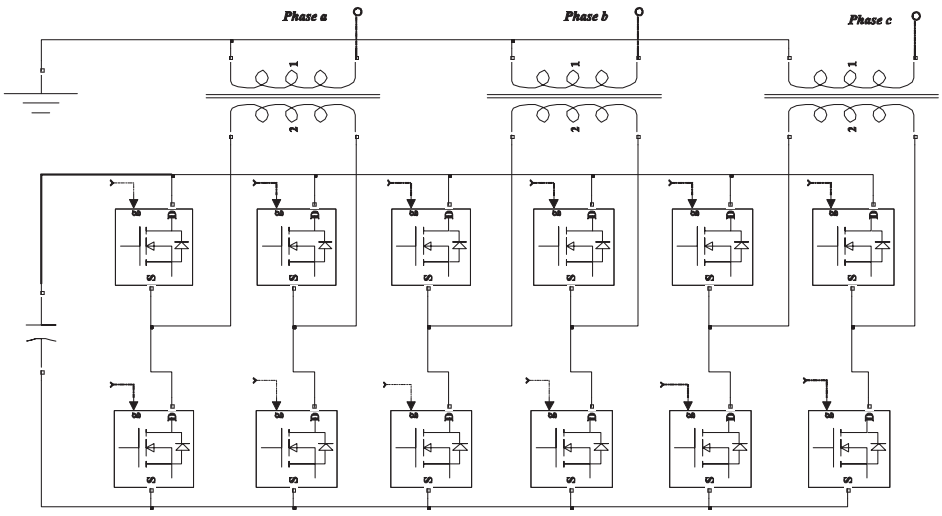

Figure 2.9 Three-Bridge Four-Wire voltage source inverter.

For the case studies presented in this research work, the three-leg full bridge VSI as well as the three-leg split-capacitor VSI have been used in the low power shunt APF compensation scheme for three-phase three-wire and three-phase four-wire electric systems, respectively.

2.4.3.1 Energy bus storage

The dc-bus capacitor of the voltage source inverter is used for energy storage, and it is required that the dc-bus capacitor maintains a constant dc voltage to allow a proper performance of the shunt APF. Nevertheless, due to the harmonics and switching commands the dc voltage slightly fluctuates. To avoid the incorrect performance of the shunt APF and to supply the energy losses, a power loss signal P_{loss} (controlled via a PI controller) is added to P_T in the reference current calculator, e.g. equation (2.9). In this way, the power losses are supplied from the source and the dc voltage is maintained nearly constant. Some references have attained this particular situation for the case of the three-leg full-bridge VSI and the three-leg split-capacitor VSI in shunt APF applications. Even more, it has been reported the use of the energy balance approaches in the dc capacitor to determine the reference filtering currents of the shunt APF. This is not the case of the research work presented in this thesis.

2.5 Conclusions

In this chapter the main components of the shunt active power filter have been described in detail. Even though, there is a wide range of options on the election of structures and control algorithms, a meaningful explanation/justification and motivation of the techniques adopted and applied in the development of the shunt APF model have been established.

The bases for the implementation of the shunt APF digital model in Matlab/Simulink® are also given in detail. Matlab/Simulink® is a powerful computational package and since Matlab/Simulink® provides full capabilities required for the analysis, implementation and developing of all the case studies reported in this thesis, it has been adopted for the realization of this investigation work.

Chapter 3. Real-Time Simulation of Shunt APF Compensation

3.1 Introduction

In this chapter, the control strategy in phase coordinates developed in Chapter 2 to derive the reference filtering currents is proposed and tested for a real-time application. The development of the proposed shunt APF control strategy is described in detail, and its application is analyzed with two case studies which include a real-time application for steady-state and dynamic nonlinear compensation. The proposed control strategy for calculating the reference filtering currents of the shunt active power filter was tested using Matlab/Simulink®, with the incorporation of the Real-Time Workshop for the simulation of the APF in real-time. This real-time application makes possible the observation and evaluation of simulation conditions close to the true real-time environment under study using a single computer, it gives accurate results with relatively low-cost hardware, and also it provides a more complete evaluation of the applied control strategy for the calculation of the reference current signals. The control strategies for calculating the reference filtering currents are of vital importance in the final performance that the shunt APF is able to provide, comparisons of the performance for different strategies can be found in [Chang and Shee 2002], [Chang and Shee 2004]. An effective control strategy for the computation of the reference filtering currents is required by the APF, in order to be able to eliminate the harmonic distortion in the source currents, and to provide reactive power compensation to the electric system, keeping other important characteristics on its performance, such as the no consumption of average real power and feasibility of physical implementation, which implies the affordable computational demand required by its algorithm.

With the growing importance of power quality problems to electric utilities and customers, there is an increasing interest on the search of new techniques for the accurate analysis and resolution of such problems. The real-time simulation techniques are used for several studies of power systems containing nonlinear loads. Available literature details several techniques developed and implemented to perform real-time simulations in power system analysis [Pak *et al*. 2007].

In this Chapter, the real-time operation of the APF compensation is developed with the incorporation of the Real-Time Windows Target (RTWT) toolbox of Matlab/Simulink [RTWT 2007], which is used as a PC solution for prototyping and testing real-time systems, where a single computer is used as a host and as a target [RTWT 2007], [RTW 2007].

Taking the above aspects into consideration, the real-time performance of the proposed control strategy, which can be described as simple and efficient, is tested and it is pointed-out to be a suitable option for further physical implementation of the device for either three-phase or single-phase systems. The details for its digital design and dynamic operation analysis are given in the following sections.

3.2 Real-Time Simulation Software

The simulation of the APF connected to the power system provides advantages in the design process by allowing options to be tried-out before the hardware is built. After creating a Simulink model, the simulation parameters are used by a Real-Time Workshop [RTW 2007] to generate C code and to build the real time application. Real-Time Workshop generates optimized, portable, and customizable ANSI C or C++ code from Simulink models to create standalone implementations of models that operate in real-time in a variety of target environments, and with commercial or proprietary real-time operating systems.

In this investigation, the real-time application of the shunt APF_*abc* compensation was developed with the incorporation of the Real-Time Windows Target (RTWT) toolbox of Matlab/Simulink. RTWT is a PC solution for prototyping and testing real-time systems. It is an environment where a single computer is used as a host and as a target. After creating a model and simulating it with Simulink in normal mode, it is possible to generate executable code; then the application in real time is achieved with the Simulink external mode. RTWT uses a small real-time kernel to ensure that the real-time application runs in real time. The real-time kernel runs at CPU ring zero (privileged or kernel mode) and uses the built-in PC clock as its primary source of time [RTWT 2007], [RTW 2007]. The kernel intercepts the interrupt from the PC clock before the Windows operating system receives it, this blocks any calls to the Windows operating system [RTWT 2007].

Communication between Simulink and the real-time application is through the Simulink external mode interface module. This module talks directly to the real-time kernel, and is used to start the real-time application. External mode requires a communication interface to

pass external parameters to Simulink, and on the receiving end the same communications protocol must be used to accept new parameter values, and to insert them in the proper memory locations to be used by the real-time application. For the case of this investigation, the host computer also serves as the target computer. Therefore, only a virtual device driver is needed to exchange parameters between the Matlab and Simulink memory space and the memory that is accessible by the real-time application [RTWT 2007].

RTWT provides the necessary software that uses the real-time resources on the computer hardware. Based on the selected sample rate, RTWT uses interruptions to set the application in real time at a proper rate [RTWT 2007]. With each new interrupt, the executable program generated by RTW computes all of the block outputs from the model.

3.3 Case Studies

Both case studies are intended to demonstrate the efficiency of the control strategy for determining the reference filtering current with an affordable computational effort in a real-time application. Case study 3.1 provides a comparison between the results obtained with the real-time simulation against the results obtained with other integration method in an off-line simulation. The mismatch error in the results is illustrated.

In the case study 3.2 the dynamic shunt APF compensation of nonlinear loads under unbalanced conditions has been implemented.

3.3.1 Case Study 3.1

The purpose of the case study is to show the usefulness of using RTWT for real-time applications giving accurate results and with all the advantages of a real-time simulation. The electric system under analysis is a three-phase three-wire system with distorted source voltages, as given in (3.1)-(3.3), supplying a non controlled 11.6 KVA six-pulse rectifier.

$$v_a(t) = 250\sin(\omega t) + 11\sin(5\omega t) + 5\sin(7\omega t) \tag{3.1}$$

$$v_b(t) = 250\sin(\omega t - 120°) + 11\sin(5\omega t + 120°) + 5\sin(7\omega t - 120°) \tag{3.2}$$

$$v_c(t) = 250\sin(\omega t + 120°) + 11\sin(5\omega t - 120°) + 5\sin(7\omega t + 120°) \tag{3.3}$$

The Figure 3.1 illustrates the shunt active power filter connected to the three-phase three-wire electric system. The reference current calculator is implemented according with the proposed strategy control in Chapter 2. Once the reference compensating currents are obtained, they are used as inputs to a hysteresis band current controller to produce the control signals of the PWM inverter and to generate the actual filtering currents. The capacitor is used for energy storage and for maintaining a constant dc voltage. The capacitor voltage slightly fluctuates due to the harmonic power flow, since the capacitor voltage at the inverter terminal must be maintained at a constant level; the loss caused by switching and capacitor voltage variations is supplied by the source. Figure 3.2 shows the report of code generation for the real-time application.

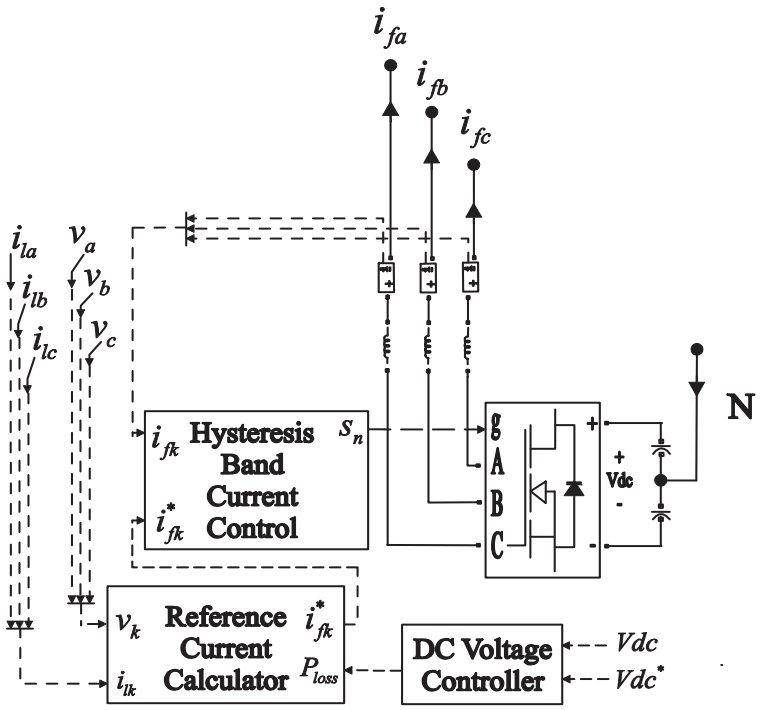

Figure 3.1 Shunt APF connected to a three-phase three-wire electric system.

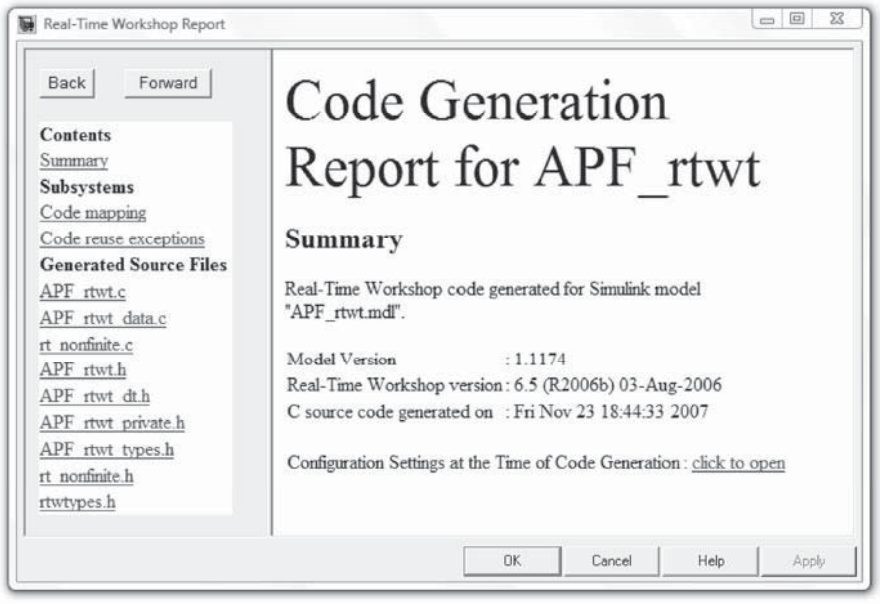

Figure 3.2 Code generation report for APF_rtwt.mdl as reported by RTW.

Figure 3.3 illustrates the results obtained by the real-time simulation using RTWT for (a) three-phase source voltages, (b) three-phase load currents, and (c) three-phase source currents before/after APF compensation.

For the test system under study the results were obtained using a fixed step solver provided by Matlab/Simulink®, a Finite Dif. method, as non continuous states were included in the model, and a sample time of $T_s = 5\text{x}10^{-5}$ was used in the experiment. An execution time of 0.11 seconds was observed.

For comparison purposes, the same electric system was analyzed with different fixed step solvers available from the RTWT toolbox of Matlab/Simulink® in off-line simulations. Figure 3.4 shows the comparison of the results shown in Figure 3.3(c) for phase *a*, i.e. the source current at phase *a*, including before/after compensation stages, against the results obtained using the fixed step solver ODE4 provided also in Matlab/Simulink toolbox; the absolute error between the results of both simulations is negligible.

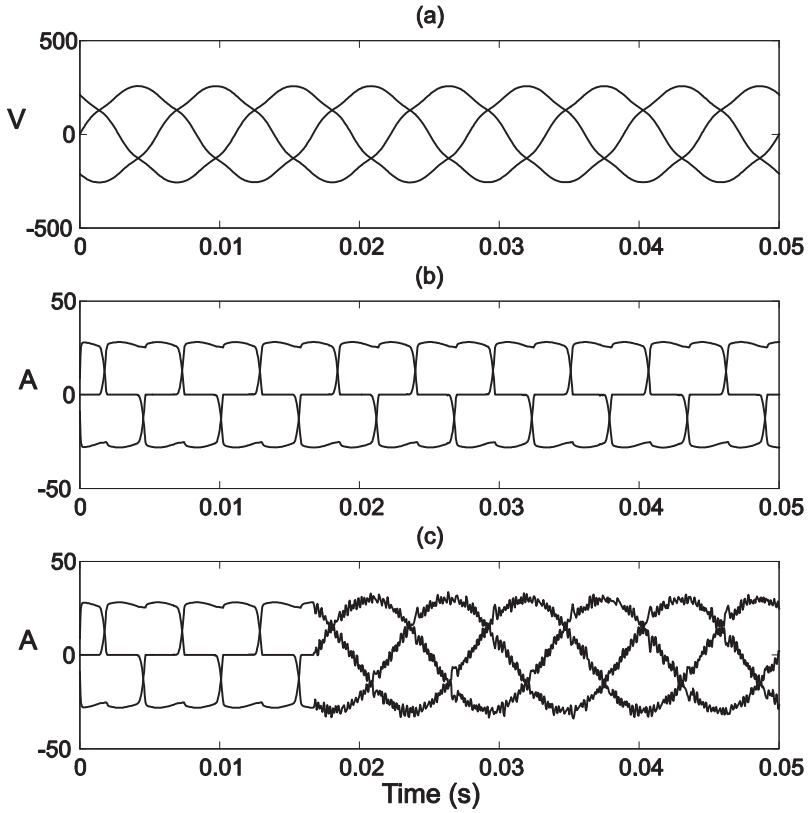

Figure 3.3 Real-time simulation results for shunt APF compensation case study 3.1. (a) Three-phase source voltages, (b) Nonlinear loads currents, (c) Source currents before/after compensation.

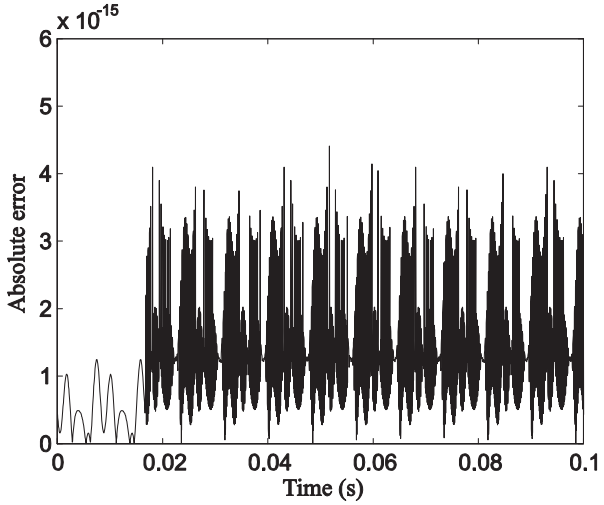

Figure 3.4 Error-mismatch between real-time simulation and off-line simulation.

3.3.2 Case Study 3.2

The potential of the developed control strategy for calculating the reference filtering currents in phase coordinates is illustrated with the analysis of the test system of Figure 3.5. The three-phase balanced source voltages supply an assumed unbalanced nonlinear load. In this scenario, there are three different distorting loads connected between each phase and neutral wires, which give place to a highly heterogeneous three-phase harmonic composition at the PCC. These loads consist on a single-phase full-wave rectifier with a high inductance on the dc side for phase *a*; a single-phase full-wave rectifier with a high capacitance on the dc side for phase *b*, and multiple current injections for phase *c*, which represent a given single-phase non linear load, as shown in Figure 3.5. For phases *a* and *b* the single-phase transformer is assumed to be linear, and the multiple current injections information of the non linear load at phase *c* is given by (3.4).

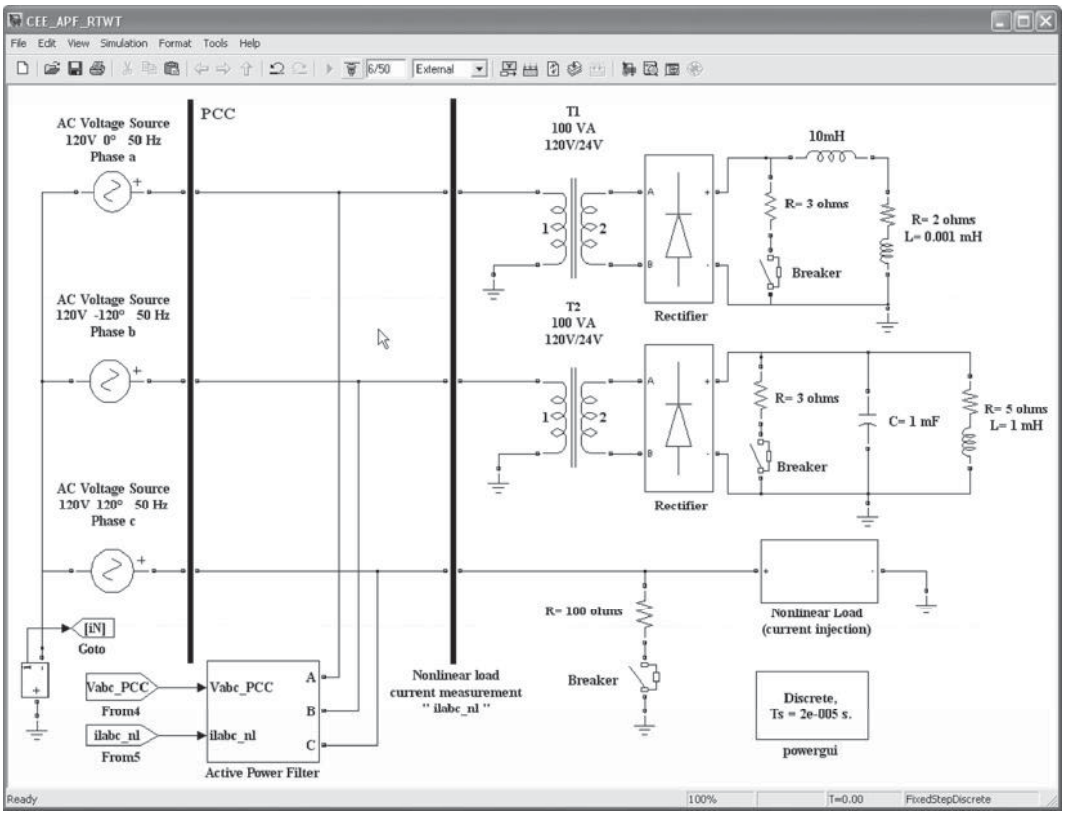

Figure 3.5 APF in Matlab/Simulink® for Real-Time application in case study 3.2.

$$i_{lc}(t) = 3.9862\sin(\omega t + 172.77°) + 0.28479\sin(3\omega t + 2.26°) + 1.5125\sin(5\omega t + 4.43°) + 0.4846\sin(7\omega t + 6.17°)\ \text{A} \tag{3.4}$$

In order to simulate a load change during the shunt APF compensation and be able to observe the transient performance of the control strategy in real-time, a load change after 3 cycles of simulation (switching ON all breakers at T=0.6 s) is programmed, see Figure 3.5. The load changes consist on a pure resistive load is connected in parallel on the dc side for phases *a* and *b*, and a pure resistive load is connected in parallel with the multiple current injections that simulate the single-phase non linear load for phase *c*, see Figure 3.5.

The electric circuit conditions of the test system under study are shown in Figure 3.6. The source voltages are sinusoidal and balanced, see Figure 3.6(a), and the total load currents are highly distorted/unbalanced, as shown in Figure 3.6(b). In particular, a meaningful and detailed analysis of the load currents behavior during the simulation illustrated through Figure 3.7, Figure 3.8 and Figure 3.9, for phases *a*, *b* and *c*, respectively, is given next.

Figure 3.7(a) shows the load current waveform for phase *a*, where the total harmonic distortion (THD) along with the current waveform is varying after 3 cycles of simulation, at T=0.06 s. As a result of the load change condition the harmonic currents and fundamental frequency also change their values. This situation is illustrated in Figure 3.7(b) and Figure 3.7(c) where the magnitude of the harmonic content is given in amperes and % of the fundamental, respectively. A similar condition is presented for phase *b*, in Figure 3.8(a), (b) and (c). For these two phases, after the load change condition at T=0.06s, the harmonic content in the load current varies. Due to the change in the harmonic content and fundamental component the THD index also varies. This situation will require a dynamic response on the calculation of the reference filtering currents.

On the other hand, the load change condition for phase *c* is illustrated in Figure 3.9(a). Please noticed that after the load change condition in phase *c* at T=0.06s, the load current has the same harmonic content in amperes as illustrated in Figure 3.9(b). This situation become clear and actually expected since the harmonic injection currents using for modeling the load current at phase *c* are not changed at all. Nevertheless, the addition of the parallel resistance produces that the fundamental current increases, which results in a variation of the waveform, the THD index value, and harmonic content expressed as a magnitude of the fundamental, see Figure 3.9(c).

After the dynamic simulation conditions of the nonlinear load explained above, it will be expected that the proposed control algorithm for calculating the reference filtering currents dynamically re-calculate their values during the entire compensation process, especially after the load change condition at T=0.06s. Thus, in order to ensure a good performance of the compensation device, it will be expected that the reference filtering currents for phases *a* and *b* re-calculate their values, due to the load change condition at T=0.06 s. On the other hand, for phase *c*, despite the continuous recalculation, the reference filtering current will be required to remains nearly constant during the entire shunt APF compensation process.

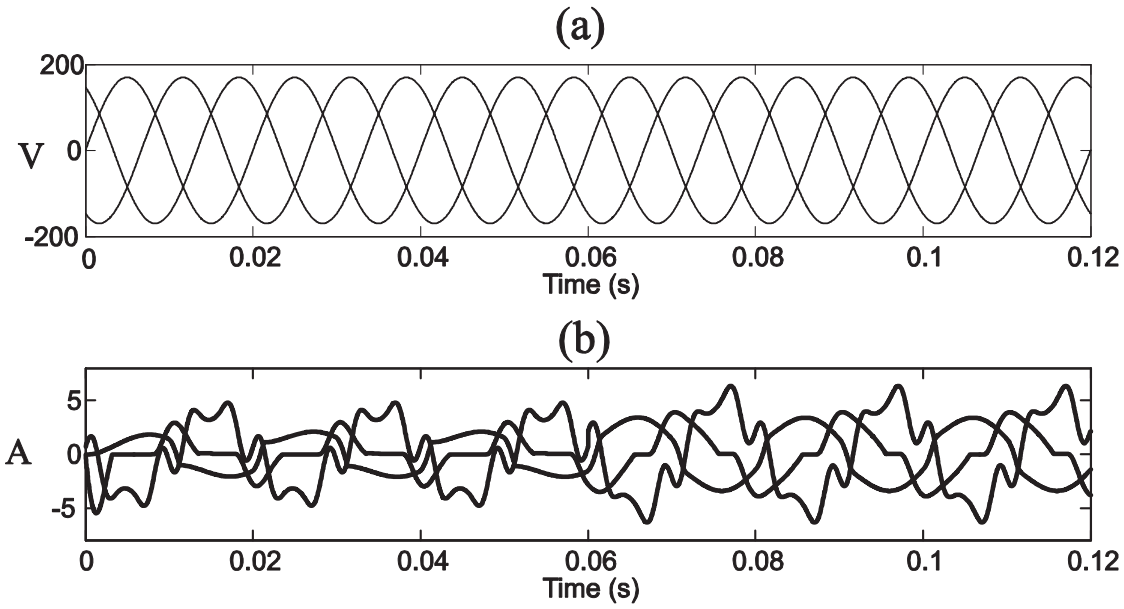

Figure 3.6 Electric circuit conditions of the case of study 3.2. (a) Source Voltages, (b) Load currents.

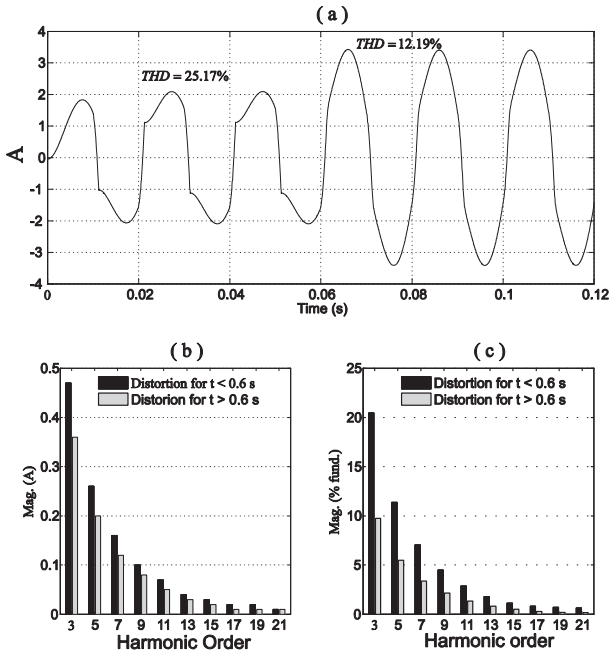

Figure 3.7 Load current at phase *a* for case study 3.2. (a) Load current at phase *a*, (b) Harmonic content in amps, (c) Harmonic content in percent of the fundamental.

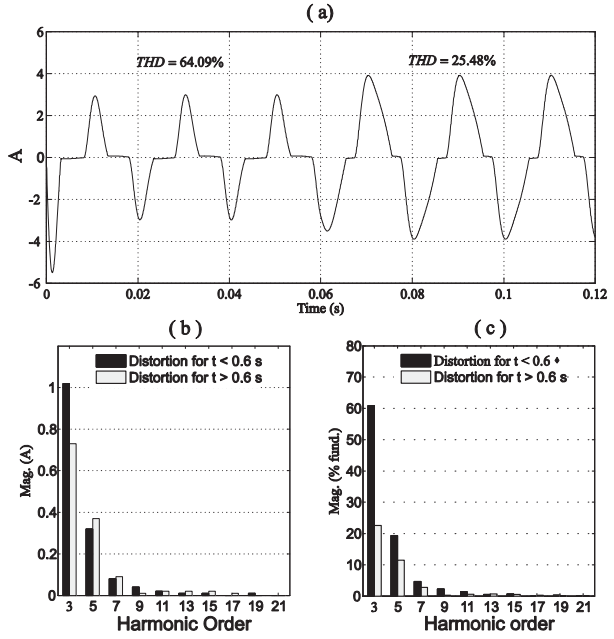

Figure 3.8 Load current at phase *b* for case study 3.2. (a) Load current at phase *b*, (b) Harmonic content in amps, (c) Harmonic content in percent of fundamental.

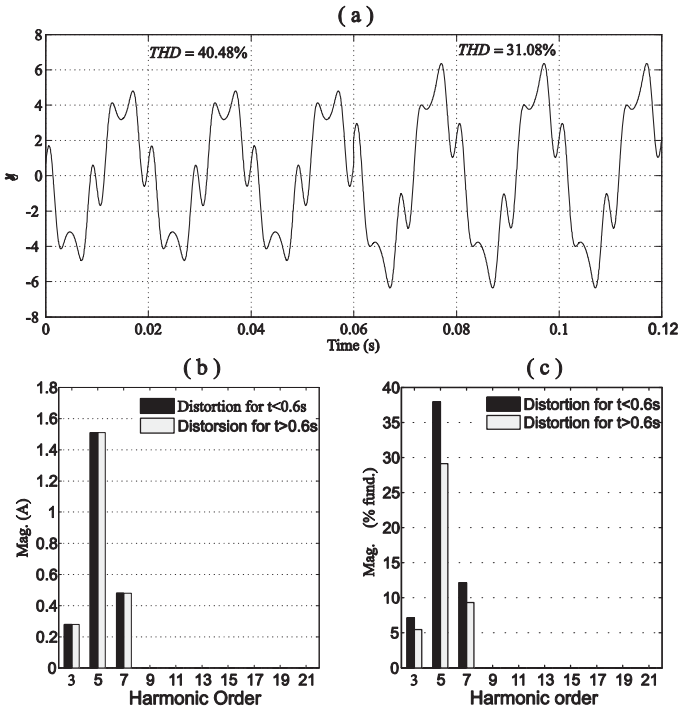

Figure 3.9 Load current at phase *c* for case study 3.2. (a) Load current at phase *c*, (b) Harmonic content in amps, (c) Harmonic content in percent of the fundamental.

The results of the shunt APF compensation are illustrated in Figure 3.10 and Figure 3.11. Figure 3.10, illustrates the source currents at the point of common coupling (PCC), where the elimination of the harmonic currents in all phases can be observed. The neutral current shown in Figure 3.11 is well controlled during the complete compensation process despite the load change conditions.

The injection currents by the APF are shown in Figure 3.12(a), (b), and (c), for phases *a*, *b*, and *c*, respectively. As it was expected, after the load change condition at T=0.06 s, the filtering currents of phases *a* and *b* update their values to be able to achieve an adequate performance of the APF, meanwhile the filtering current for phase *c* remains nearly constant as it was required and calculated by the control strategy. It important to mention that the little variation on the filtering current for phase *c* after the load change condition, is due to the increase of the fundamental component produced by the parallel resistance. Actually, this variation is a non-active fundamental frequency current, injected for purposes of source currents balance and reactive power compensation.

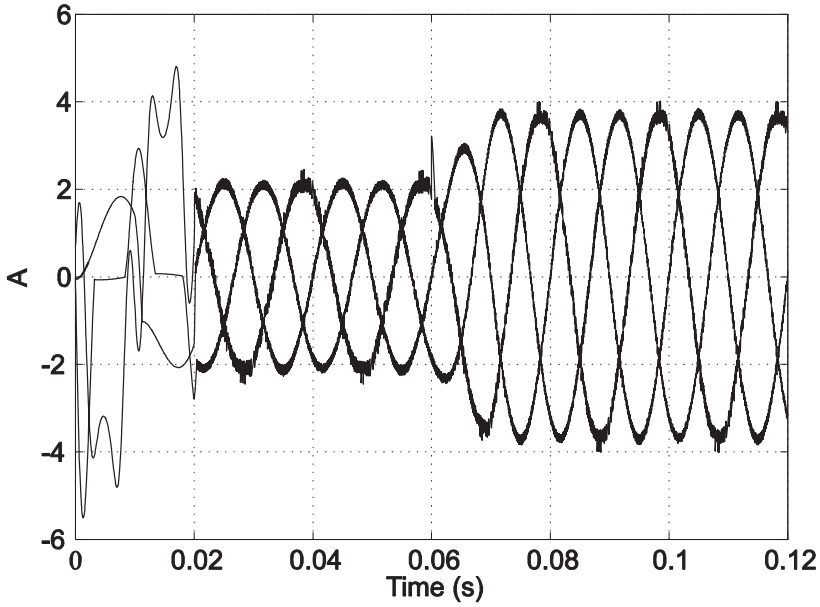

Figure 3.10 Source currents at the PCC with shunt APF compensation.

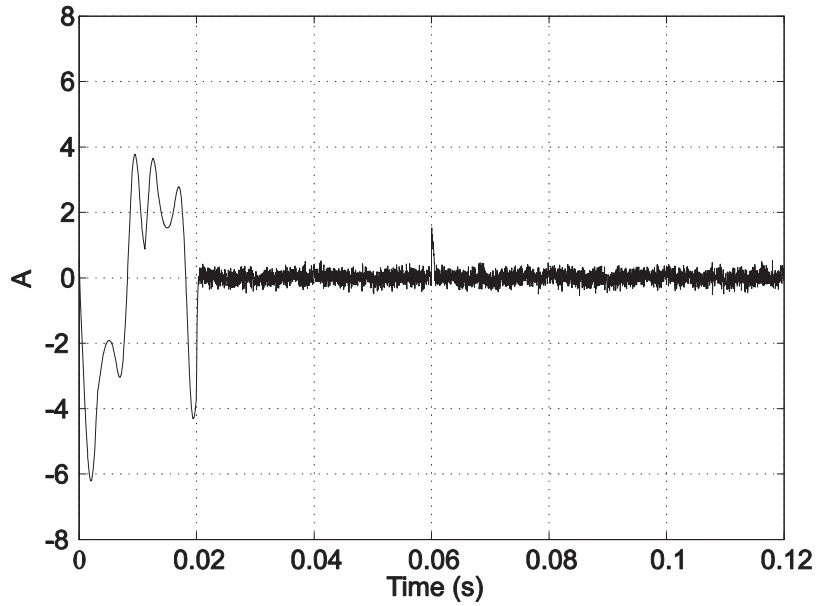

Figure 3.11 Neutral current during shunt APF compensation.

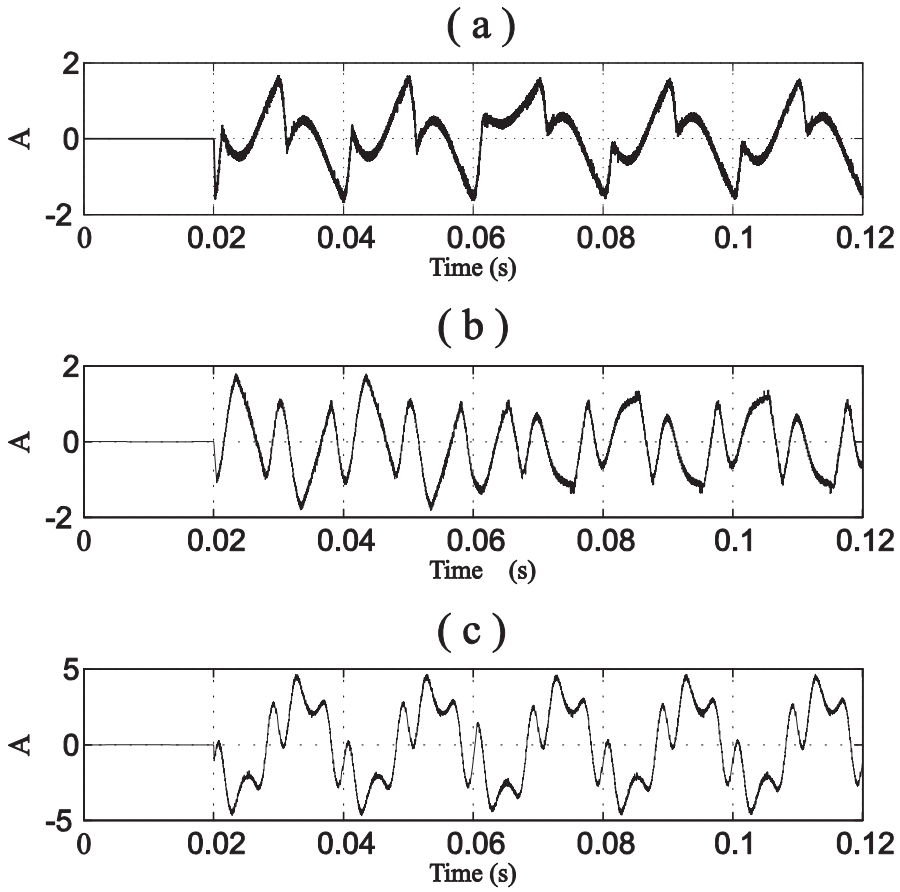

Figure 3.12 Shunt APF compensation currents. (a) Filtering current at phase *a*, (b) Filtering current at phase *b*, (c) Filtering current at phase *c*.

3.4 Conclusions

The electric systems under study and the complete dynamic model of the shunt APF_*abc* has been implemented in the real-time simulation package RTWT, which includes the VSI, the modulation technique, and the control strategy. In fact, it is important to note that in order to be able to compensate unbalanced nonlinear currents by the APF and to maintain the neutral current controlled, the use of a Three-Leg Split-Capacitor (TLSC) as the converter configuration of the VSI was required. The converter configuration and the modulation technique used for generating the switching commands allow the control of the

injection currents of each phase to be independent to each other, working directly over the reference filtering current with a low computational demand required for that purpose.

On the other hand, when using simulating modulation techniques with a fixed-step solver, the integration step should be small enough to provide accurate solutions, or the inclusion of another software package would be necessary for obtaining a feasible solution. Giving the characteristics of the commutation technique used in this real-time application, a maximum of 50-kHz commutation frequency was used for the appropriated real-time operation of the shunt APF.

The control strategy in phase coordinates has been developed avoiding the transformation between different frameworks. In this control strategy and for the work presented in this thesis, the sliding window DFT for the extraction of the fundamental component of the source voltage has been used, which provides a good behavior of the method, taking full advantage from the Matlab/Simulink and its embedded functions supported by RTWT.

After the shunt APF is in operation; effective harmonic distortion mitigation in the source currents has been achieved, and as they are balanced, the neutral current is practically null. The THD of the source currents has been reduced on average 43% and 22%, respectively, for both scenarios of the nonlinear load represented in the analysis.

The APF compensation ensures the mitigation of the harmonic content in the source currents at all times despite the harmonic content present in the source currents, thus maintaining the THD on average close to 1%. This final value of THD is due to the ripple current inherent to the APF injection currents. In addition, the reactive power compensation has been conveniently achieved since the source currents have been placed in phase with the source voltages at fundamental frequency.

In the control algorithm to determine the reference filtering currents, developed in Chapter 2, it has been used the reference signal voltages expressed in equations (2.9)-(2.11) to develop the formulation for calculating the reference filtering currents. These reference signal voltages achieve well their purpose as a reference and simplify the formulae needed for the calculation of the reference filtering currents, providing as well a low computational effort demand. Nevertheless, for the case of compensation in non-stiff systems, e.g. electric systems with phase/unbalance at fundamental frequency in the source voltages, it is recommendable the use of the positive sequence of the source voltages at fundamental frequency as the reference signal voltages. By including the positive sequence source voltages at fundamental frequency as the reference voltages, the reactive power compensation would be conveniently achieved. Even though, by obtaining the positive sequence the amount of computational effort demand needed for the control algorithm will

be increased. Similar results obtained with the strategy control to derive the reference injection currents and the real-time application are reported in [Medina-Rios and Ramos-Carranza 2007], [Ramos-Carranza *et al*. 2008].

Finally, we can conclude that based on the results observed through the case studies, until now, the control strategy to derive the reference filtering currents has proved to have an affordable computational demand under an emulation environment of a digital signal processor. The next step to ensure that the control strategy will work in a practical implementation will be a Hardware-in-the-loop simulation. In this way, the control algorithm will be directly implemented in the actual digital signal processor, and the electric system could be simulated by a personal computer.

Chapter 4. Shunt Compensation of Nonlinear Loads in Electric Systems

4.1 Introduction

This Chapter examines the use of shunt filtering techniques such as shunt APF and shunt hybrid filter (SHF), to mitigate harmonic distortion and to compensate reactive power.

A major drawback of APFs is their high rating, e.g. up to 80% of the nonlinear load in some practical applications [Singh *et al*. 2005], [Fuchs and Mosoum 2008]; and the problems emerge when they become a costly solution to harmonics mitigation and reactive power compensation. The economic concerns and other problems such as insulation, and series or parallel connection of switches associated with the high rating of APFs have derived to propose different structures of hybrid filters that have evolved as a cost-effective solution for the compensation of nonlinear loads [Singh *et al*. 2005], [Fuchs and Mosoum 2008], [Akagi *et al*. 2003].

In Addition, in actual shunt APF applications it is known that a path should be provided to drain the high frequency ripple current associated to the nonlinear nature of the inverter and the control current modulation technique. In general, a LC ripple-filter [Akagi *et al*. 2003] or a compensator-passive filter structure is designed for this particular purpose is required [Gosh and Ledwich 2003].

The aim of this chapter is to illustrate the usefulness of combining together the advantages of both, shunt active and passive filtering techniques, as well as to provide the details of the control design to be applied. Under the scheme presented in this investigation; the shunt APF performs harmonic current mitigation, and a shunt passive element is placed to compensate reactive power (this reduces the APF kVA rating) and to provide a path to drain the high frequency ripple current.

For this shunt hybrid filter scheme, a Linear Quadratic Regulator (LQR) switching controller scheme, based on that proposed in [Gosh and Ledwich 2003], is designed and implemented. This switching controller scheme allows an effective operation of the shunt hybrid filter, maintaining the source currents balanced and free of harmonic distortion after compensation; the compensation of reactive power is achieved with the passive element.

In addition, the ripple current is drained through the passive element, thus avoiding undesired ripple current associated effects, such as resonance phenomenon and harmonic voltage contamination in the voltages at the PCC, as it will be shown in the following sections.

4.2 Shunt Filtering Performance in Electric Systems

In this section the shunt APF filter and shunt hybrid filter compensation schemes are analyzed in a weak power system. The harmonic voltage contamination at the PCC, for the case of shunt active filter compensation, and the resonance phenomenon, for the case of shunt hybrid filter compensation, are illustrated.

4.2.1 Shunt Active Power Filter.

The shunt APF compensation scheme for a three-phase four-wire electric system is illustrated in Figure 4.1. In this system an unbalanced linear load in parallel with a nonlinear load are supplied by a balanced voltage source.

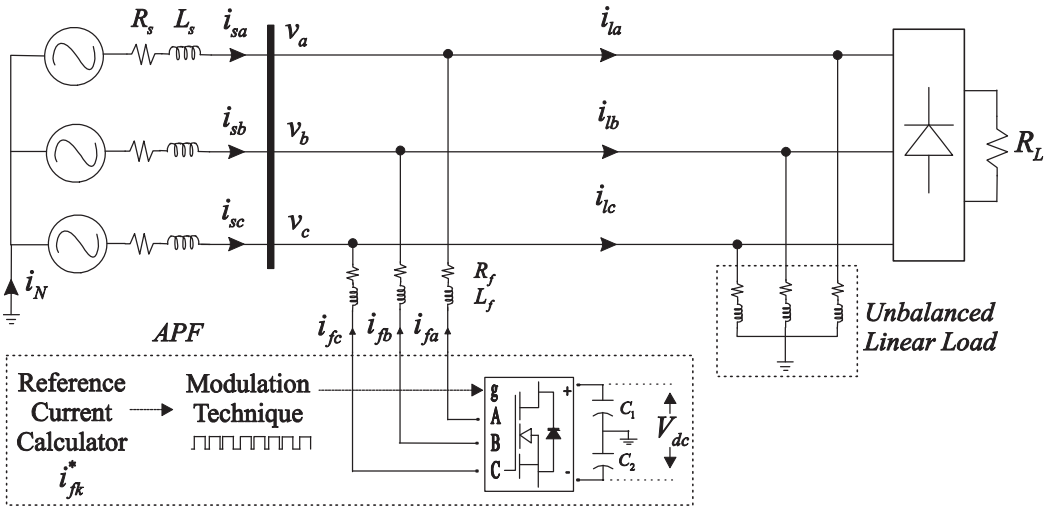

Figure 4.1 Shunt APF compensation scheme in a 3P3W electric system.

The nonlinear load is a 9.41 KVA, 6-pulse diode rectifier and the linear load is a series resistance-inductance branch per phase; Table 4.1 shows the system parameters. Once the

reference currents are calculated using the control strategy described in Chapter 2, they are inputted to a hysteresis-band current controller to generate the control signals of the VSI and to generate the actual filtering current to be injected into the electric system by the APF.

Table 4.1 Circuit Parameters

v_k	Supply phase voltage	176.77V
L_S	Source inductance	0.1mH
R_s	Source resistance	0.0015Ω
L_f	Energy link inductance	2mH
R_f	Energy link resistance	0.1Ω
R_L	Rectifier load resistance	100Ω
R_a	Load resistance at phase *a*	15.4Ω
R_b	Load resistance at phase *b*	15.4Ω
R_c	Load resistance at phase *c*	7Ω
L_a	Load inductance at phase *a*	11.5mH
L_b	Load inductance at phase *b*	15.4mH
L_c	Load inductance at phase *c*	23.5mH
C_1, C_2	*DC* capacitors	1000μF, V_{dc} = 1000V

The electric system in Figure 4.1 was implemented in Matlab/Simulink® and the results obtained from the simulation are illustrated in Figure 4.2. The load voltages v_k are shown in Figure 4.2(a); it can be noticed that the voltages are harmonic contaminated as soon as

the APF goes into operation at one cycle of simulation. The total harmonic distortion THD_v of the voltages at phases *a, b, c* at the time of the shunt APF compensation is on average 10%, beyond the imposed limit in Std. IEEE-519. This harmonic contamination of the load voltages will cause current distortion in any other load that may be connected at its terminal bus, as it can be observed from Figure 4.2(b). These currents, i_{lk} , are distorted/unbalanced and harmonic ripple contaminated.

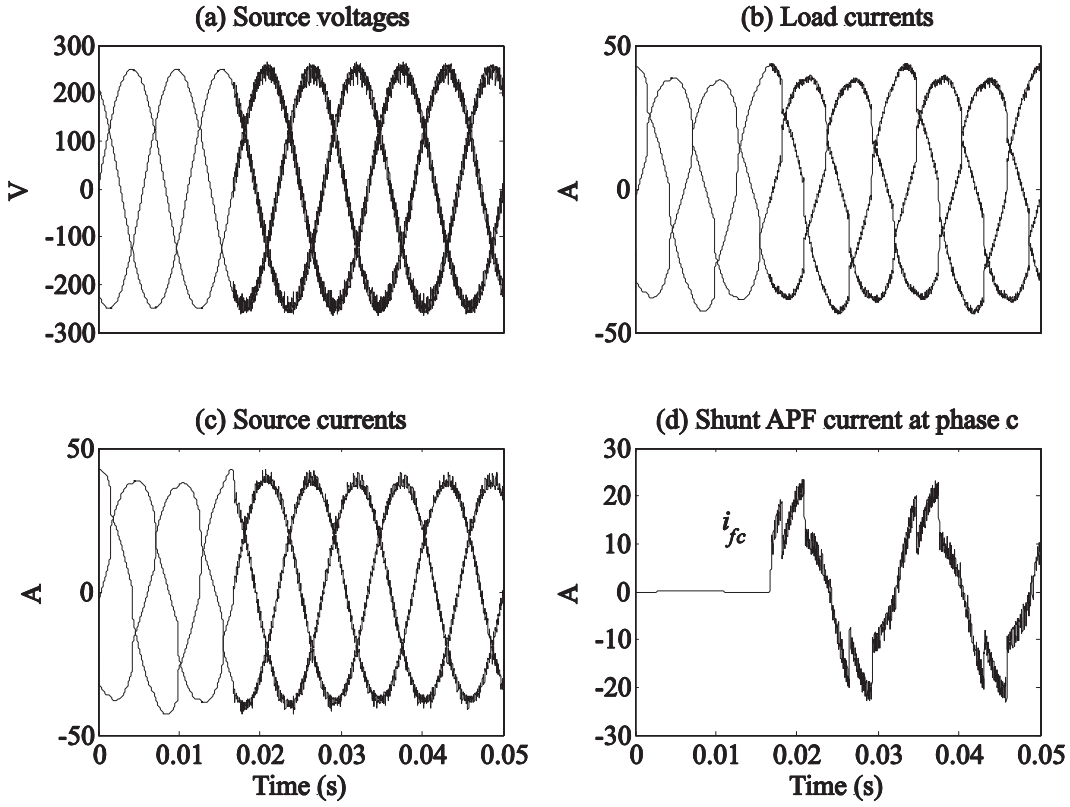

Figure 4.2 Results of the shunt APF compensation. (a) Source voltages, (b) Load currents, (c) Source currents and (d) Shunt APF current at phase *c*

The source currents i_{sk} are shown in Figure 4.2(c). It can be noticed that those are balanced, as soon as the APF goes into operation. The harmonic current cancellation by the APF is well identified by observing the current waveforms. The total harmonic distortion THD_{i_s} of the source currents, before the shunt APF compensation is on average 8.8%; and

after the compensation the value of THD_{i_s} has been reduced to 6.5%. The resulting THD_{i_s} after the shunt APF compensation is due the ripple current. The current injected by the shunt APF in phase *c* is shown in Figure 4.2(d).

Figure 4.3 shows the power flows during the shunt APF compensation. When the APF is placed to perform reactive power compensation, the shunt APF has the capability to inject a controlled three-phase reactive current component at fundamental frequency, in order to deliver the reactive power required by the load. After this process, the source currents are placed in phase with the load voltages at fundamental frequency. This injection of reactive current component at fundamental frequency increases the *rms* filtering current, therefore, increasing the necessary APF KVA rating to compensate both harmonic currents and reactive power. The three-phase *rms* filtering current was observed to be 14.49A, giving an APF KVA rating of 4.43KVA, which for practical applications can be a costly solution.

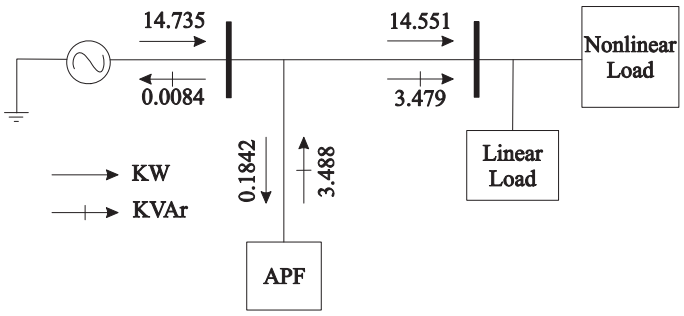

Figure 4.3 Power flow during the shunt APF compensation.

At this stage, it is clear that conventional reactive power compensation, e.g. using a capacitor bank, may be useful in the reduction of the necessary APF KVA rating, so that with the inclusion of the capacitor bank the compensation of harmonic currents and reactive power is separately achieved by the shunt APF and the shunt capacitor bank, respectively.

4.2.2 Shunt Hybrid Filter

The hybrid filter structure studied in this research work consists of a shunt APF, and a capacitor bank acting as a reactive power compensator, as shown in Figure 4.4. The APF is designed to perform harmonic cancelation; however, reactive power is not included in its compensation mechanism. Therefore, under this compensation scheme, the APF sees the

capacitor bank as an added load component using i_{lk}, see Figure 4.4, for the calculation of the reference filtering currents, as it was implemented in the previous subsection.

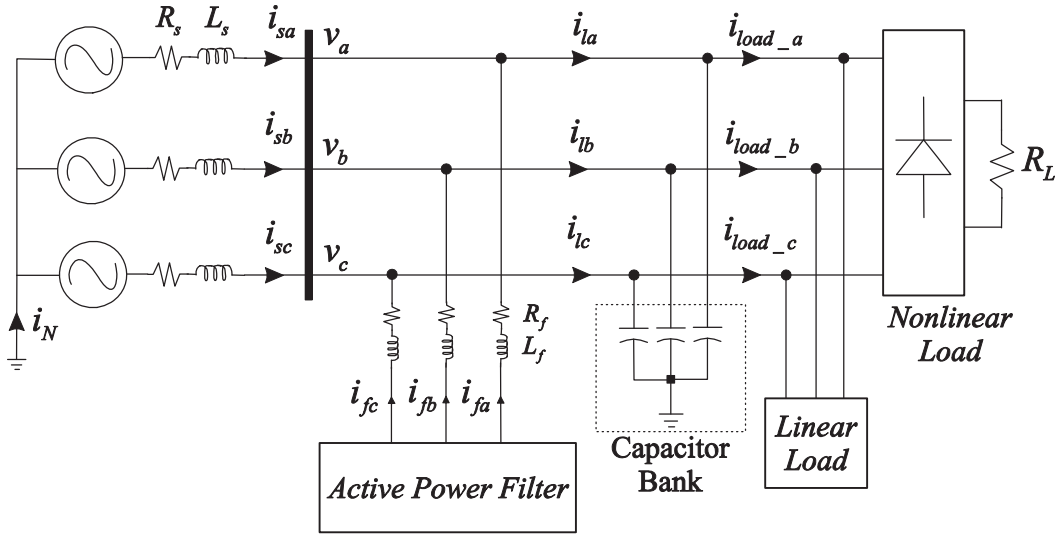

Figure 4.4 Shunt hybrid filter compensation scheme.

The capacitor bank in Figure 4.4 is placed to supply the three-phase reactive power $Q_{3\phi} = 3.479\,\text{KVAr}$, consumed by the load, see Figure 4.3.

The capacitor reactance and capacitance are calculated as [Acha and Madrigal 2001],

$$X_{C_f} = \frac{V_{LL}^2}{Q_{3\phi}} \tag{4.1}$$

$$C_f = \frac{1}{\omega X_{C_f}} \tag{4.2}$$

where X_{C_f} is the capacitive reactance, V_{LL} is the line-to-line *rms* voltage, and C_f is the capacitance per phase. To achieve reactive power compensation, the capacitance of the capacitor bank per phase was found to be $C_f = 99.30\,\mu\text{F}$.

The system of Figure 4.4 was implemented in Matlab/Simulink and the simulation results are shown in Figure 4.5. Figure 4.5(a) shows the voltages at the PCC once the shunt APF is switched on at one cycle of simulation. It can be noticed that discordant waveforms appear. This situation may be caused by a resonance condition produced by the harmonic interaction of the shunt APF, the capacitor bank and the load. Consequently, the same situation is presented in the source currents shown in Figure 4.5(b).

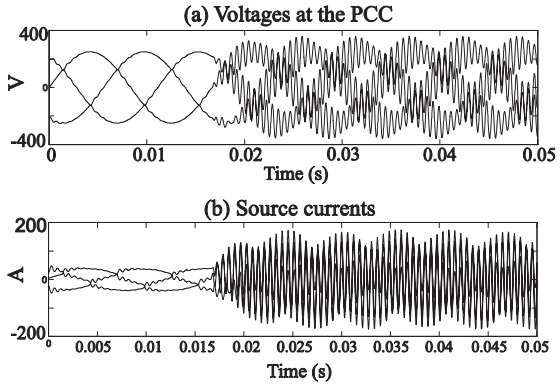

Figure 4.5 SHF compensation in a weak system using hysteresis band current controller.

In order to identify the possible resonance problem illustrated in Figure 4.5, a frequency scan analysis is performed with the equivalent circuit of the electric system for phase *a* shown in Figure 4.6, where the linear load impedance is also included in the analysis.

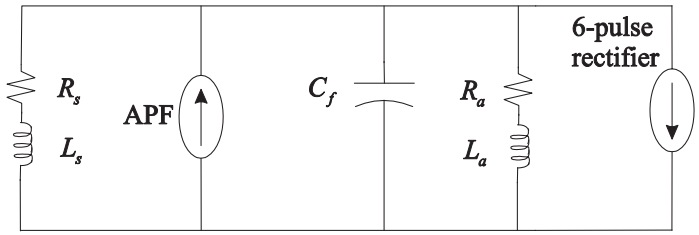

Figure 4.6 Equivalent circuit for parallel resonance analysis.

The source impedance and load data are the same given in Table 4.1 and the equivalent impedance of the circuit at any harmonic order *h* is given by,

$$Z_a = \frac{1}{\left(1/\left(R_s + jh\omega L_s\right)\right) + \left(1/\left(R_a + jh\omega L_a\right)\right) + \left(1/\left(-j\dfrac{1}{h\omega C_f}\right)\right)} \tag{4.3}$$

The response of the equivalent impedance $|Z_a|$ at harmonic frequencies is illustrated in Figure 4.7(a); similar results were obtained for phases *b* and *c*. It can be seen that there is a strong parallel resonant frequency taking place at the 27th harmonic.

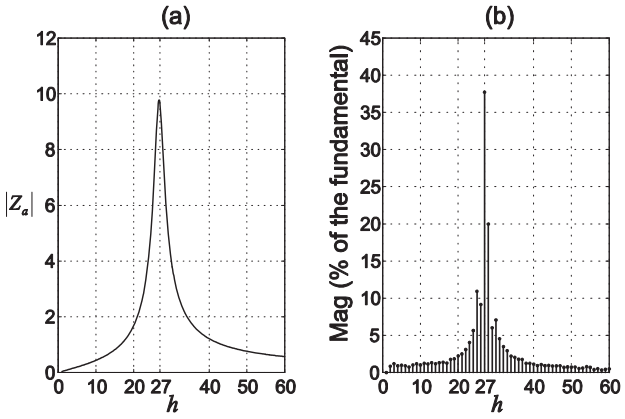

Figure 4.7 Resonance analysis. (a) Driving point impedance at phase *a*, (b) Harmonic content of voltage at the PCC for phase *a*.

The resonance peak in Figure 4.7, mainly occurs by the addition of the capacitor bank, and it is excited by the ripple current inherent to the APF currents. On the other hand, consistent information with the above observation is obtained from the harmonic spectrum of the load voltage for phase *a* illustrated in Figure 4.7(b); it shows that the harmonic magnitude for any frequency is, in general, higher as get closer to the harmonic resonance identified in Figure 4.7(a).

Though there are many approaches for reference filtering currents calculation, for theoretical purposes, they are presented without including a high-pass filter for the harmonic ripple current. It is obvious that in the control strategy the path to drain this high

frequency ripple current should be included in order to avoid undesirable effects associated with the parallel resonance phenomenon observed above.

4.3 Shunt Hybrid Filter Control for Compensation in Weak Systems

When an active filter is considered to provide compensation in practical applications, a high-pass passive filter should be considered in order to drain the high frequency current, e.g. ripple current, produced by the transistors commutation action. This procedure is intended to avoid possible undesired effects that may be present in the electric system, such situations can be a parallel resonance and/or harmonic ripple contamination to the supply voltages [Akagi *et al* 2003].

4.3.1 LQR-Based Switching Controller

In this section, a LQR based switching controller is designed to generate the inverter control signals. This switching controller restricts the ripple current propagation into the power system by actually forcing the ripple current to follow a given path, e.g. through the shunt capacitor, thus, ensuring a correct performance of the shunt hybrid filter process. The LQR-based switching controller is finally incorporated as a fundamental part of the proposed control strategy for the shunt hybrid filter.

For the used LQR-based switching controller the optimum system control is based on minimizing the performance index of the form [Gosh and Ledwich 2003],

$$J = \int_0^\infty \left\{ \left(w - w_{ref} \right)^T Q \left(w - w_{ref} \right) + u^T R u \right\} dt \tag{4.4}$$

where w is the state vector and w_{ref} is the desired reference state vector, Q is a Hermitian matrix or a symmetric positive definite matrix. For this particular case, R is a scalar and sets a penalty on the maximum control action, u is the optimal control law and T is the transpose operator. The minimized cost function results in a feedback control, i.e.

$$u = -K \left(w - w_{ref} \right) \tag{4.5}$$

where the gain matrix K is obtained with the solution of the steady-state Ricatti equation [Gosh and Ledwich 2002], and the switching control is obtained from [Gosh and Ledwich 2002], [Gosh and Ledwich 2003],

$$u = -hys\left(K\left(w - w_{ref}\right)\right) \tag{4.6}$$

Where the *hys* function is defined as the hysteresis band current controller technique, e.g.,

$$\begin{aligned} &\text{if } K\left(w - w_{ref}\right) > \Delta_i / 2 \text{ then } hys\left(K\left(w - w_{ref}\right)\right) = 1 \\ &\text{else if } K\left(w - w_{ref}\right) < \Delta_i / 2 \text{ then } hys\left(K\left(w - w_{ref}\right)\right) = -1 \end{aligned} \tag{4.7}$$

This switching technique is called switching band tracking control in [Gosh and Ledwich 2002], and the selection of Δ_i determines the switching frequency while tracking the reference.

Figure 4.8 shows the equivalent circuit used for the time domain analysis of the SHF compensation scheme, where the nonlinear load is represented by a series *RL* equivalent load. The state vector x and the state-space equation are given in (4.8) and (4.9), respectively.

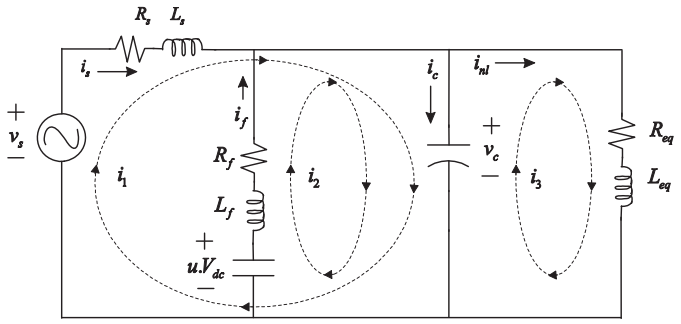

Figure 4.8 Equivalent circuit of the SHF compensation scheme used for the analysis in the time domain.

$$x = \begin{bmatrix} i_1 & i_2 & i_3 & v_c \end{bmatrix}^T \tag{4.8}$$

$$\dot{x} = \begin{bmatrix} -\frac{R_s}{L_s} & 0 & 0 & -\frac{1}{L_s} \\ 0 & -\frac{R_f}{L_f} & 0 & -\frac{1}{L_f} \\ 0 & 0 & -\frac{R_{eq}}{L_{eq}} & -\frac{1}{L_{eq}} \\ \frac{1}{C} & \frac{1}{C} & -\frac{1}{C} & 0 \end{bmatrix} x + \begin{bmatrix} \frac{1}{L_s} \\ 0 \\ 0 \\ 0 \end{bmatrix} v_s + \begin{bmatrix} 0 \\ \frac{V_{dc}}{L_f} \\ 0 \\ 0 \end{bmatrix} u \tag{4.9}$$

For convenience, the estate vector *x* can be transformed into a new state vector *w* which is expressed in terms of the variables of interest and/or control, e.g. i_f, i_c, i_{nl} and v_c. From Figure 4.8 the relationship between the state vector *x* of (4.8) and the new state vector *w* is observed; the state transformation is performed by using the transformation matrix *V* as given by (4.10). Then, the state equation (4.9) can be transformed into a new state equation having the form expressed in (4.11).

$$w = \begin{bmatrix} i_f \\ i_c \\ v_c \\ i_{nl} \end{bmatrix} = \begin{bmatrix} 0 & 1 & 0 & 0 \\ 1 & 1 & -1 & 0 \\ 0 & 0 & 0 & 1 \\ 0 & 0 & 1 & 0 \end{bmatrix} \begin{bmatrix} i_1 \\ i_2 \\ i_3 \\ v_c \end{bmatrix} \tag{4.10}$$

$$\dot{w} = VAV^{-1}w + VB_1v_s + VB_2u = \Lambda w + \Upsilon_1 v_s + \Upsilon_2 u \tag{4.11}$$

It is assumed that we have full control over *u* and that the switching control is based on a linear combination of multiple states [Gosh and Ledwich 2003]. Hence, for a calculated matrix of optimum feedback control *K*, the law (4.6) minimizes the performance index (4.4) subject to the constraint (4.11).

Figure 4.9 illustrates the control diagram of the active filter. It can be observed how the control strategy for the calculation of the reference currents and the LQR-based switching current controller are incorporated to complete the control strategy. Figure 4.10 shows the

flow chart of the LQR calculations to obtain the feedback gain matrix *K*. The low complexity in the implementation of the LQR switching current control, to generate the switching commands of the inverter, is similar to the hysteresis band current controller [Gosh and Ledwich 2002], which is widely used in active power filter applications.

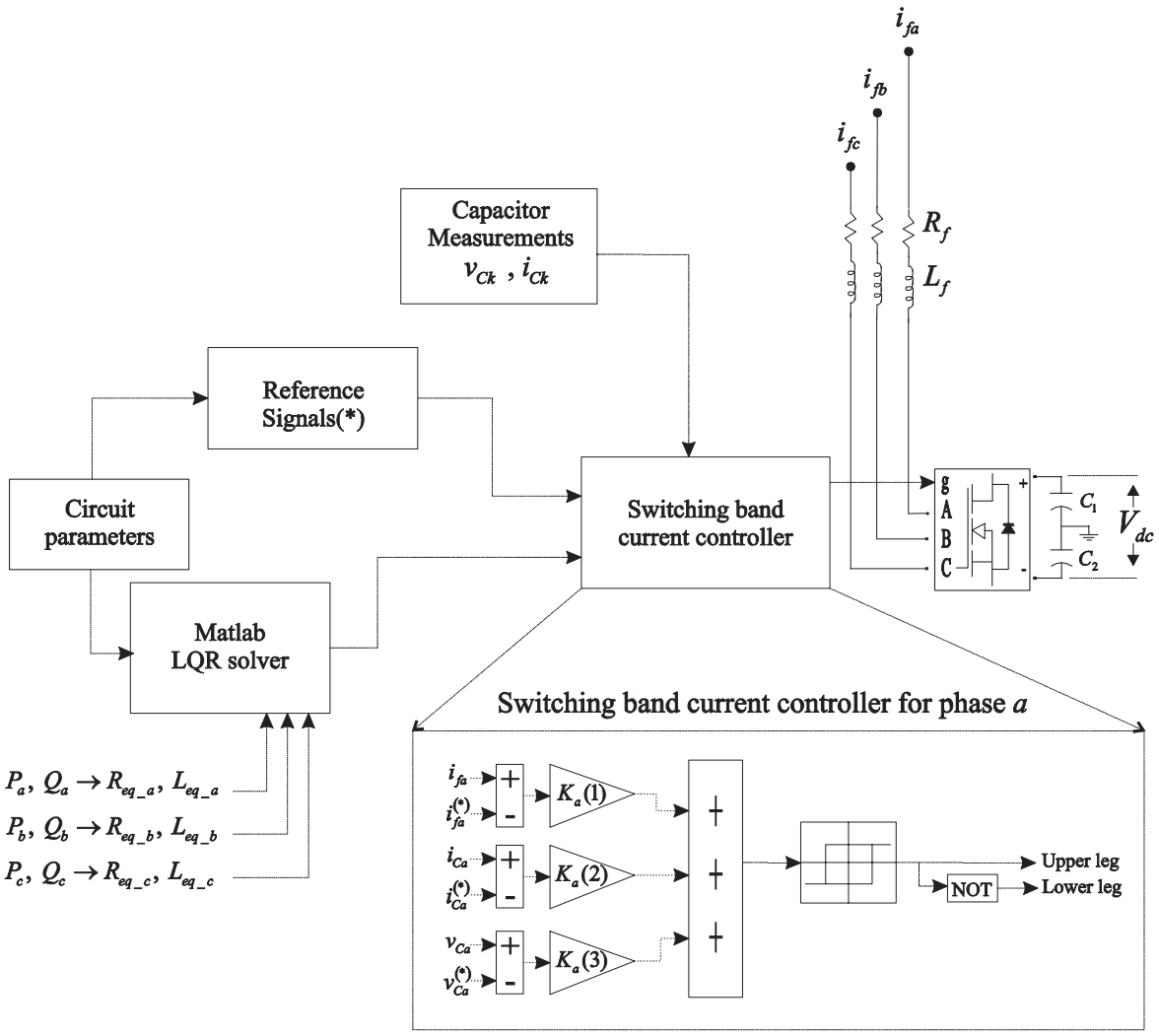

Figure 4. Control diagram of the Active Filter.

Figure 4.9 Control diagram of the shunt APF under SHF compensation scheme.

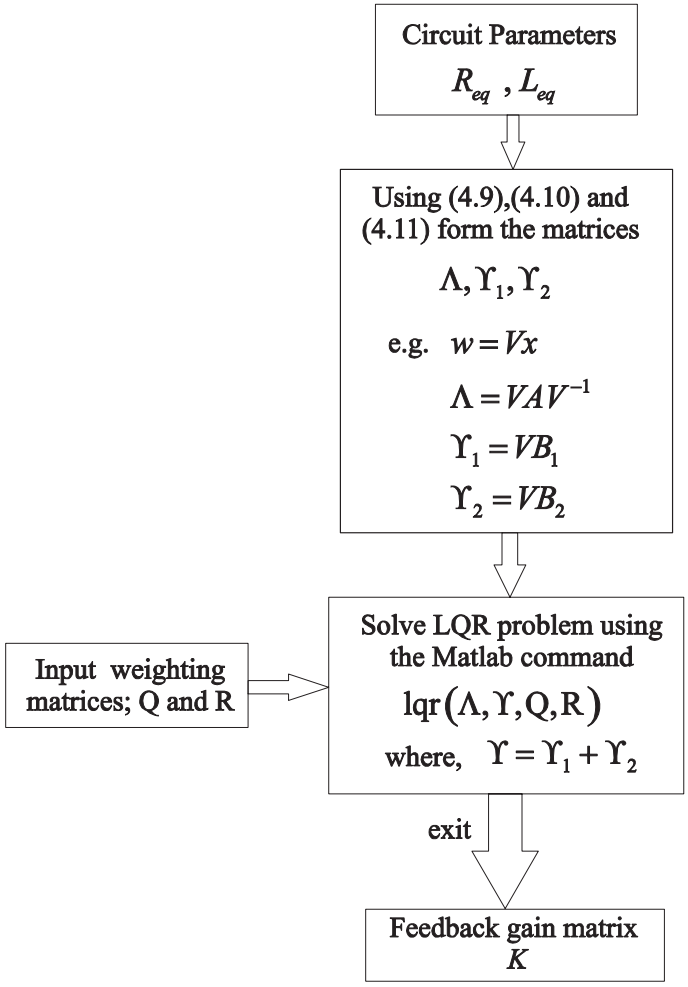

Figure 4.10 Flow chart of the LQR calculation feedback gain matrix.

The linear quadratic regulator method is a powerful technique for designing controllers for complex systems that have stringent performance requirements. The LQR method seeks to find the optimal controller that minimizes a given cost function. This cost function is parameterized by two matrices, *Q* and *R*, that weight the state vector and the system input, respectively. For most realistic applications, the LQR problem (4.11) is solved via a Computer Aided Design (CAD) package such as Matlab. The Matlab command $\mathrm{lqr}(\Lambda, \Upsilon, Q, R)$, with $\Upsilon = \Upsilon_1 + \Upsilon_2$, solves the LQR problem and the associated Ricatti equation, and it then calculates the matrix of optimum feedback control *K*. However, some difficulties may arise on determining how the matrices *Q* and *R* are chosen. Most of the

times the weighting matrix Q reflects the importance of the states to be controlled, and the selection of an appropriate value of R has to be chosen to provide the system control effort and to obtain a finite time convergence of the regulator [Gosh and Ledwich 2003]. To avoid the complexity of forming a reference for the load current, the gain matrix K is reduced to $K = \begin{bmatrix} K_1 & K_2 & K_3 & 0 \end{bmatrix}$; checking that this reduction of the state feedback results in shifting the closed-loop eigenvalues to the left of s, in order to maintain the system stable.

4.4 Case Study 4.1

The same electric system of Figure 4.4 and Table 4.1 is analyzed using the LQR-based switching technique. The weighting matrix to minimize the performance index of the LQR problem is $Q = diag\left(\begin{bmatrix} 25 & 10 & 3 & 0 \end{bmatrix}\right)$, where *diag* is a diagonal matrix, and $R = 0.01$. The reduced feedback gain matrices for each phase *a*, *b*, *c*, are calculated and given by,

$$K_a = \begin{bmatrix} 49.9468 & 9.3787 & 34.5637 \end{bmatrix}$$
$$K_b = \begin{bmatrix} 49.9460 & 9.3795 & 34.7046 \end{bmatrix}$$
$$K_c = \begin{bmatrix} 49.9450 & 9.3805 & 34.7665 \end{bmatrix}$$

4.4.1 Simulation Results

The results obtained from the simulation with Matlab/Simulink are shown in Figure 4.11. It can be observed that both load voltages, Figure 4.11(a), and source currents, Figure 4.11(b), become balanced and free of harmonics once the shunt APF goes into operation at one cycle of simulation, the resulting value of the THD_i is null, and the source currents are placed in phase with the load voltages, thus achieving a unit load power factor. As the high-frequency ripple current has been drained-out through the capacitor branch, it avoids the parallel-resonance effects shown in Figure 4.5, as well as there is no harmonic ripple contamination in the currents drawn by the load, as shown Figure 4.11(c). The shunt APF injected current in phase *c* is illustrated in Figure 4.11(d). It can be noticed that there is a reduction on the amount of necessary shunt current injection, in comparison to the case when only the shunt APF technique is applied, see Figure 4.2(d). The three-phase *rms* filtering current was 8.54A, giving an APF KVA rating of 2.61 KVA.

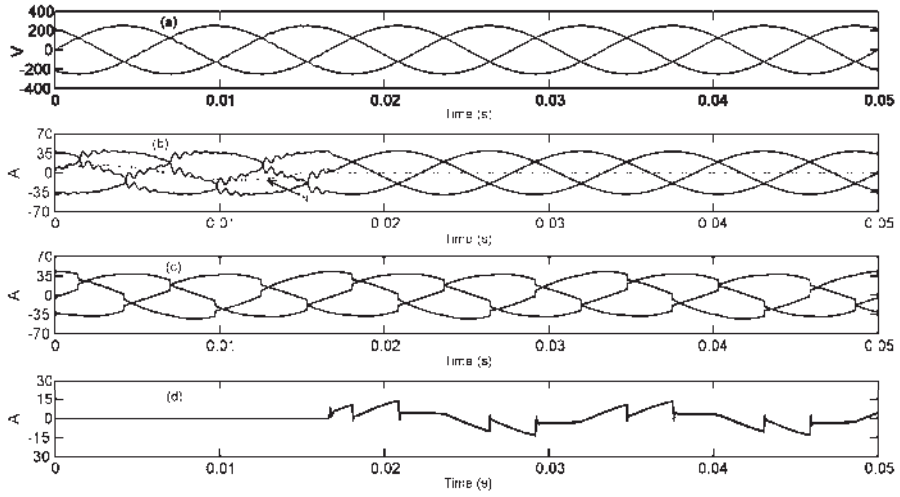

Figure 4.11 Results of the shunt hybrid filter compensation. (a) Load voltages, (b) Source currents, (c) Load currents and (d) Shunt APF current at phase *c*

It becomes clear that the reactive power compensation using the capacitor bank has reduced the necessary APF KVA rating by approximately 1.81KVA which represents a 41% reduction of the KVA rating of the APF, and obviously the reduction of the necessary APF KVA rating will depend on the amount of reactive power compensation achieved with the capacitor bank for each particular case.

The power flows during the shunt hybrid filter compensation are shown in Figure 4.12. It can be observed that the capacitor bank is supplying the reactive power consumed by the load, and as a consequence of a better tracking control over the filtering currents, the losses have been significantly reduced and the desired performance of the shunt hybrid filter has been achieved.

Under this compensation scheme, the sinusoidal voltages across the capacitor are the supplying voltages, thus allowing the better operation of the nonlinear load as observed in Figure 4.11(c). The currents through the capacitor are shown in Figure 4.13. It can be seen that the high-frequency ripple current has been drained-out thorough the capacitor as it was specified in the control design. The total harmonic distortion of the capacitor current was found to be $THD_i = 3.1\%$, barely increasing the *rms* current in about 1% of the fundamental component. The ripple current drained through the capacitor contains high frequency harmonics with relatively low amplitude; similar results will be expected for any

other particular case. Since both, the terminal capacitor voltage and the current through the capacitor were included in the state vector control *w*, this ensures that the voltage and current restrictions for the shunt power capacitor meet the restrictions imposed by IEEE-18 [IEEE-18 Std. 1992].

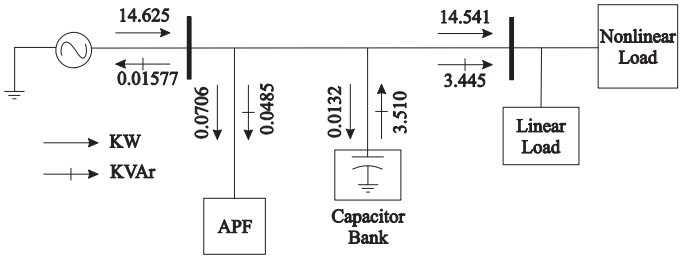

Figure 4.12 Power flow during SHF compensation using LQR switching technique.

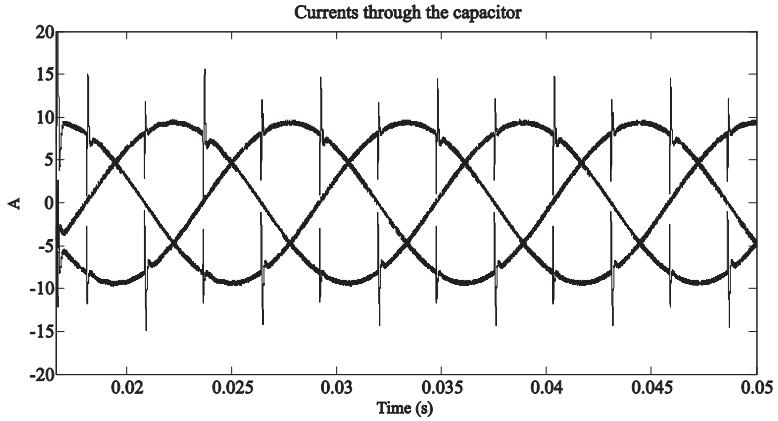

Figure 4.13 Capacitor current during shunt hybrid filter compensation.

4.5 Optimization Based Method for Shunt Hybrid Filter Compensation

The aim of this section is to present a shunt hybrid filter control algorithm able to obtain an optimal reduction in the APF rating and at the same time preserving, during the process, the main performance advantages of both, the shunt APF and the shunt capacitor compensation.

The main concept of the proposed steady-state control lies on a new control design for the SHF topology which includes the formulation of a nonlinear programming problem that is

solved to find the optimal injection currents of the APF that satisfy practical constraints such as harmonic limits, unbalance limits, minimum load power factor, as well as other constraints associated to the shunt capacitor such as current and voltage *rms* limits. The practical aspect of compensation applied in non-stiff systems is taken into account.

4.5.1 Proposed Control Strategy for the Derivation of the Optimal Reference Signals

The proposed control strategy for the SHF compensation consists of two main stages. The first stage provides the formulation theory of the nonlinear programming problem obtained from the analysis in the frequency domain of the equivalent circuit for the SHF compensation scheme, where all the constraints associated to the electric system operation limits and shunt APF performance are included. Since the proposed compensation scheme includes a shunt capacitor, to provide reactive power compensation, special care must be taken on the parallel resonance analysis of the system. The LQR based switching current control technique is also implemented.

4.5.1.1 Determining Optimal Shunt APF Reference Currents

The proposed control strategy for the shunt hybrid control is based on the requirements that the source currents and voltages at the PCC after compensation must be maintained sinusoidal and balanced or meet the current and voltage harmonic distortion limits imposed by Std. IEEE-519 [IEEE-519 1992], permissible levels of source current unbalance, as well as to meet permissible *rms* values of voltage and current of the shunt capacitor set by Std IEEE-18 [IEEE-18 1992], and to provide an acceptable load power factor. To satisfy these requirements, the formulation to obtain the reference currents of the shunt APF are determined from the analysis in the frequency domain of the equivalent circuit for the proposed scheme of shunt hybrid compensation shown in Figure 4.14, and solving the nonlinear programming problem formulated from this analysis.

In Figure 4.14 the source voltage V_S is supplying a nonlinear load I_{nl}, where the injection currents of the nonlinear load are assumed to be known, and the shunt hybrid filter is placed to control the mitigation of the harmonics of voltage and current, and to provide reactive power compensation.

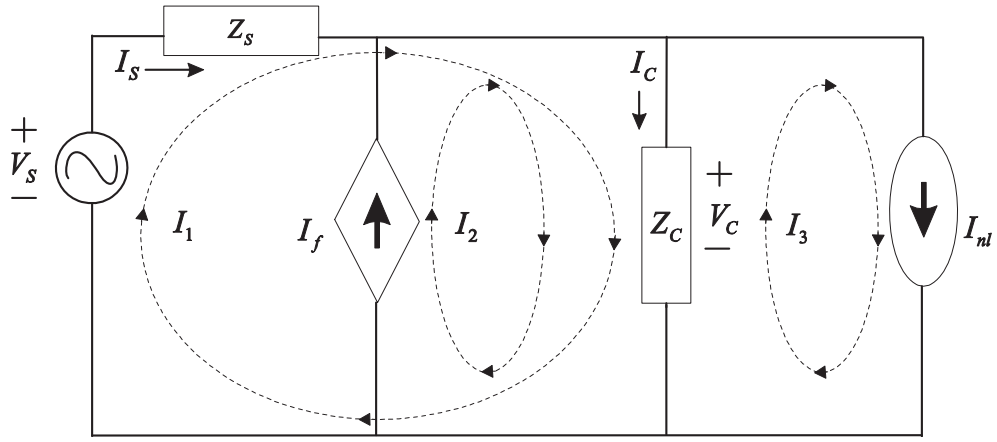

Figure 4.14 Equivalent circuit of the SHF compensation scheme used for the analysis in the frequency domain.

From the mesh analysis using the Kirchhoff's Voltage Law (KVL) gives

$$I_1^h = \frac{V_S^h}{Z_S^h + Z_C^h} + \frac{Z_C^h}{Z_S^h + Z_C^h}\left(I_3^h - I_2^h\right) \tag{4.12}$$

$$I_2^h = I_f^h \tag{4.13}$$

$$I_3^h = I_{nl}^h \tag{4.14}$$

where $Z_S^h = R_S + ihX_S$ is the system impedance, $Z_C^h = -iX_C / h$ is the impedance of the shunt capacitor, and h is the harmonic order. The reactance of the shunt capacitor per phase is calculated as

$$X_C = \frac{V_{LL}^2}{Q_C} \tag{4.15}$$

where V_{LL} is the *rms* line-to-line voltage and Q_C is the three-phase reactive power supplied to the system by the shunt capacitor. Thus, by substituting (4.13)-(4.14) into (4.12) and expressing the equation in rectangular form; the source current for the harmonic *h* at phase *k* is obtained as

$$I_{Sk}^{h}\left(I_{fk}^{h,r}, I_{fk}^{h,i}, X_C\right) = \frac{V_{Sk}^{h,r} + iV_{Sk}^{h,i}}{R_S + i\left(hX_S - \dfrac{X_C}{h}\right)} + \frac{Z_C^h}{Z_S^h + Z_C^h}\left(\left(I_{nlk}^{h,r} - I_{fk}^{h,r}\right) + i\left(I_{nlk}^{h,i} - I_{fk}^{h,i}\right)\right) \quad (4.16)$$

where $h \in H$, and H is the set of harmonics under consideration, k= *a, b, c*, and the superscripts *r* and *i* represents the real and imaginary components of the electrical system quantities. From Figure 4.14 the current through the shunt capacitor I_{Ck}^{h} and the voltage across the capacitor V_{Ck}^{h}, both for any harmonic order *h* at phase *k*, can be expressed as

$$I_{Ck}^{h} = \left(I_{Sk}^{h,r} + I_{fk}^{h,r} - I_{nlk}^{h,r}\right) + j\left(I_{Sk}^{h,i} + I_{fk}^{h,i} - I_{nlk}^{h,i}\right) \quad (4.17)$$

$$\begin{aligned} V_{Ck}^{h}\left(I_{fk}^{h,r}, I_{fk}^{h,i}, X_C\right) &= Z_C^h I_{Ck}^h \\ &= -I_{Ck}^{h,i} Z_C^h + iI_{Ck}^{h,r} Z_C^h \\ &= -\left(I_{Sk}^{h,i} + I_{fk}^{h,i} + I_{nlk}^{h,i}\right) Z_C^h + j\left(I_{Sk}^{h,r} + I_{fk}^{h,r} + I_{nlk}^{h,r}\right) Z_C^h \end{aligned} \quad (4.18)$$

By observing (4.16)-(4.18), the optimal control strategy for the SHF implies the determination of the real and imaginary components of the shunt APF currents $\left(I_{fk}^{h,r}, I_{fk}^{h,i}\right)$ for a given capacitor reactance X_C, appropriate to compensate reactive power, and henceforth, the desired source current for each harmonic order I_{Sk}^{h}, the current through the capacitor I_{Ck}^{h}, and the voltage at the capacitor terminals V_{Ck}^{h}, which meet the operation requirements of the electrical system imposed by the IEEE-519 and IEEE-18 standards. From Figure 4.4 and Figure 4.14 it is noticed that the voltage across the capacitor V_{Ck}^{h} is the voltage at the PCC. The constrained problem formulation of the SHF optimal control strategy is given below.

1) Individual Harmonic Distortion and Total Harmonic Distortion constraints

The individual harmonic distortion limits of the source current and voltage at the PCC after SHF compensation is defined as [IEEE-519 1992],

$$(IHD_I)_k^h = \frac{\left|I_{Sk}^h\right|}{\left|I_{Sk}^1\right|} \le \alpha_I^h \qquad h \in H, \quad h \ne 1 \tag{4.19}$$

$$\left(IHD_V\right)_k^h = \frac{\left|V_{Ck}^h\right|}{\left|V_{Ck}^1\right|} = \alpha_V \qquad h \in H, \quad h \ne 1 \tag{4.20}$$

In (4.19) and (4.20), α_I^h and α_V are the imposed individual harmonic distortion limits of the source current and voltage at the PCC, respectively, by the IEEE-519 harmonic standard. The total harmonic distortion limits of the source current and voltage at the PCC are defined as [IEEE-519 1992]

$$\left(THD_I\right)_k = \sqrt{\frac{\sum_{h \in H}\left|I_{Sk}^h\right|^2}{\left|I_{Sk}^1\right|^2}} \le \beta_I \tag{4.21}$$

$$\left(THD_V\right)_k = \sqrt{\frac{\sum_{h \in H}\left|V_{Ck}^h\right|^2}{\left|V_{Ck}^1\right|^2}} \le \beta_V \tag{4.22}$$

Similarly, in (4.21) and (4.22), β_I and β_V are the imposed total harmonic distortion limits of the source current and voltage at the PCC, respectively, by the IEEE-519 harmonic standard.

2) Source Current Imbalance Limits

In a three-phase four-wire system the neutral current after SHF compensation must be restricted to an acceptable level. In terms of the source sequence components the following sequence harmonic relationships can be defined as

$$U^{h,(0)} = \frac{\left|I_S^{h,(0)}\right|}{\left|I_S^{h,(+)}\right|} \le \gamma^0 \qquad h \in H \tag{4.23}$$

$$U^{h,(-)} = \frac{\left|I_S^{h,(-)}\right|}{\left|I_S^{h,(+)}\right|} \le \gamma^- \qquad h \in H \tag{4.24}$$

where γ^0 and γ^- are unbalance limits for negative and zero sequence components of source currents. $\left|I_S^{h,(0)}\right|$, $\left|I_S^{h,(+)}\right|$ and $\left|I_S^{h,(-)}\right|$ are determined by the symmetrical components transformation, as given in (4.25)-(4.27), for each harmonic order.

$$I_S^{h,(0)} = 1/3\left(I_{Sa}^h + I_{Sb}^h + I_{Sc}^h\right) \tag{4.25}$$

$$I_S^{h,(+)} = 1/3\left(I_{Sa}^h + aI_{Sb}^h + a^2 I_{Sc}^h\right) \tag{4.26}$$

$$I_S^{h,(-)} = 1/3\left(I_{Sa}^h + a^2 I_{Sb}^h + aI_{Sc}^h\right) \tag{4.27}$$

where $a = e^{j2h\pi/3}$ and +, –, and 0 represent the positive-, negative-, and zero-sequence components, respectively.

3) Load Power Factor

The constraint imposed on the load power factor can be enforced to be not less than a lower bound $\underline{\lambda}$,

$$\frac{P_L}{V_{C,rms} I_{S,rms}} \geq \underline{\lambda} \tag{4.28}$$

where P_L is the total active power consumed by the load, $V_{C,rms}$ is the three-phase *rms* voltage at the PCC, $I_{S,rms}$ is the three-phase *rms* source currents, as defined in (4.29), (4.30) and (4.31) respectively.

$$P_L = \sum_{k\in K}\sum_{h\in K} real\left(V_{Ck}^{h}\, conj\left(I_{nlk}^{h}\right)\right) = \sum_{k\in K}\sum_{h\in H}\left(V_{Ck}^{h,r} I_{nlk}^{h,r} + V_{Ck}^{h,i} I_{nlk}^{h,i}\right) \tag{4.29}$$

$$V_{C,rms} = \sqrt{\sum_{h\in H}\sum_{k\in K}\left|V_{Ck}^{h}\right|^2} \tag{4.30}$$

$$I_{S,rms} = \sqrt{\sum_{h\in H}\sum_{k\in K}\left|I_{Sk}^{h}\right|^2} \tag{4.31}$$

4) Reactive Power Compensation

The reactive power compensation constraint is referred to the fundamental frequency only, as recommended by IEEE-519 standard. In this sense, after SHF compensation the relation in (4.32) must hold

$$Q_F + Q_C = Q_L \tag{4.32}$$

where Q_F is the reactive power supplied by the shunt APF, and Q_L is the reactive power consumed by the load. In terms of the currents I_{fk}^{1}, I_{Ck}^{1} and I_{nlk}^{1}, Eq. (4.32) can be expressed as,

$$\sum_{k\in K}\left(V_{Ck}^{1,r}\left(-I_{fk}^{1,i}+I_{Ck}^{1,i}+I_{nlk}^{1,i}\right)+V_{Ck}^{1,i}\left(I_{fk}^{1,r}-I_{Ck}^{1,r}-I_{nlk}^{1,r}\right)\right)=0 \tag{4.33}$$

5) Shunt APF Active Power Consumption

It is required that the shunt APF does not consume/supply any active power before and after the SHF compensation. That is,

$$\begin{aligned} P_F &= \sum_{k\in K}\sum_{h\in K} real\left(V_{Ck}^{h}.\left(I_{fk}^{h}\right)^{*}\right)=0 \\ &= \sum_{k\in K}\sum_{h\in H}\left(V_{Ck}^{h,r}I_{fk}^{h,r}+V_{Ck}^{h,i}I_{fk}^{h,i}\right)=0 \end{aligned} \tag{4.34}$$

6) Capacitor Harmonic Constraints

The installation of any capacitor at the design or operating stages should also include harmonic and power quality analyses. If the capacitor contains voltage and current harmonics, then appropriate constraints for *rms* voltage $V_{C,rms}$, *rms* current $I_{C,rms}$, and the reactive power Q_C must be satisfied, as indicated by IEEE-18 [IEEE-18 1992], and these are given as,

$$\frac{V_{C,rms}}{V_{C,rms}^{1}}\le 1.10 \tag{4.35}$$

$$\frac{I_{C,rms}}{I_{C,rms}^{1}}\le 1.80 \tag{4.36}$$

$$\frac{Q_C\big|_{h\in H}}{Q_C}\le 1.35 \tag{4.37}$$

where $V_{C,rms}^{1}$ and $I_{C,rms}^{1}$ are the three-phase *rms* values of the shunt capacitor evaluated at fundamental frequency, and $I_{C,rms}$ is the three-phase *rms* current through the capacitor given by,

$$I_{C,rms} = \sqrt{\sum_{h\in H}\sum_{k\in K}\left|I_{Ck}^{h}\right|^{2}} \tag{4.38}$$

and $Q_C\big|_{h\in H}$ is calculated as,

$$\begin{aligned} Q_C\big|_{h\in H} &= \sum_{k\in K}\sum_{h\in K} imag\left(V_{Ck}^{h}\, conj\left(I_{nlk}^{h}\right)\right) \\ &= \sum_{h\in H}\sum_{k\in K}\left(-V_{Ck}^{h,r} I_{Ck}^{h,i} + V_{Ck}^{h,i} I_{Ck}^{h,r}\right) \end{aligned} \tag{4.39}$$

7) Objective Function

The performance index to be minimized is the injection current of the shunt APF, e.g.

$$f_{obj} = I_{f,rms} \tag{4.40}$$

where $I_{f,rms}$ is given as,

$$I_{f,rms} = \sqrt{\sum_{h\in H}\sum_{k\in K}\left|I_{fk}^{h}\right|^{2}} \tag{4.41}$$

Recapitulating, the constrained optimization problem (4.19)-(4.41) for determining the optimal injection currents at each phase for any harmonic order $\left(I_{fk}^{h,r}, I_{fk}^{h,i}\right)$ considers a given set of permissible harmonic and unbalanced limits. It is noted from (4.16)-(4.18) that all the associated constraints to the optimization problem are function of the injection

currents and the reactance of the shunt capacitor. The constrained optimization problem is summarized as follows,

$$
\begin{aligned}
&\text{Min} \quad f_{obj} \\
&\text{s.t.} \\
&\quad \left(IHD_I\right)^h \le \alpha_I^h \qquad h \in H, \quad h \ne 1, \\
&\quad \left(IHD_V\right) \le \alpha_V \qquad h \in H, \quad h \ne 1, \\
&\quad \left(THD_I\right)_k \le \beta_I \qquad k \in K \\
&\quad \left(THD_V\right)_k \le \beta_V \qquad k \in K \\
&\quad U^{h,(0)} \le \gamma^0 \qquad h \in H \\
&\quad U^{h,(-)} \le \gamma^- \qquad h \in H \\
&\quad \frac{P_L}{V_{C,rms} I_{S,rms}} \ge \underline{\lambda} \\
&\quad \frac{V_{C,rms}}{V_{C,rms}^1} \le 1.10 \\
&\quad \frac{I_{C,rms}}{I_{C,rms}^1} \le 1.80 \\
&\quad \frac{Q_C\big|_{h \in H}}{Q_C} \le 1.35 \\
&\quad \sum_{k \in K} \left(V_{Ck}^{1,r} \left(-I_{fk}^{1,i} + I_{Ck}^{1,i} + I_{nlk}^{1,i} \right) + V_{Ck}^{1,i} \left(I_{fk}^{1,r} - I_{Ck}^{1,r} - I_{nlk}^{1,r} \right) \right) = 0 \\
&\quad \sum_{k \in K} \sum_{h \in H} \left(V_{Ck}^{h,r} I_{fk}^{h,r} + V_{Ck}^{h,i} I_{fk}^{h,i} \right) = 0
\end{aligned}
\tag{4.42}
$$

4.6 Case Study 4.2

The designed case study has the purpose of showing the usefulness and efficiency of the proposed optimal SHB control strategy. Because the Matlab/Simulink provides full capabilities for obtaining the solution of the optimization problems (4.42) and (4.11), and the simulation of the SHF compensation, these are adopted as the simulation tools to perform the case study. The advantage of adopting the optimization toolbox of Matlab is that it can be used in combination with Simulink, providing an integrated simulation environment where the SHF compensation scheme is built with computational efficiency and solution accuracy. The formulated problem (4.42) is a nonlinear constrained

optimization problem, and its performance index and the associated constraints are highly nonlinear, among several efficient routines for solving different types of optimization algorithms, available in the optimization toolbox of Matlab [MathWorks Inc. 1999], the solution method of Sequential Quadratic Programming [Nocedal 1999] is used to obtain the optimal solution for the optimization problem (4.42). The weighting matrices, to minimize the performance index of the switching control technique used in the experiment were Q=*diag*[30, 400, 0, 0] and R=0.01. The reduced feedback gain matrix obtained after solving the LQR problem and used in the experiment for all phases was $K = \begin{bmatrix} 171.7 & 486.2 & 197.4 \end{bmatrix}$.

Figure 4 illustrates the control diagram of the active filter. It can be observed how the nonlinear programming problem and the LQR-based switching current controller are incorporated to complete the control strategy.

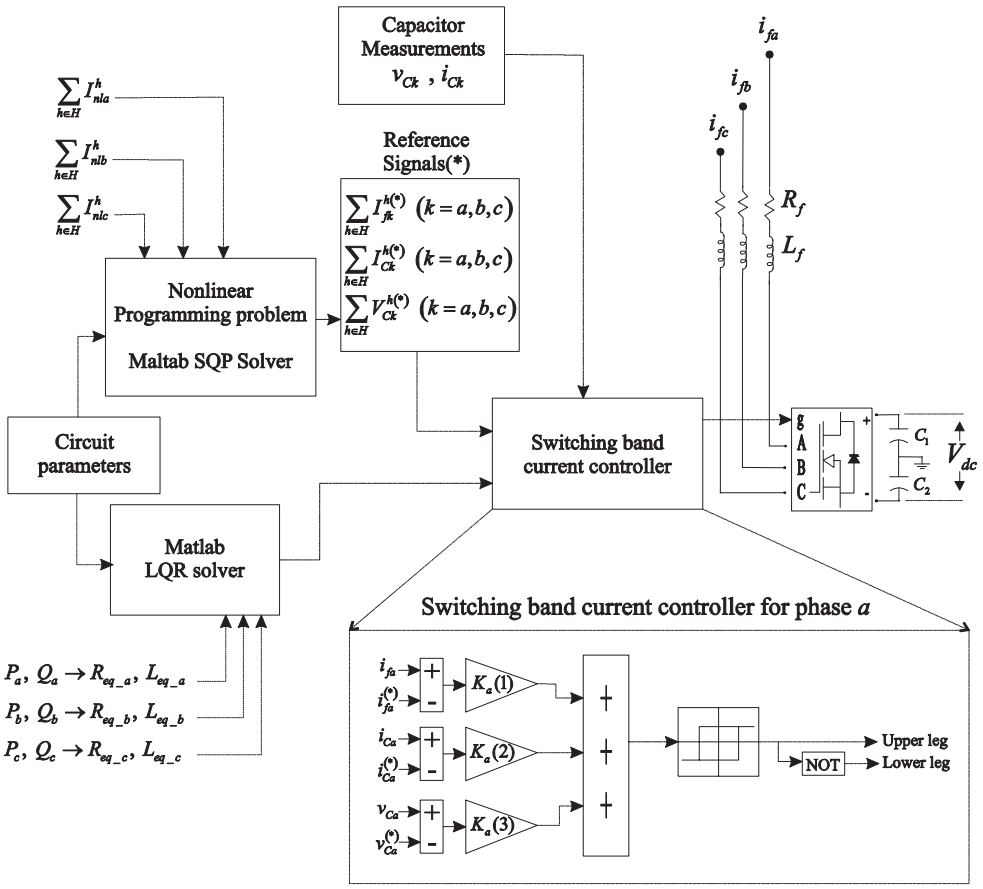

Figure 4.15 Control diagram for the optimal APF under SHF compensation.

4.6.1 Simulation Results

The case study consists of an unbalanced linear load in parallel with a nonlinear load, supplied by a balanced voltage source as shown in Figure 4.4. The nonlinear load is a 6-pulse diode rectifier and the linear load is a series resistance-inductance branch per phase. Table 4.2 shows the system parameters.

Figure 4.16 shows the distorted waveforms of voltage at the PCC and source current without compensation, where the total harmonic distortion indices are on average $THD_I = 13.5\%$ and $THD_V = 5.1\%$. The three-phase reactive power consumed by the load was 2.065 kVAr.

Table 4.2 Circuit parameter for case study 4.2.

v_S	Supply phase voltage	120V
L_S	Source inductance	0.55mH
R_S	Source resistance	0.0083Ω
L_f	Energy link inductance	2mH
R_f	Energy link resistance	0.1Ω
R_L	Rectifier load resistance	20Ω
R_a	Load resistance at phase *a*	15.4Ω
R_b	Load resistance at phase *b*	15.4Ω
R_c	Load resistance at phase *c*	7Ω
L_a	Load inductance at phase *a*	11.5mH
L_b	Load inductance at phase *b*	15.4mH
L_c	Load inductance at phase *c*	23.5mH
C_1, C_2	*DC* capacitors	500μF, $V_{dc} = 600$V

Due to the discrete size nature of capacitor banks, the three-phase reactive power supplied to the system by the shunt capacitor was considered to be $Q_C = 2$ kVAr, so that the reactance of the shunt capacitor per phase was found to be $X_C = 21.6\Omega$, which was substituted in (4.16)-(4.18) to solve the nonlinear programming problem (4.42). The optimization problem has been solved by considering partial and full compensation.

The limits imposed for partial compensation are those recommended by Std. IEEE-519, for a short-circuit ratio of 20< R_{SC} <50, and Std. IEEE-18; harmonics distortion limits $\beta_V = 5\%$, $\beta_I = 8\%$, $\alpha_V = 3\%$, $\alpha_I^h = 7\%,\ 3.5\%,\ 2.5\%,$ and 1% for h<11, $11 \le h \le 17$, $17 \le h \le 23$ and $23 \le h \le 35$, respectively, with unbalance limits $\gamma^0 = 5\%$ and $\gamma^- = 5\%$. Other constraint limits associated to shunt capacitor are as given in (4.35)-(4.37); and the lower bound of the load power factor for both scenarios is $\underline{\lambda} = 0.9$. In order to provide good accuracy on the representation of the nonlinear load currents, the highest order harmonic taken under consideration is h=31. The current of the nonlinear load I_{nlk}^h and the APF current injections I_{fk}^h obtained with the solution of the optimization problem for partial and full compensation are summarized in Table 4.3.

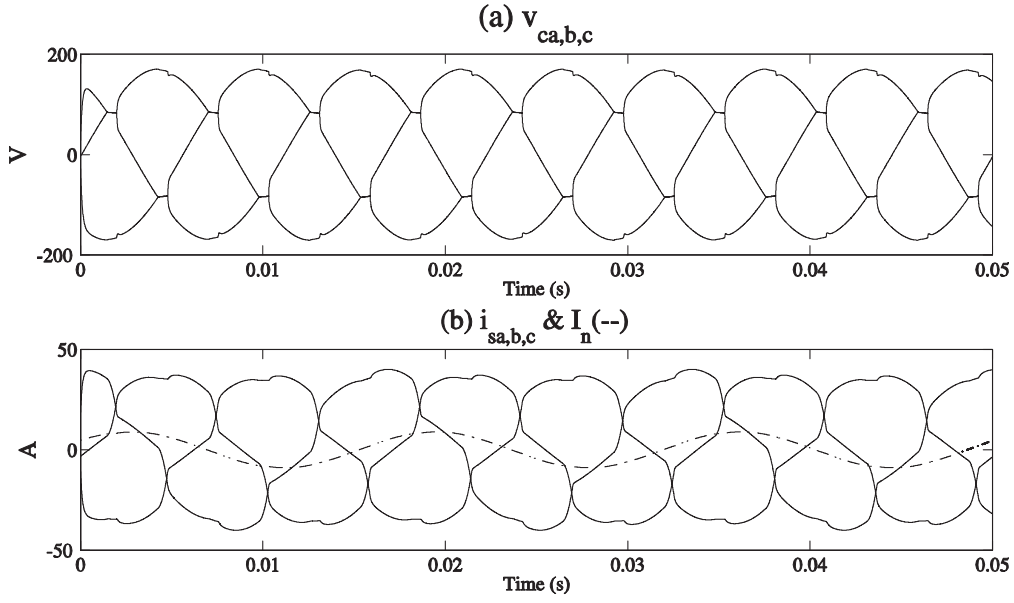

Figure 4.16 Electric circuit conditions for the case study 4.2, (a) Voltages at the PCC, (b) Source current and neutral current without compensation.

The result of the optimal SHF compensation for both scenarios, partial and full compensation, is shown from Figure 4.17 to Figure 4.20. Figure 4.17(a) illustrates the voltages at the PCC considering partial compensation, and Figure 4.17(b) for full compensation. The source currents and neutral current are shown in Figure 4.17(c) for partial compensation and, Figure 4.17(d) for full compensation. These results are consistent with the expected performance of the SHF compensation.

For the case of the partial compensation scenario, the harmonic distortion indices for voltage at the PCC and source current illustrated in Figure 4.17(a) and Figure 4.17(b), respectively, properly meet the imposed limits by Std. IEEE-519; the corresponding APF injection currents are given in Table 4.3.

Table 4.3 Optimal APF currents considering partial and full compensation obtained with Matlab

		Phase a (A) (peak values)	*Phase b* (A) (peak values)	*Phase c* (A) (peak values)
I_{nl}^{1}		$38.8\angle -9.9°$	$38.0\angle -131.9°$	$39.8\angle 97.3°$
I_{f}^{1}	Part	$0.8\angle 51.3°$	$0.5\angle 18.0°$	$2.1\angle 24.7°$
	Full	$3.3\angle 75.3°$	$2\angle -25.4°$	$5.6\angle 22.9°$
I_{nl}^{5}		$4.4\angle 135.4°$	$4.4\angle -104.7°$	$4.5\angle 16.0°$
I_{f}^{5}	Part	$2.4\angle 135.3°$	$2.4\angle -104.8°$	$2.5\angle 15.9°$
	Full	$4.4\angle 135.4°$	$4.4\angle -104.7°$	$4.5\angle 16.0°$
I_{nl}^{7}		$2\angle 104.9°$	$2\angle -15.9°$	$2\angle -135.1°$
I_{f}^{7}	Part	$1.3\angle 104.9°$	$1.4\angle -16.1°$	$1.3\angle -135.2°$
	Full	$2\angle 104.9°$	$2\angle -15.9°$	$2\angle -135.1°$
I_{nl}^{11}		$1.5\angle -105.7°$	$1.5\angle 13.1°$	$1.6\angle 133.9°$
I_{f}^{11}	Part	$1.5\angle -105.6°$	$1.5\angle 13.2°$	$1.5\angle 134.0°$
	Full	$1.5\angle -105.7°$	$1.5\angle 13.1°$	$1.6\angle 133.9°$

I_{nl}^{13}		$0.9\angle -130.8°$	$0.9\angle 106.7°$	$0.9\angle -11.9°$
I_{f}^{13}	Part	$0.6\angle -130.5°$	$0.6\angle 106.9°$	$0.5\angle -11.6°$
	Full	$0.9\angle -130.8°$	$0.9\angle 106.7°$	$0.9\angle -11.9°$
I_{nl}^{17}		$0.7\angle 10.2°$	$0.8\angle 128.2°$	$0.8\angle -110.4°$
I_{f}^{17}	Part	$0.1\angle 11.2°$	$0.1\angle 129.2°$	$0.1\angle -109.7°$
	Full	$0.7\angle 10.2°$	$0.8\angle 128.1°$	$0.8\angle -110.4°$
I_{nl}^{19}		$0.5\angle -7.1°$	$0.5\angle -131.1°$	$0.5\angle 111.4°$
I_{f}^{19}	Part	$0.04\angle -5.7°$	$0.04\angle -129.5°$	$0.04\angle 112.9°$
	Full	$0.5\angle -7.1°$	$0.5\angle -131.1°$	$0.5\angle 111.4°$
I_{nl}^{23}		$0.4\angle 121.0°$	$0.4\angle -121.8°$	$0.4\angle 0.1°$
I_{f}^{23}	Part	$0.01\angle 125.0°$	$0.01\angle -118.8°$	$0.01\angle 2.2°$
	Full	$0.4\angle 121.0°$	$0.4\angle -121.8°$	$0.4\angle 0.1°$
I_{nl}^{25}		$0.3\angle 113.2°$	$0.3\angle -12.1°$	$0.2\angle -127.9°$
I_{f}^{25}	Part	$0.006\angle 118.8°$	$0.006\angle -10.4°$	$0.004\angle -123.3°$
	Full	$0.3\angle 113.2°$	$0.3\angle -12.1°$	$0.2\angle -127.9°$
I_{nl}^{29}		$0.2\angle -137.8°$	$0.2\angle -21.1°$	$0.2\angle 101.6°$
I_{f}^{29}	Part	$0.002\angle -147.2°$	$0.002\angle -4.5°$	$0.003\angle 113.6°$
	Full	$0.2\angle -137.8°$	$0.2\angle -21.1°$	$0.2\angle 101.6°$
I_{nl}^{31}		$0.1\angle -135.5°$	$0.1\angle 97.8°$	$0.1\angle -15.6°$
I_{f}^{31}	Part	$0.003\angle -99.9°$	$0.003\angle 34.8°$	$0.002\angle 104.9°$
	Full	$0.1\angle -135.5°$	$0.1\angle 97.8°$	$0.1\angle -15.6°$

For the full compensation scenario, the voltages at the PCC and the source currents illustrated in Figure 4.17(b) and Figure 4.17(d), respectively, are balanced and free of harmonic distortion.

As observed from Table 4.3, the APF injection current I_{fk}^{h} equals the injection current of the nonlinear load for any h>1, which agrees with equation (4.16), if it is desired to completely eliminate the harmonic distortion. For h=1 the phase current injection I_{fk}^{1} of the APF, observed in Table 4.3, corresponds to only the compensation of reactive power and current unbalance.

Figure 4.17(e) shows the currents through the capacitor for partial compensation, and Figure 4.17(f) for full compensation. The shunt capacitor yielding reactive power compensation also provides the path to drain the ripple current inherent to the shunt APF injection currents.

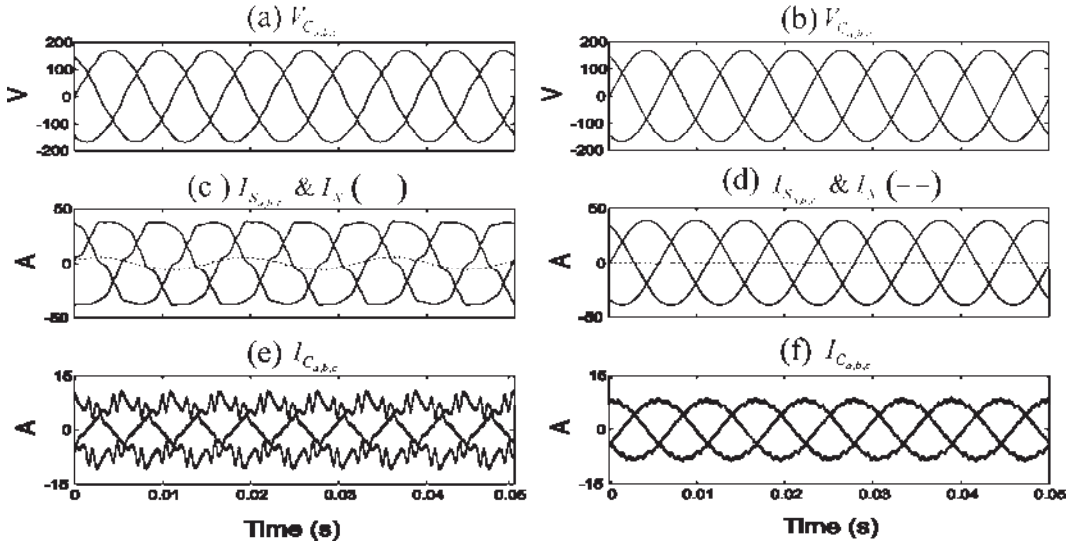

Figure 4.17 Simulink simulation results for optimal SHF compensation. (a) Voltages at the PCC with partial compensation, (b) Voltages at the PCC with full compensation, (c) Source currents and neutral current with partial compensation, (d) Source currents and neutral current with full compensation, (e) Currents through the shunt capacitor with partial compensation, (f) Currents through the shunt capacitor with full compensation. Figures in (a), (b), (c), and (d) have the same time scale on x axis as for (e) and (f).

The LQR switching technique, in particular designed for the proposed SHF topology, satisfies the stringent performance requirements of the system, allowing the correct performance of the SHF process by forcing the ripple current to be drained out through the

capacitor. This technique also prevents possible parallel resonance phenomenon, which for this case, it is clearly not present despite the resonant frequency of the system at 610Hz (h=10.3), which is very close to a characteristic harmonic present in the nonlinear load current spectrum at h=11. The driving point phase impedance is illustrated in Figure 4.18.

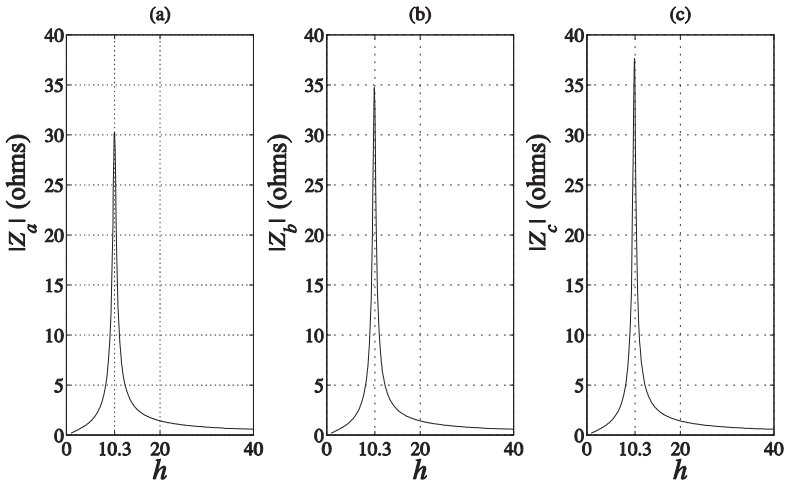

Figure 4.18 Driving point impedance. (a) Phase *a*, (b) Phase *b*, (c) Phase *c*.

Table 4.4 summarizes the constraints output of the nonlinear programming problem for both compensation scenarios. For partial compensation the inequality constraints $\left(THD_V\right)_k$ are under the limit $\beta_V = 5\%$, and the inequality constraints of $\left(THD_I\right)_k$ are active at the imposed limit $\beta_I = 8\%$. For both compensation scenarios null APF active power consumption/supplying P_F can be observed, which results in $P_S = P_L$, in other words, the active power is only supplied from the source. Besides, for both compensation scenarios, as a result of the equality constraint (21), $Q_F + Q_C = Q_L$, the reactive power compensation from the source Q_S is null, and the reactive power Q_F from the APF only provides a refined adjustment to efficiently achieve reactive power compensation, and satisfies its mathematical constraint. The load power factor is close to or equal to unit load power factor above the selected lower bound, e.g. $\lambda \geq 0.9$. Capacitor associated constraints are also given; these constraints are under safety operation limits of the shunt capacitor as

recommended by Std. IEEE-18. It is observed that for partial compensation f_{obj} is significantly reduced in about 47%, compared with the full compensation scenario.

The APF kVA rating is calculated with the three-phase *rms* voltage at the PCC and the three-phase *rms* APF injection current, e.g. f_{obj}, as given in (4.43).

$$APF_{rating} = I_{f,rms} V_{C,rms} \tag{4.43}$$

Therefore, the resulting APF kVA rating for partial compensation scenario (0.872 kVA) is reduced by almost half of the size of the APF kVA necessary rating when the full compensation scenario (1.663 kVA) is considered.

Table 4.4 Matlab Simulation summary for partial and full compensation.

	Without Comp.	Partial Comp.	Full Comp.		Without Comp.	Partial Comp	Full Comp
$(THD_I)_a$	13.46%	8.00%	0.0%	$(THD_V)_a$	4.98%	2.41%	0.0%
$(THD_I)_b$	13.36%	8.00%	0.0%	$(THD_V)_b$	5.02%	2.41%	0.0%
$(THD_I)_c$	13.35%	8.00%	0.0%	$(THD_V)_c$	5.12%	2.41%	0.0%
f_{obj} (A)	---	4.207	8.024	λ	0.97	0.99	1
P_L (kW)	9.534	9.602	9.602	Q_L (VAr)	2065	2084.0	2087.2
P_S (kW)	9.534	9.602	9.602	Q_S (VAr)	2065	0.000	0.000
P_F (kW)	---	0.000	0.000	Q_F (VAr)	---	95.720	98.94
$Q\|_{h\in H}/Q_C$	---	1.005	1	Q_C (VAr)	---	1988.3	1988.3
$\frac{V_{C,rms}}{V^1_{C,rms}}$	---	1.0003	1	$\frac{I_{C,rms}}{I^1_{C,rms}}$	---	1.0292	1

Finally, the harmonic content of the source currents and voltages at the PCC are illustrated in Figure 4.19 and Figure 4.20, respectively. From Figure 4.19 it is observed that only the inequality constraints associated to the $\left(IHD_I\right)^5$ of the source currents at the fifth harmonic are active at $\alpha_I^{h<11} = 7\%$ for the case of partial compensation; for the full compensation case all the harmonic content has been fully removed. On the other hand, from Figure 4.20 it is observed that the IHD_V of the source voltage at the PCC is under the imposed limit $\alpha_V = 3\%$ for partial compensation and completely removed for full compensation. In particular, the percent of decrease of THD is for both cases, on average 100% and 60% for current and 100% and 47% for voltage considering full and partial compensation, respectively.

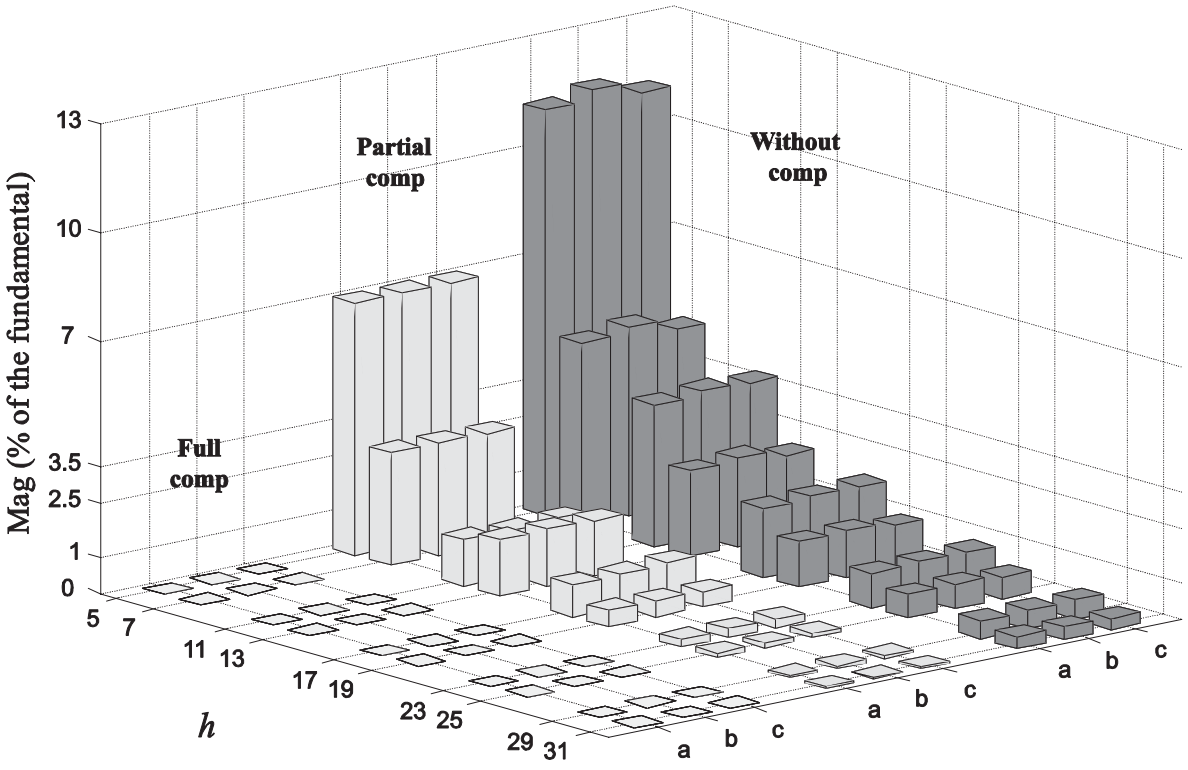

Figure 4.19 Harmonic content of the source currents for case study 4.2.

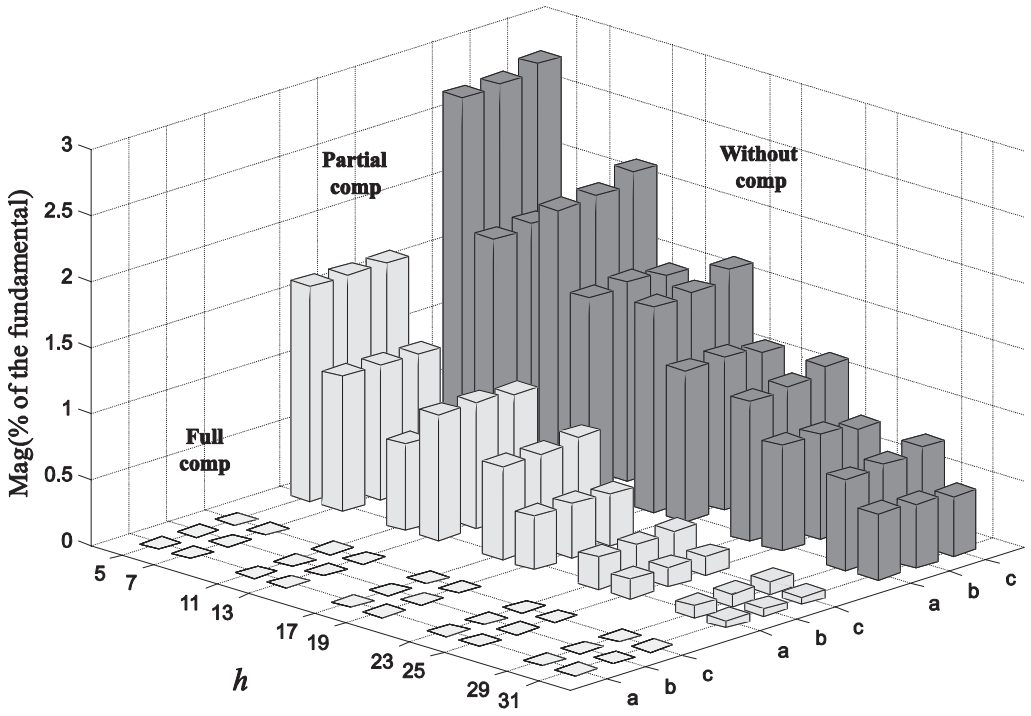

Figure 4.20 Harmonic content of the voltages at the PCC for case study 4.2.

By way of complementation to the results presented in this case study, in the Simulink experiment the capacitors C_1 and C_2 of Figure 4.4 are used for energy storage, and even though the capacitors instantaneous voltage slightly fluctuates due to harmonics, they must maintain a constant *dc* voltage V_{dc} at the inverter terminals. The losses produced by switching and capacitor voltage variations must be supplied by the source, thus a power loss signal, controlled via a PI controller, is added to the fundamental component of the source currents I_{sk}^1. The addition of the power loss component in the source currents at fundamental frequency, causes that for the case of partial compensation the harmonic distortion indices decrease just a bit below those reported in Table 4.4. For instance, the harmonic distortion indices of the source current and voltage at the PCC in the simulation were found to be on average $THD_I = 7.8\%$ and $THD_V = 2.3\%$, respectively.

4.7 Conclusions

The formulation and control of a proposed steady-state method for the optimal SHF compensation have been described in detail. According to the reported simulation results, it has been found that the proposed method is suitable for effective harmonic control

mitigation and reactive power compensation providing optimal injection currents of the APF reducing the APF KVA rating.

The harmonic control mitigation under the proposed SHF compensation scheme is able to handle two scenarios of compensation:
1. Full compensation. The harmonic distortion of voltage and current are completely removed from the voltage and current waveforms, the percentage of harmonic distortion reduction for this compensation scheme is 100%. The control strategy of Chapter 2 is also providing this level of performance.
2. Partial compensation. The harmonic distortion of voltage and current and other constraints associated to the shunt capacitor are forced to meet permissible/safety operation levels imposed by Std. IEEE-519 and Std. IEEE-18. In particular, for the presented case study II, given the short circuit ratio of the system and proper characteristics of the nonlinear load, the percent of decrease in terms of the harmonic index THD is close to 50%.
For both compensation scenarios the proposed optimization-based theory ensures the null APF active power consumption/supplying. Besides, the reactive power supplied from the source is null, and provides a load power factor close to unity in both cases. Similar results are reported in [Ramos-Carranza and Medina 2010].
Practical aspects such as non-ideal supply voltages and draining of the ripple current inherent to the APF injection currents have been also taken into consideration in the analysis, formulation and solution of the proposed method. The designed LQR switching technique for this particular scheme of compensation prevents possible parallel resonance effects and has allowed the correct performance of the proposed SHF process, by including stringent performance requirements on the switching controller to generate the inverter control signals. In this way, the propagation into the electric system of the ripple current, inherent to the APF injection current, has been restricted to a given path (e.g., to be drained out through the shunt capacitor), thus allowing the correct performance of the hybrid filtering process. This control action also avoids the harmonic ripple contamination of the source voltages at the PCC.

Once the LQR algorithm is solved, and the feedback matrices obtained, the implementation would proceed with no further calculations of the LQR algorithm, unless the circuit conditions are changed. If this is the case not only the LQR algorithm would need to be recalculated but also the nonlinear programming problem needs to be again solved. At this stage of research, the theory of the proposed control strategy has been designed to work as a steady state control technique. Future work will focus on the search of be able to handle dynamic compensation.

Chapter 5. Active Power Line Conditioner Planning for Harmonic Distortion Control in Distribution Power Systems

5.1 Introduction

Harmonic distortion is increasing in distribution power systems due to the proliferation of nonlinear distorting loads, such as adjustable speed drives and rectifiers. To correct this quality problem the Active Power Line Conditioner (APLC), has demonstrated to be an appropriated tool for holding harmonic distortion indices in the power system within the recommended guidelines [Grady *et al* 1992a], [Chang *et al*. 1994], [Grady *et al*. 1992b], [Grady *et al*. 1991], [Hong and Chang 1996], [Fuchs and Mosoum 2008]. The APLC is a type of Active Power Filter (APF); a converter-based compensation device designed to improve the harmonic distortion of the entire power system by injecting corrective harmonic currents at selected (sensitive) buses. Their placement, sizing, and their injection currents are usually determined by using an optimization-based approach.

Different authors have proposed different alternatives about the necessary number of APLC units to reduce the harmonic distortion levels to the required quality of the electric system, as specified by IEEE-519 [IEEE-519 1992]. In [Chang *et al*. 1994], a single APLC is used (and sufficient) to achieve acceptable harmonic distortion indices in the electric network. On the other hand, arguing the severity of a high harmonic pollution in the power system and a restriction on the maximum permissible rating (maximum affordable size) of the APLC unit. It has been proposed [Hong and Chang 1996] that multiple APLC units are necessary to mitigate the harmonic distortion below recommended limits. Even though it is clear that both viewpoints are valid, at some point it is important to clarify some situations. In the case of a single unit APLC planning; is it equally convenient to inject the correction harmonic currents, for each different harmonic h, from the same (selected) node of connection? Moreover, for the case of multiple APLC planning; how convenient is to afford the control algorithm for all the APLC units, for all the harmonics, at the same time?

In this chapter, a methodology is developed that takes into account both situations mentioned above on the decision making of APLC planning to mitigate harmonic distortion in the power system, maintaining the harmonic distortion indices of voltage below permissible levels imposed by the IEEE-519 Standard [IEEE-519 1992].

Foremost it is proposed to use a Single-Harmonic Active Power Line Conditioner (SHAPLC), a variant of the traditional APLC, which in this case only injects a single harmonic current. The intended goal at this stage is to mitigate the Individual Harmonic Distortion (IHD) index at all buses of the distribution power system for a given harmonic *h*. To do so, it is necessary to establish which nodes of the power system are feasible nodes to achieve this purpose, for each harmonic *h*. Once the feasible nodes are properly identified, with a sensitivity analysis, the "best" candidate node for the location of the SHAPLC is determined. This procedure would be repeated for each harmonic frequency of interest. Then, to complete the SHAPLC planning, a feasibility analysis is conducted for determining if the multiple SHAPLCs are able to provide also a reduction of the Total Harmonic Distortion (THD) of voltage, for all nodes of the power system, under the recommended limits.

Since for each one of the SHAPLCs it is only required to determine a single harmonic current to be injected into the electric system as a corrective measure, the aim is to present a methodology that uses multiple (necessary number) SHAPLCs with low computational effort on the control algorithm, which also ensures that the harmonic distortion indices IHD and THD meet the recommended Standard guidelines.

The total number of SHAPLC could be limited to the number of harmonic frequencies for which the recommendation for the IHD index is violated, at any of the buses of the electric network, according with recommended Standards. In this way, the total number of SHAPLCs is justified by the need of compensate the harmonic distortion in the power system at harmonic frequencies for which their presence in the power system is dominant. Finally, the size of the SHAPLCs will be optimally obtained, by solving a nonlinear programming problem that minimizes the injections currents of the SHAPLCs for the corrective measure.

5.2 Statement and Formulation of the Problem

For a given electric power system under analysis containing nonlinear loads, and where its harmonic distortion indices are beyond recommendable levels, the Active Power Line Conditioners (APLCs) have shown to be a useful tool to mitigate voltage harmonic distortion in a network by injecting corrective-harmonic currents [Grady *et. al*. 1991], [Grady *et. al*. 1992]; the main idea is to control the harmonic distortion of the electric network below permissible levels. The main stages of APLC planning are for determining their sizing, placement, and their injection currents. In order to be able to achieve that purpose, an optimization-based methodology is presented in this section. We assume that

the system harmonic impedances are known, as well as all the bus voltage harmonics, and we also assume that there is no coupling between harmonics.

Conventionally, the APLC is placed to compensate the harmonic voltage magnitudes at different harmonic frequencies in the network. Here, a Single-Harmonic Active Power Line Conditioner (SHAPLC) is presented as a complete concept for controlling the harmonic distortion indices, IHD and THD. Though a previous concept of harmonic mitigation for the single harmonic problem was presented in [Chang *et al*. 1994], the procedure was not finally intended assure that the levels of THD satisfy Standard requirements, while on the other hand, their placement is chosen by proving the algorithm for all buses.

There are two main stages during the development of the proposed methodology:

First, it is necessary to determine the number and location of SHAPLCs to ensure that the reduction of the levels of the harmonic indices, IHD and THD, is able to meet the requirements of the Standard IEEE-519.

Second, once we have the number and placement of SHAPLCs needed for harmonic distortion mitigation of the network, it is necessary to determine the injection corrective-harmonic currents of the SHAPLCs. This procedure will also result in an automatic determination of the optimal sizing of the SHAPLCs.

5.2.1 Harmonic Propagation Due to the SHAPLC Injection Current and the IHD Index

The SHAPLC injection current should mitigate the voltage magnitudes for harmonic *h* throughout the network. The change in the nodal harmonic voltage can be expressed as

$$V_{n,new}^{h} = V_{n,old}^{h} + \Delta V_{n}^{h} \tag{5.1}$$

where the subscripts *old* and *new* correspond to bus voltages at bus *n* before and after SHAPLC injection current, and superscript *h* refers to harmonic *h*. In terms of the elements of the network impedance matrix, the voltage change at bus *n* due to SHAPLC injection current at bus *p* can be expressed as

$$\Delta V_{n}^{k} = Z_{np}^{k} I_{p}^{k} \tag{5.2}$$

Where n=1, 2…,N, and where Z^h_{np} is the harmonic transfer impedance between buses n and p, which includes both real and imaginary parts. The harmonic transfer impedance is determined according to the system harmonic impedance matrix as

$$Z^h_{bus} = \begin{vmatrix} Z^h_{11} & Z^h_{12} & \cdots & Z^h_{1p} & \cdots & Z^h_{1N} \\ Z^h_{21} & Z^h_{22} & \cdots & Z^h_{2p} & \cdots & Z^h_{2N} \\ \vdots & \vdots & \ddots & \vdots & \ddots & \vdots \\ Z^h_{n,1} & Z^h_{n2} & \cdots & Z^h_{np} & \cdots & Z^h_{nN} \\ \vdots & \vdots & \ddots & \vdots & \ddots & \vdots \\ Z^h_{N1} & Z^h_{N2} & \cdots & Z^h_{Np} & \cdots & Z^h_{NN} \end{vmatrix} \tag{5.3}$$

Individually, the new harmonic voltage at bus n, can be expressed as,

$$V^h_{n,new} = V^{k,r}_{n,old} + jV^{h,i}_{n,old} + \left(Z^{h,r}_{np} + jZ^{h,i}_{np}\right)\left(I^{h,r}_{p} + jI^{h,i}_{p}\right) \tag{5.4}$$

where the superscripts r and i refers to the real and imaginary components, respectively for the harmonic voltage, the elements of the impedance matrix, and the SHAPLC injection current. The magnitude of the nodal harmonic voltage after SHAPLC injection current at bus p, can be expressed as

$$\left|V^h_{n,new}\right| = \sqrt{\left(Z^{h,r}_{np}I^{h,r}_{p} - Z^{h,i}_{np}I^{h,i}_{p} + V^{h,r}_{n,old}\right)^2 + \left(Z^{h,r}_{np}I^{h,i}_{p} - Z^{h,i}_{np}I^{h,r}_{p} + V^{h,i}_{n,old}\right)^2} \tag{5.5}$$

Expanding the terms inside the square root of (5.5), we have that the new magnitude of the harmonic voltage at bus n, is,

$$\left|V^h_{n,new}\right| = \sqrt{\begin{pmatrix} \left(I^{(h,r)2}_{p} + I^{(h,i)2}_{p}\right)\left(Z^{(h,r)2}_{np} + Z^{(h,i)2}_{np}\right) + 2I^{h,r}_{p}\left(Z^{h,r}_{np}V^{h,r}_{n,old} + Z^{h,i}_{np}V^{h,i}_{n,old}\right) + \\ 2I^{h,i}_{p}\left(Z^{h,r}_{np}V^{h,i}_{n,old} - Z^{h,i}_{np}V^{h,r}_{n,old}\right) + V^{(h,r)2}_{n,old} + V^{(h,i)2}_{n,old} \end{pmatrix}} \tag{5.6}$$

According with the Standard IEEE-519 [IEEE-519 1992], the *IHD* index for the harmonic *h* at bus *n* is given by

$$IHD_n^h = \frac{\left|V_{n,new}^h\right|}{\left|V_n^1\right|} \tag{5.7}$$

Where the restriction imposed by the IEEE-519 establishes that for all harmonic *h* at bus *n* must satisfy,

$$IHD \leq \alpha \tag{5.8}$$

with α=3%. Substituting (5.6) into (5.7) and using Equation (5.8), the inequality restriction is now expressed as,

$$\frac{\sqrt{\begin{pmatrix}\left(I_p^{(h,r)2}+I_p^{(h,i)2}\right)\left(Z_{np}^{(h,r)2}+Z_{np}^{(h,i)2}\right)+2I_p^{h,r}\left(Z_{np}^{h,r}V_{n,old}^{h,r}+Z_{np}^{h,i}V_{n,old}^{h,i}\right)\\ +2I_p^{h,i}\left(Z_{np}^{h,r}V_{n,old}^{h,i}-Z_{np}^{h,i}V_{n,old}^{h,r}\right)+V_{n,old}^{(h,r)2}+V_{n,old}^{(h,i)2}\end{pmatrix}}}{\left|V_n^1\right|} \leq \alpha \tag{5.9}$$

For convenience on further analysis, the inequality in (5.9), can be expressed also as,

$$\begin{aligned}\left(I_p^{(h,r)2}+I_p^{(h,i)2}\right)\left(Z_{np}^{(h,r)2}+Z_{np}^{(h,i)2}\right)+2I_p^{h,r}\left(Z_{np}^{h,r}V_{n,old}^{h,r}+Z_{np}^{h,i}V_{n,old}^{h,i}\right)+\\ 2I_p^{h,i}\left(Z_{np}^{h,r}V_{n,old}^{h,i}-Z_{np}^{h,i}V_{n,old}^{h,r}\right)+V_{n,old}^{(h,r)2}+V_{n,old}^{(h,i)2} \;\leq\; \left(\alpha\left|V_n^1\right|\right)^2\end{aligned} \tag{5.10}$$

The inequality restriction given in (5.10) represents the IHD index, at bus *n* for the harmonic *h*, and is in function of the SHAPLC injection current. From Eq. (5.10) we will have a proper expression to work with, in order to examine the performance we are looking for in the methodology of the SHAPLC planning, as given in the subsections to follow.

5.2.2 Determination of Number and Location of the SHAPLCs

In order to determine the number and location of SHAPLCs, to ensure that the harmonic distortion indices IHD and THD are under recommended levels, and in addition taking into consideration the operation principle of the SHAPLC; the number of SHAPLC will depend on the severity of harmonic distortion present in the electric system for each harmonic *h*. On the other hand, the location of each one of the SHAPLCs is obtained from a feasibility analysis on the harmonic compensation capabilities of the SHAPLC, combined with a sensitivity analysis to assure the best candidate bus is chosen among the feasible buses.

5.2.2.1 Number of SHAPLCs

Given the harmonic pollution information of a particular electric system, initially, one SHAPLC has to be considered for each harmonic *h* for which the IHD index, at any bus of the system, is beyond the recommended level. In this way, the number of SHAPLCs will be associated to the severity of harmonic distortion present in the electric system. The SHAPLC should provide harmonic mitigation for the harmonics *h* for which the mitigation control is needed and the distortion is most present.

The best location for each one of the SHAPLCs is identified according the analysis described in subsection 5.2.2.2. Then, the set (number and location) of the SHAPLCs has to be evaluated for the THD index consideration, according with subsection 5.2.2.3. If this set of SHAPLCs is able to meet the Standard guidelines then we have the number and location of SHAPLCs needed for harmonic distortion mitigation.

On the other hand, if the set of SHAPLCs is not able to provide enough mitigation to meet the THD index recommendation, then we incorporate an extra SHAPLC that would be considered for a new harmonic *h*, at which the harmonic distortion is most present in the electric system. Although for this *h* the IHD index is not beyond the recommended limits, once again determine the best location according the procedure detailed in subsection 5.2.2.2 for this extra SHAPLC, and re-evaluate the THD index recommendation according with subsection 5.2.2.3. The incorporation of extra SHAPLCs will be repeated until the arrangement of number and location of SHAPLCs meets with THD index recommendation.

5.2.2.2 Identification of Feasible Buses

Once we have expressed the IHD index as a inequality restriction in function of the new harmonic voltage in terms of the SHAPLC injection currents, e.g. Equation (5.10), it is

necessary to determine if the SHAPLC injection current at bus *p* results on Equation (5.10) being satisfied for all buses of the electric system at harmonic *h*. In [Chang *et al.* 1994] a graphical representation of Eq. (5.10) as the general form of a circle is used to determine the feasible area of solution. In this case, a graphical representation of Equation (5.10) is proposed. By rearranging (5.10) and it in taking it from the general form of a circle to the canonic form of a circle, which has a center (*q*, *w*) and radius *r*, e.g.,

$$\left(I_p^{h,r} - q\right)^2 + \left(I_p^{h,i} - w\right)^2 = r^2 \tag{5.11}$$

In this way, for different values of *r* we can graphically see Equation (5.11) as the concentric circles of Figure 5.1(a). For a value of $r = 0$, the circle is a single point, e.g. the center (*q*, *w*), which represent null harmonic distortion due to the injection currents, see Figure 5.1(a). On the other hand, the largest value of *r*, e.g. the exterior circle of Figure 5.1(a), represents the maximum value for which the inequality condition of Equation (5.10) still holds. We will call this exterior circle the Harmonic Distortion Circle (HDC). Hereby, it is convenient to convert the inequality condition expressed in Equation (5.10) into an equality, which we can later evaluate as the exterior circle, e.g. the HDC.

We have expressed Equation (5.10) as,

$$\begin{aligned}
&\left(Z_{np}^{(h,r)2} + Z_{np}^{(h,i)2}\right)\left(I_p^{(h,r)2} + 2I_p^{h,r}\left(\frac{Z_{np}^{h,r}V_{n,old}^{h,r} + Z_{np}^{h,i}V_{n,old}^{h,i}}{Z_{np}^{(h,r)2} + Z_{np}^{(h,i)2}}\right)\right) + \\
&\left(Z_{np}^{(h,r)2} + Z_{np}^{(h,i)2}\right)\left(I_p^{(h,i)2} + 2I_p^{h,i}\left(\frac{\left(Z_{np}^{h,r}V_{n,old}^{h,i} - Z_{np}^{h,i}V_{n,old}^{h,r}\right)}{Z_{np}^{(h,r)2} + Z_{np}^{(h,i)2}}\right)\right) = \\
&-\left(V_{n,old}^{(h,r)2} + V_{n,old}^{(h,i)2}\right) + \left(\alpha\left|V_n^1\right|\right)^2
\end{aligned} \tag{5.12}$$

Let us continue with the transformation of (5.10) to the form of (5.11). By completing the squares in Equation (5.12) results in,

$$\left(Z_{np}^{(h,r)2}+Z_{np}^{(h,i)2}\right)\left(\begin{array}{l} I_p^{(h,r)2}+2I_p^{h,r}\left(\dfrac{Z_{np}^{h,r}V_{n,old}^{h,r}+Z_{np}^{h,i}V_{n,old}^{h,i}}{Z_{np}^{(h,r)2}+Z_{np}^{(h,i)2}}\right)+ \\ \dfrac{Z_{np}^{(h,r)2}V_{n,old}^{(h,r)2}+Z_{np}^{(h,i)2}V_{n,old}^{(h,i)2}+2Z_{np}^{h,r}Z_{np}^{h,i}V_{n,old}^{h,r}V_{n,old}^{h,i}}{Z_{np}^{(h,r)4}+Z_{np}^{(h,i)4}+2Z_{np}^{(h,r)2}Z_{np}^{(h,i)2}} \end{array}\right)+$$

$$\left(Z_{np}^{(h,r)2}+Z_{np}^{(h,i)2}\right)\left(\begin{array}{l} I_p^{(h,i)2}+2I_p^{h,i}\left(\dfrac{Z_{np}^{h,r}V_{n,old}^{h,i}-Z_{np}^{h,i}V_{n,old}^{h,r}}{Z_{np}^{(h,r)2}+Z_{np}^{(h,i)2}}\right)+ \\ \dfrac{Z_{np}^{(h,r)2}V_{n,old}^{(h,i)2}+Z_{np}^{(h,i)2}V_{n,old}^{(h,r)2}-2Z_{np}^{h,r}Z_{np}^{h,i}V_{n,old}^{h,r}V_{n,old}^{h,i}}{Z_{np}^{(h,r)4}+Z_{np}^{(h,i)4}+2Z_{np}^{(h,r)2}Z_{np}^{(h,i)2}} \end{array}\right)=$$

$$-\left(V_{n,old}^{(h,r)2}+V_{n,old}^{(h,i)2}\right)+\left(\alpha\left|V_n^1\right|\right)^2+ \tag{5.13}$$

$$\left(\frac{Z_{np}^{(h,r)2}V_{n,old}^{(h,r)2}+Z_{np}^{(h,i)2}V_{n,old}^{(h,i)2}+2Z_{np}^{h,r}Z_{np}^{h,i}V_{n,old}^{h,r}V_{n,old}^{h,i}}{Z_{np}^{(h,r)4}+Z_{np}^{(h,i)4}+2Z_{np}^{(h,r)2}Z_{np}^{(h,i)2}}\right)\left(Z_{np}^{(h,r)2}+Z_{np}^{(h,i)2}\right)+$$

$$\left(\frac{Z_{np}^{(h,r)2}V_{n,old}^{(h,i)2}+Z_{np}^{(h,i)2}V_{n,old}^{(h,r)2}-2Z_{np}^{h,r}Z_{np}^{h,i}V_{n,old}^{h,r}V_{n,old}^{h,i}}{Z_{np}^{(h,r)4}+Z_{np}^{(h,i)4}+2Z_{np}^{(h,r)2}Z_{np}^{(h,i)2}}\right)\left(Z_{np}^{(h,r)2}+Z_{np}^{(h,i)2}\right)$$

After factorizing the left side of Equation (5.13), and some algebraic manipulation on the right side, the equation can be reduced to the form,

$$\left(I_p^{h,r}+\frac{Z_{np}^{h,r}V_{n,old}^{h,r}+Z_{np}^{h,i}V_{n,old}^{h,i}}{Z_{np}^{(h,r)2}+Z_{np}^{(h,i)2}}\right)^2+\left(I_p^{h,i}+\frac{Z_{np}^{h,r}V_{n,old}^{h,i}-Z_{np}^{h,i}V_{n,old}^{h,r}}{Z_{np}^{(h,r)2}+Z_{np}^{(h,i)2}}\right)^2=\frac{\left(\alpha\left|V_n^1\right|\right)^2}{Z_{np}^{(h,r)2}+Z_{np}^{(h,i)2}} \tag{5.14}$$

Equation (5.14) finally has the same form of (5.11). From (5.14), it can be demonstrated that for α=0, e.g. null distortion equivalent to a radius $r = 0$, the values of the SHAPLC injection current at bus p are,

$$\left[I_p^{h,r}=-\left(\frac{Z_{np}^{h,r}V_{n,old}^{h,r}+Z_{np}^{h,i}V_{n,old}^{h,i}}{Z_{np}^{(h,r)2}+Z_{np}^{(h,i)2}}\right),I_p^{h,i}=-\left(\frac{Z_{np}^{h,r}V_{n,old}^{h,i}-Z_{np}^{h,i}V_{n,old}^{h,r}}{Z_{np}^{(h,r)2}+Z_{np}^{(h,i)2}}\right)\right] \tag{5.15}$$

and for different values of α, e.g. $0<\alpha\leq 0.03$, the value of the radiuses of the concentric circles illustrated in Figure 5.1(b) are given by,

$$r = \frac{\alpha.\left|V_n^1\right|}{\left|Z_{np}^h\right|} \tag{5.16}$$

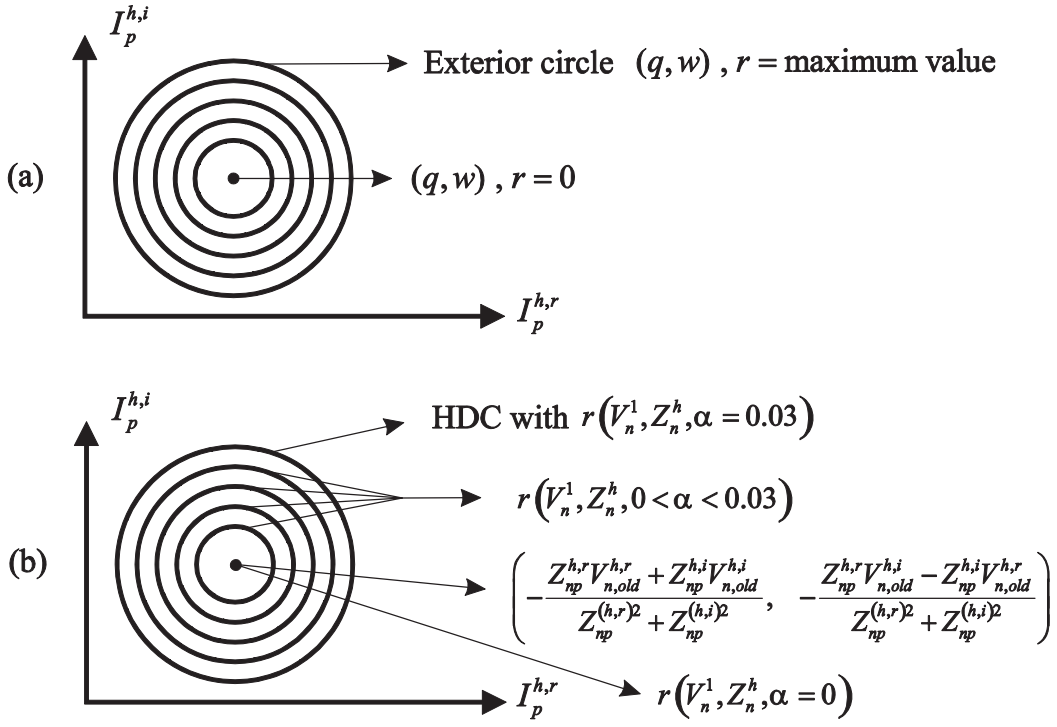

Figure 5.1 Individual harmonic distortion represented as concentric circles. (a) Concentric circles from the canonic form of a circle, (b) Harmonic Distortion Circle for the bus *n* from the injection current at bus *p*.

In Equation (5.15) we have the injection currents, at the bus *p*, which will produce a null harmonic distortion at bus *n* for the harmonic *h*. From an optimization point of view, it is easy to demonstrate that the injection currents in (5.15) are the minima of (5.12), see Appendix A. On the other hand, from (5.16) it is clear that the diameter of the concentric circles of Figure 5.1(b) for a bus *n* at the harmonic *h*, is in function of the impedance matrix element between the bus *n* and the bus of SHAPLC injection current *p*, the nodal voltage at fundamental frequency, and α. Therefore, the exterior circle, denominated above as HDC,

will be found at the recommended value α=0.03, see Figure 1(b), and the center of the HDC is given for the values of the injection current as expressed in (5.15).

It is important to mention that the HDC of Figure 5.1(b) represents the feasible region for which the values of the injection currents from bus *p* are able to meet the inequality condition of (5.10) at a specific bus *n* for the harmonic *h*.

In order to determine if a bus *p* is a feasible bus for the placement of the SHAPLC, to mitigate the *IHD* index below the permissible value α in each bus of the electric network, and for harmonic *h*, it is necessary that the HDC of all nodes do share a feasibility region for which every HDC has an $IHD \leq 3\%$.

Here, it is proposed a three-step procedure which consists of three conditions that have to be taken into account to ensure feasibility. Though a similar procedure was proposed in [Chang *et al.* 1994], the Equations (5.14)-(5.16) will enable us to get closed formulae for these three conditions, and then further evaluations can be easily done by a programmed computational algorithm.

First condition: redundant circles must be taken out of the analysis. As indicated by Equation (5.16) the radiuses of the circles will be different for each one of the HDC, then if a larger circle contains a smaller circle, the larger circle must be ignored. This condition is intended to simplify the procedure by eliminating larger circles in further analysis; in such case, the feasibility region of the larger circle, to be taken into account, will be represented by the smaller circle.

The identification of a larger circle containing a smaller circle can be done by comparing the distance between the centers of both circles with the difference between their radiuses, as illustrated in Figure 5.2, so that if the relationship of Equation (5.17) is meet for any bus *m*, the HDC of the respective bus *n* must be taken out of further analysis.

$$\sum_{n=1}^{N}\sum_{\substack{m=1 \\ m\neq n}}^{N} d_{nm} < \left| r_n - r_m \right| \quad \&\& \quad r_n > r_m \tag{5.17}$$

Where

$$r_n = \frac{\alpha . \left| V_n^1 \right|}{\left| Z_{np}^h \right|} \quad , \quad r_m = \frac{\alpha . \left| V_m^1 \right|}{\left| Z_{mp}^h \right|}$$

$$d_{nm} = \sqrt{\left(-\left(\frac{Z_{np}^{h,r}V_{n,old}^{h,r} + Z_{np}^{h,i}V_{n,old}^{h,i}}{Z_{np}^{(h,r)2} + Z_{np}^{(h,i)2}} \right) + \left(\frac{Z_{mp}^{h,r}V_{m,old}^{h,r} + Z_{mp}^{h,i}V_{m,old}^{h,i}}{Z_{mp}^{(h,r)2} + Z_{mp}^{(h,i)2}} \right) \right)^2 + \left(-\left(\frac{Z_{np}^{h,r}V_{n,old}^{h,i} - Z_{np}^{h,i}V_{n,old}^{h,r}}{Z_{np}^{(h,r)2} + Z_{np}^{(h,i)2}} \right) + \left(\frac{Z_{mp}^{h,r}V_{m,old}^{h,i} + Z_{mp}^{h,i}V_{m,old}^{h,r}}{Z_{mp}^{(h,r)2} + Z_{mp}^{(h,i)2}} \right) \right)^2}$$

$$d_{nm} \leq |r_n - r_m| \quad \&\& \quad r_n > r_m$$

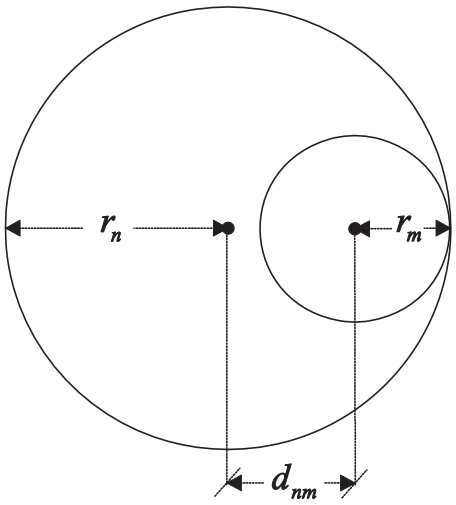

Figure 5.2 Largest circle *n* containing a smaller circle *m*.

At the end, the remaining circles must be included in a set NC1, which includes all the HDCs representing each bus of the electric system, except those which have been identified as larger circles containing smaller circles.

Second condition: All the HDCs remaining in the set NC1 have to share a feasibility region with each other. One way of knowing if two HDCs, let's say for a bus *n* and a bus *m*, do share a feasibility region, for the harmonic *h*, can be determined by comparing the distances between their centers with the sum of their radiuses, see Figure 5.3. Therefore, when two HDCs do share a feasibility region in common the following relationship holds,

$$d_{nm} \leq \left(r_n + r_m\right) \tag{5.18}$$

In a similar manner, Equation (5.18) can be expressed in a general form that includes all the buses of the electric system, such as given in (5.19). If the general relationship of (5.19) holds for all *n*, *m*, the second condition is satisfied and the procedure can continue to the third condition, otherwise the bus *p* is not a feasible bus for the placement of the SHAPLC.

$$\sum_{n=1}^{NC1-1} \sum_{m=n+1}^{NC1} d_{nm} \leq \left(r_n + r_m\right) \tag{5.19}$$

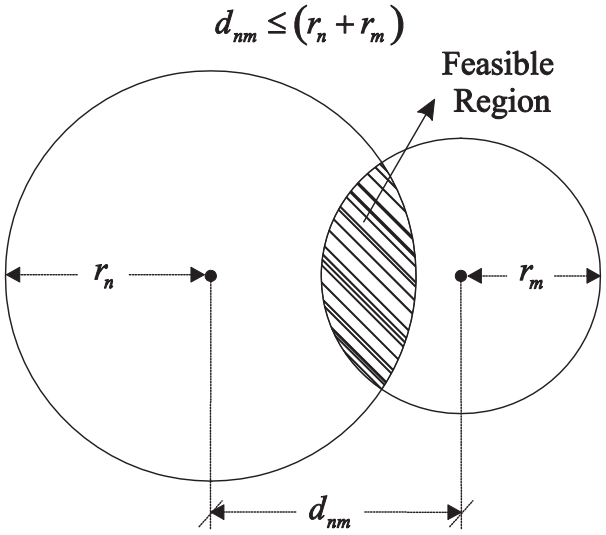

Figure 5.3 Intersection of two circles.

Third condition: Proof for the existence of a common feasibility region for all the remaining circles in the set NC1. Once the second condition is satisfied, it must be ensured that a common feasibility region exists for all the circles in set NC1. For this case, a point *F* can be identified as contained into a common feasible region by comparing the distance from the center of the HDC in question to the feasible region with the radius of the HDC. Figure 5.4 illustrates this condition where *F* is any point contained in the feasible region. Therefore, if the condition (5.20) is satisfied, for all the HDC included in the set NC1, *F* is

contained in the common feasible region, proving that the common feasible region does actually exist. The detailed derivation for correctly choosing the F to be evaluated in (5.20) is given in Appendix B.

$$\sum_{n=1}^{NC1} d_{nF} \leq r_n \tag{5.20}$$

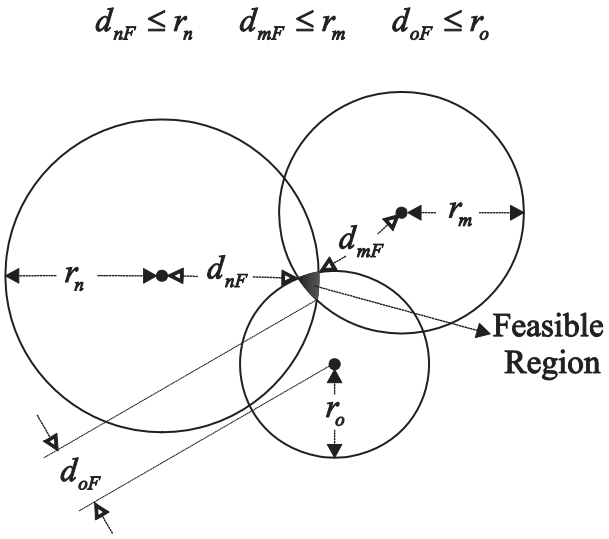

Figure 5.4 Feasible region condition.

If (5.19) and (5.20) are satisfied for the set NC1, the bus p is a feasible bus for the placement of the SHAPLC, and hereby to provide enough harmonic mitigation to decrease the harmonic index IHD below the maximum permissible value α at all buses of the electric network.

For the particular harmonic h, the group of feasible buses will be placed in a set P^h.

5.2.2.2.1 Sensitivity Analysis over the Feasible Buses

Once we have determined the buses that are feasible candidates for the placement of the SHAPLC for the harmonic h, it is necessary to determine, among the feasible buses, which bus is the best option for the SHAPLC location. To achieve this aim, a sensitivity analysis

is proposed. Here, we have used the simplest interpretation of the sensitivity analysis, e.g. the rate of change of a function due to the unit change of a dependent variable,

$$\delta = \frac{\partial \Phi(x)}{\partial x} \tag{5.21}$$

Therefore, it is required to estimate the rate variation of the harmonic voltage in the electric network produced by the injection current of a SHAPLC at bus *p*. According to Equation (5.2) the harmonic voltage variation produced by the SHAPLC injection current at bus *p* can be expressed in closed form as,

$$\Delta V^h = \sum_{n=1}^{N} Z_{np}^h I_p^h \tag{5.22}$$

Including the rectangular components, it can be expressed as,

$$\Delta V^h = \sum_{n=1}^{N} \left(\left(Z_{np}^{h,r} I_p^{h,r} - Z_{np}^{h,i} I_p^{h,i} \right) + j \left(Z_{np}^{h,r} I_p^{h,i} + Z_{np}^{h,i} I_p^{h,r} \right) \right) \tag{5.23}$$

The rate variation of ΔV^h with respect to a unit chance of each one of the rectangular components of the SHAPLC injection current is given by,

$$\frac{\partial \Delta V^h}{\partial I_p^{h,r}} = \sum_{n=1}^{N} \left(Z_{np}^{h,r} + j Z_{np}^{h,i} \right) \tag{5.24}$$

$$\frac{\partial \Delta V^h}{\partial I_p^{h,i}} = \sum_{n=1}^{N} \left(-Z_{np}^{h,i} + j Z_{np}^{h,r} \right) \tag{5.25}$$

Where the magnitude of the sum of the rate variations, given in (5.24) and (5.25), can be determined as follows,

$$\left|\frac{\partial \Delta V^h}{\partial I_p^{h,r}} + \frac{\partial \Delta V^h}{\partial I_p^{h,i}}\right| = \sum_{n=1}^{N} \sqrt{Z_{np}^{(h,r)2} + Z_{np}^{(h,i)2} - 2Z_{np}^{h,r} Z_{np}^{h,i} + Z_{np}^{(h,r)2} + Z_{np}^{(h,i)2} + 2Z_{np}^{h,r} Z_{np}^{h,i}}$$
$$= \sum_{n=1}^{N} \sqrt{2\left(Z_{np}^{(h,r)2}\right) + 2\left(Z_{np}^{(h,i)2}\right)} \tag{5.26}$$
$$= \sqrt{2} \sum_{n=1}^{N} \left|Z_{np}^{h}\right|$$

At this stage, the purpose is to identify which bus, among the feasible buses in the set P^h, is the best option for the SHAPLC placement. The best bus location p for the harmonic h will be the bus with the largest sensitivity value according to (5.26). This means that for the harmonic h, an injection current at the most sensitive bus will produce a higher distortion, e.g., higher than the distortion produced in any other bus in the set of feasible buses P^h. Though for this case, the distortion will be a planned and favorable distortion, provided by the SHAPLC as a corrective measure.

5.2.2.3 Test for the THD Index

Once we have selected the set (number and location) of the SHAPLCs to assure that the *IHD* index meets the recommended limits by the IEEE-519, there is still an important situation to take into consideration. Is this arrangement of number and location of SHAPLCs, able to provide enough harmonic distortion in order to meet the imposed limits by the IEEE-519, on the THD index throughout the network? To answer this question, we have to determine how much distortion mitigation can a single SHAPLC, at its respective harmonic h, is able to provide to the system. Then an evaluation on the *THD* index for all buses will give us the outcome.

According with the IEEE-519 the *THD* index is to be evaluated as,

$$THD_n = \frac{\sqrt{\sum_{h \in H} \left|V_{n,new}^h\right|^2}}{V_n^1} \tag{5.27}$$

And the *THD* index should meet the following inequality condition,

$$THD_n \leq \beta \tag{5.28}$$

Where β is the imposed limit by the IEEE-519, setting at a value of β=5%.

From Equation (5.6), the new harmonic voltage for the harmonic *h*, in all buses, as a function of the SHAPLC injection current is given as,

$$V_{AB,new}^{h} = \sqrt{\sum_{n=1}^{N}\left(\begin{array}{l}\left(I_p^{(h,r)2}+I_p^{(h,i)2}\right)\left(Z_{np}^{(h,r)2}+Z_{np}^{(h,i)2}\right)+2I_p^{h,r}\left(Z_{np}^{h,r}V_{n,old}^{h,r}+Z_{np}^{h,i}V_{n,old}^{h,i}\right)+\\ 2I_p^{h,i}\left(Z_{np}^{h,r}V_{n,old}^{h,i}-Z_{np}^{h,i}V_{n,old}^{h,r}\right)+V_{n,old}^{(h,r)2}+V_{n,old}^{(h,i)2}\end{array}\right)} \tag{5.29}$$

where the subscripts $_{AB}$ stands for *all buses*. Please notice that in the case of not presence of the SHAPLC in the network for the harmonic *h*, the value of the new harmonic voltage in (5.29) will remain constant as the old value of harmonic voltage. From an optimization point of view it is more convenient to work with the square values of the harmonic voltages, such as given in (5.30),

$$\left|V_{AB,new}^{h}\right|^2 = \sum_{n=1}^{N}\left(\begin{array}{l}\left(I_p^{(h,r)2}+I_p^{(h,i)2}\right)\left(Z_{np}^{(h,r)2}+Z_{np}^{(h,i)2}\right)+2I_p^{h,r}\left(Z_{np}^{h,r}V_{n,old}^{h,r}+Z_{np}^{h,i}V_{n,old}^{h,i}\right)+\\ 2I_p^{h,i}\left(Z_{np}^{h,r}V_{n,old}^{h,i}-Z_{np}^{h,i}V_{n,old}^{h,r}\right)+V_{n,old}^{(h,r)2}+V_{n,old}^{(h,i)2}\end{array}\right) \tag{5.30}$$

In the same way, the new harmonic voltage of Equation (5.30) for a single bus *n*, allow us to express the THD at bus *n*, in terms of the new harmonic voltage, as a the inequality condition,

$$\sum_{h\in H}\left(\begin{array}{l}\left(I_p^{(h,r)2}+I_p^{(h,i)2}\right)\left(Z_{np}^{(h,r)2}+Z_{np}^{(h,i)2}\right)+2I_p^{h,r}\left(Z_{np}^{h,r}V_{n,old}^{h,r}+Z_{np}^{h,i}V_{n,old}^{h,i}\right)+\\ 2I_p^{h,i}\left(Z_{np}^{h,r}V_{n,old}^{h,i}-Z_{np}^{h,i}V_{n,old}^{h,r}\right)+V_{n,old}^{(h,r)2}+V_{n,old}^{(h,i)2}\end{array}\right) \leq \left(\beta\left|V_n^1\right|\right)^2 \tag{5.31}$$

To proceed the search of the maximum harmonic distortion mitigation that a SHAPLC can provide throughout the network at the harmonic *h*, we have used a direct approach for minimizing the Equation given in (5.30). Deriving Equation (5.30) with respect to the rectangular components of the SHAPLC injection current we get,

$$\frac{\partial \left| V_{AB,new}^{h} \right|^2}{\partial I_{p}^{h,r}} = \sum_{n=1}^{N} \left(2I_{p}^{h,r} \left(Z_{np}^{(h,r)2} + Z_{np}^{(h,i)2} \right) + 2\left(Z_{np}^{h,r} V_{n,old}^{h,r} + Z_{np}^{h,i} V_{n,old}^{h,i} \right) \right) \tag{5.32}$$

$$\frac{\partial \left| V_{AB,new}^{h} \right|^2}{\partial I_{p}^{h,i}} = \sum_{n=1}^{N} \left(2I_{p}^{h,i} \left(Z_{np}^{(h,r)2} + Z_{np}^{(h,i)2} \right) + 2\left(Z_{np}^{h,r} V_{n,old}^{h,i} - Z_{np}^{h,i} V_{n,old}^{h,r} \right) \right) \tag{5.33}$$

Making Equations (5.32) and (5.33) equal to zero and solving both equations for each one of the rectangular components, respectively, the values of the rectangular components are obtained with Equations (5.34) and (5.35), for which the SHAPLC at the selected bus *p*, will get the maximum harmonic voltage mitigation throughout the network for the respective harmonic *h*.

$$I_{p,\max}^{h,r} = -\left(\frac{\sum_{n=1}^{N} \left(Z_{np}^{h,r} V_{n,old}^{h,r} + Z_{np}^{h,i} V_{n,old}^{h,i} \right)}{\sum_{n=1}^{N} \left(Z_{np}^{(h,r)2} + Z_{np}^{(h,i)2} \right)} \right) \tag{5.34}$$

$$I_{p,\max}^{h,i} = -\left(\frac{\sum_{n=1}^{N} \left(Z_{np}^{h,r} V_{n,old}^{h,i} - Z_{np}^{h,i} V_{n,old}^{h,r} \right)}{\sum_{n=1}^{N} \left(Z_{np}^{(h,r)2} + Z_{np}^{(h,i)2} \right)} \right) \tag{5.35}$$

where the subscript *max* stands for the SHAPLCs injection currents, which provides the maximum harmonic mitigation from bus *p* for the harmonic *h*. It is easy to demonstrate that

the equations (5.34) and (5.35) represent an unconstrained global minimum of (5.30), as given in Appendix A.

After calculating (5.34) and (5.35), for all the SHAPLCs included in the analysis, these values of the injection currents are to be substituted in (5.31). The evaluation of Equation (5.31) will tell us if the selected group of SHAPLCs is able to provide enough harmonic distortion to meet the IEEE-519 imposed limit on the THD index.

5.2.3 Determination of the Optimal Injection Currents of the SHAPLCs

The objective function considered in the SHAPLC planning is to minimize the SHAPLCs injection currents. Once again, from an optimization point of view it is more convenient to work with the square magnitudes of the SHAPLC injection currents, as given in (5.36).

$$\begin{aligned} f_{obj} &= \sum_{p \in P} \left| I_p^h \right|^2 \\ &= \sum_{p \in P} \left(I_p^{(h,r)2} + I_p^{(h,i)2} \right) \end{aligned} \tag{5.36}$$

The calculation of the optimal injection currents and sizing of the SHAPLCs, is based on solving the constrained nonlinear optimization problem, given in (5.37), while the harmonic distortion indices, IHD and THD, must meet IEEE-519 guidelines according with (5.10) and (5.31), respectively. The nonlinear optimization problem is a convex optimization problem, so a local minimum that satisfies the nonlinear conditions of (5.37) will also be a global minimum, see Appendix A.

$$\begin{aligned} &\text{Min} \quad f_{obj} \\ &\text{s.t.} \quad IHD_n^h \le \alpha \qquad h \in HC, \;\; n = 1, 2, ..., n, ..N \\ &\qquad THD_n \le \beta \qquad n = 1, 2, ..., n, ..N \end{aligned} \tag{5.37}$$

where *HC* is the set of harmonics considered for the SHAPLCs.

5.2.4 SHAPLC Planning Procedure

Recapitulating, a step by step procedure to determine the number and locations of the SHAPLCs to meet the IEEE-519 guidelines for harmonic distortion indices, IHD and THD, is given next and a flow chart of the procedure illustrated in Figure 5.5.

1. From the information, obtained priori, about the harmonic pollution on the network; identify the harmonic h for which the level of the IHD index is beyond the limit α, at any bus of the electric system. Include the harmonic h in a set HC. Notice that for each harmonic h in the set HC, one SHAPLC has to be considered for harmonic distortion mitigation planning.

2 For each harmonic h included in set HC; perform an identification of the feasible nodes as indicated in Section 5.2.2.2. Form the sets P^h with the feasible buses for each harmonic h.

3. For each harmonic h included in set HC; perform a sensitivity analysis using respectively the corresponding set P^h. According to Section 5.2.2.2.1 the bus with the highest sensitivity value will be selected for the SHAPLC location at the respective harmonic h.

4. For each harmonic h included in set HC; calculate the SHAPLC injection currents using (5.34) and (5.35), which provides the maximum harmonic distortion mitigation from the selected sensitive bus p. Using the calculated injection currents, evaluate condition (5.31) for all buses.

5. If the evaluation of condition (5.31) holds for all buses proceed to step 7. The set of SHAPLCs (number and location) are able to reduce the harmonic distortion mitigation in the electric network and meet the IEEE-519 guidelines. Otherwise proceed to next step.

6. If the condition (5.31) does not hold for all buses; identify a new harmonic h, with heavy harmonic distortion in the electric system, even though at this harmonic h the maximum limit of the IHD index is not violated for any bus, and include this new harmonic h in the set HC an go back to step 2.

7. Solve the nonlinear optimization problem (5.37). Output results.

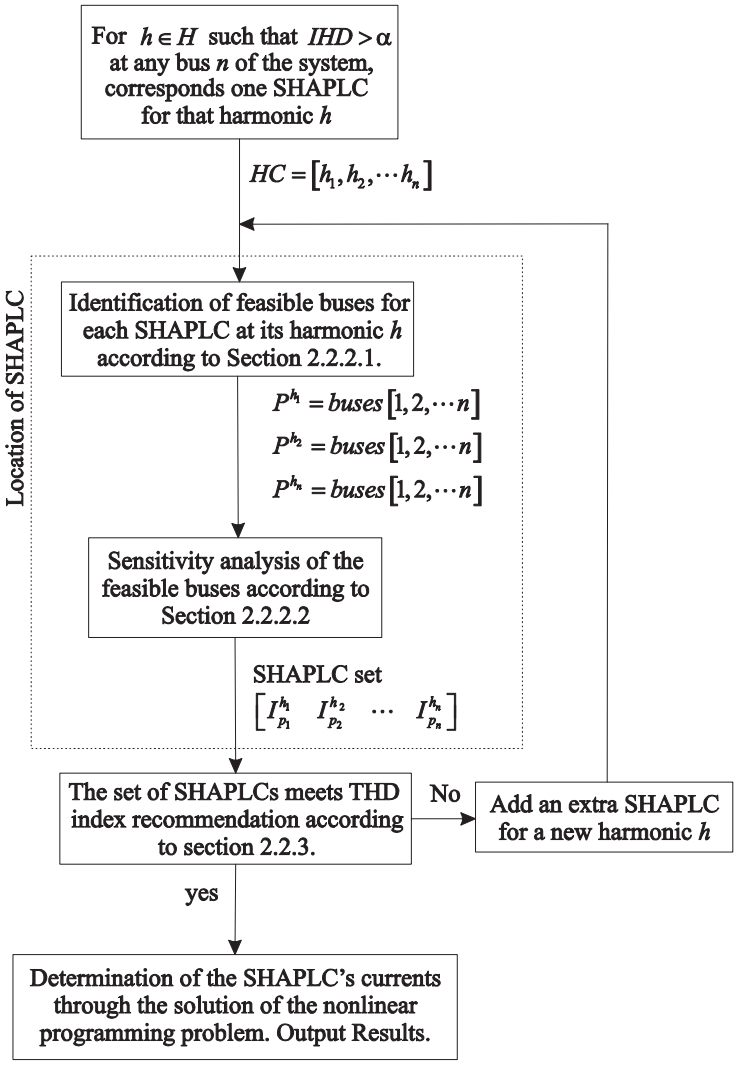

Figure 5.5 Flow chart in the SHAPLC planning.

5.3 Case Study

The proposed solution algorithm for SHAPLC planning is tested using a 30-bus distribution system shown in Figure 5.6 to demonstrate its usefulness and relative simplicity. The objective is to determine the number and location of the SHAPLCs as well as their optimal injection currents to control the system harmonic voltage distortion throughout the network. The system data is given in [Saadat 1999] and also provided in Appendix D. The harmonic sources are three six-pulse converters located at buses 16, 17, and 22, respectively.

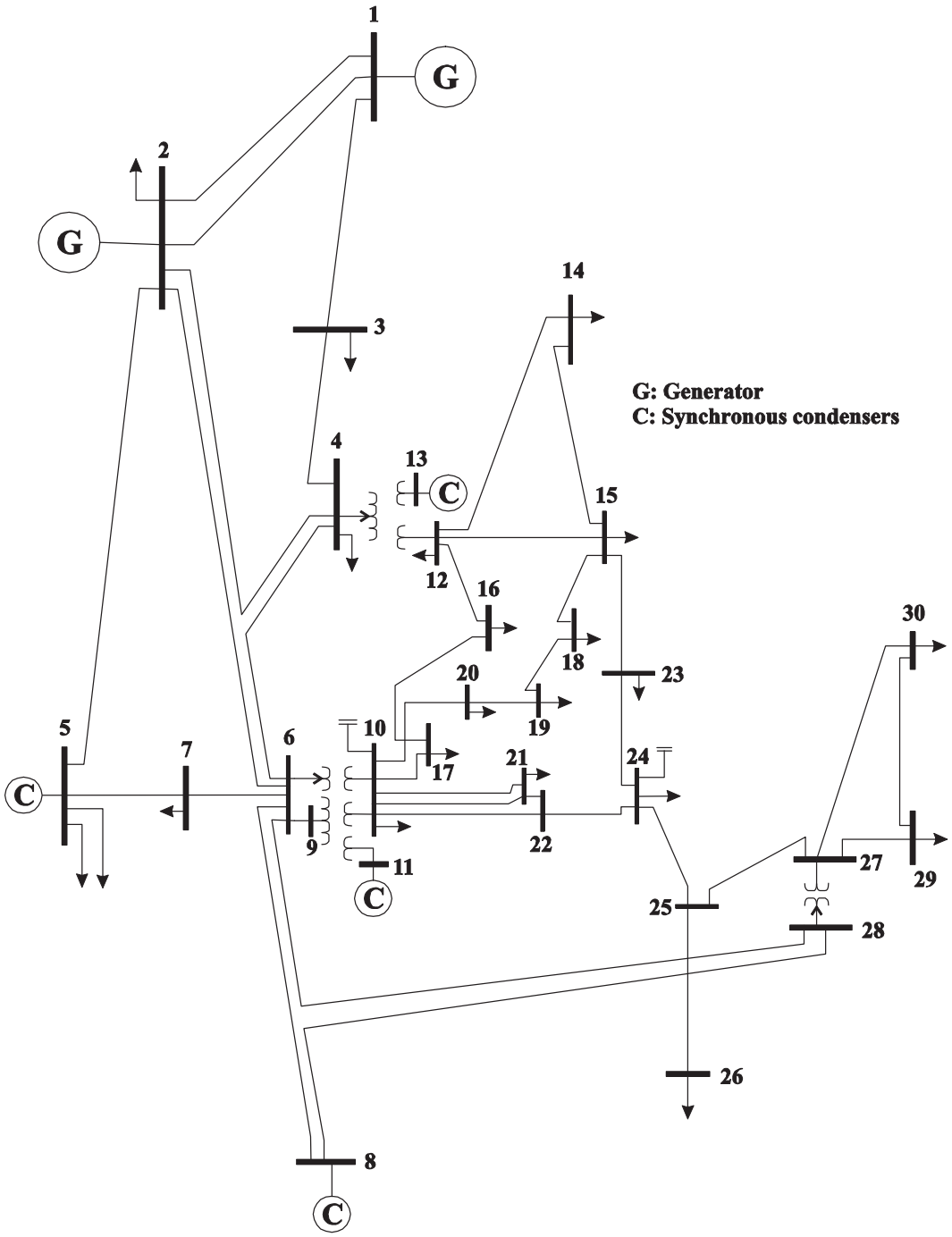

Figure 5.6 IEEE 30-bus distribution system under study.

The nonlinear loads information is given in Table 5.1. Figure 5.7 and Figure 5.8 show the harmonic contamination of the power system through the individual harmonic distortion and the total harmonic distortion indices, where it can be seen that the system is highly harmonic distorted; the values of IHD and THD are beyond the limits recommended by IEEE-519 given in Section 1.2.

Table 5.1 Harmonic injections current of the nonlinear loads at buses 22, 17 and 16.

h	**5**	**7**	**11**	**13**	**17**	**19**	**23**	**25**	**29**	**31**
Mag. (% fund.)	19.1	13.1	7.2	5.6	3.3	2.4	1.2	0.8	0.2	0.2
Angle (Deg.)	0	0	0	0	0	0	0	0	0	0

BUS	**16**	**17**	**22**
P_d (p.u.)	**0.035**	**0.09**	**0.35**
Q_d (p.u.)	**0.018**	**0.058**	**0.25**

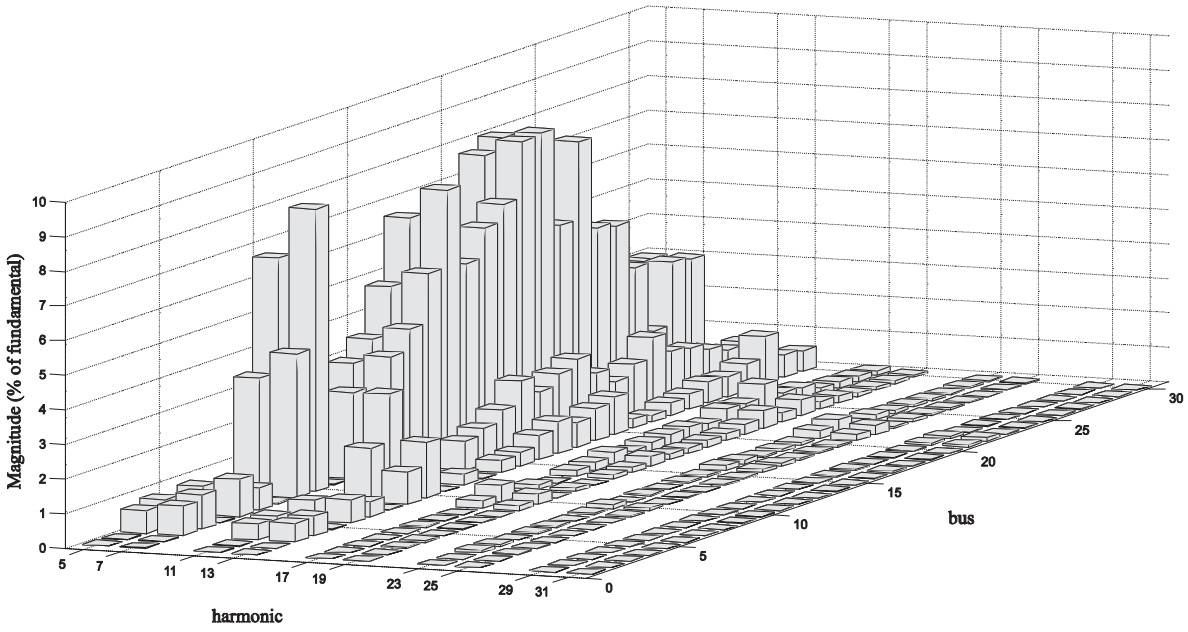

Figure 5.7 IHD in the 30-bus distribution system before SHAPLC harmonic mitigation.

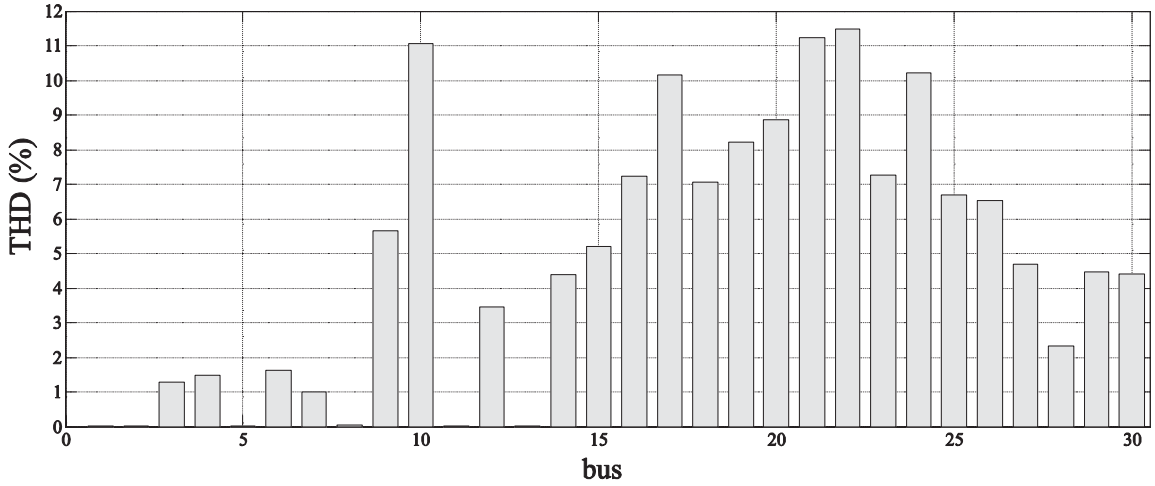

Figure 5.8 THD in the 30-bus distribution system before SHAPLC harmonic mitigation.

5.3.1 Solution Procedure

The number and locations of the SHAPLCs are then obtained from the proposed seven-step procedure in section 5.2.4.

1. From the harmonic distortion information, illustrated in Figure 5.7, it has been founded that the maximum permissible limit α for the IHD index is violated for the harmonics 5 and 7, at several buses of the electric system for both harmonics. Even though the harmonic distortion contamination is present for other harmonics, their IHD index values are not beyond the maximum permissible limit. Therefore, the set HC will be formed with the harmonics HC= [5 7].

2. According with the feasibility analysis for IHD mitigation; for the harmonic 5 the set of feasible nodes is P^5= [10, 17, 21, 22], and coincidentally for the harmonic 7 the set of feasible node is P^7= [10, 17, 21, 22].

3. The sensitivity values, δ_h, for each bus included in sets P^5 and P^7, at their respective harmonic *h*, are summarized in Table 5.2. The sensitivity analysis shows that the best option for the placement of the SHAPLCs for the harmonics 5 and 7, are the buses 22 and 10, respectively. Comparative analyses to demonstrate that these buses are the best option, at their respective harmonic *h*, are given in Appendix C.

Table 5.2 Sensitivity analysis results for feasible nodes at harmonics h = 5, 7.

Bus	δ_5	δ_7
10	11.8094	21.5499
17	11.3038	19.2617
21	12.1539	20.3415
22	12.2268	20.1767

4. Using (5.34) and (5.35); we have calculated the injection currents of the SHAPLCs for maximum harmonic mitigation from the buses 22 and 10, for harmonics 5 and 7, respectively.

$$I_{22,\max}^{5,r} = -0.03883052 \qquad I_{22,\max}^{5,i} = -0.09959600\,j$$

$$I_{10,\max}^{7,r} = 0.00368110 \qquad I_{10,\max}^{7,i} = -0.06832709\,j$$

5. Taking the above values as the SHAPLCs injection currents, which are for the maximum harmonic distortion mitigation achievable with the SHAPLCs, results in the harmonic mitigation illustrated in Figure 5.9. Figure 5.9(a) shows the maximum reduction of IHD index for harmonic 5 with a SHAPLC placed at bus 22, and Figure 5.9(b) shows the maximum reduction of IHD index for harmonic 7 with a SHAPLC placed at bus 10. Also, substituting the values of the SHAPLC injection currents obtained in step 4 into (5.30) and evaluating (5.27), we get that condition (5.31) holds for all buses of the system. Therefore, the set of SHAPLCs are able to mitigate the harmonic distortion throughout the network to meet the harmonic distortion indices IHD and THD as recommended by IEEE-519. Two SHAPLCs are necessary to achieve the goal; one for the harmonic 5 at bus 22, and another for the harmonic 7 at bus 10.

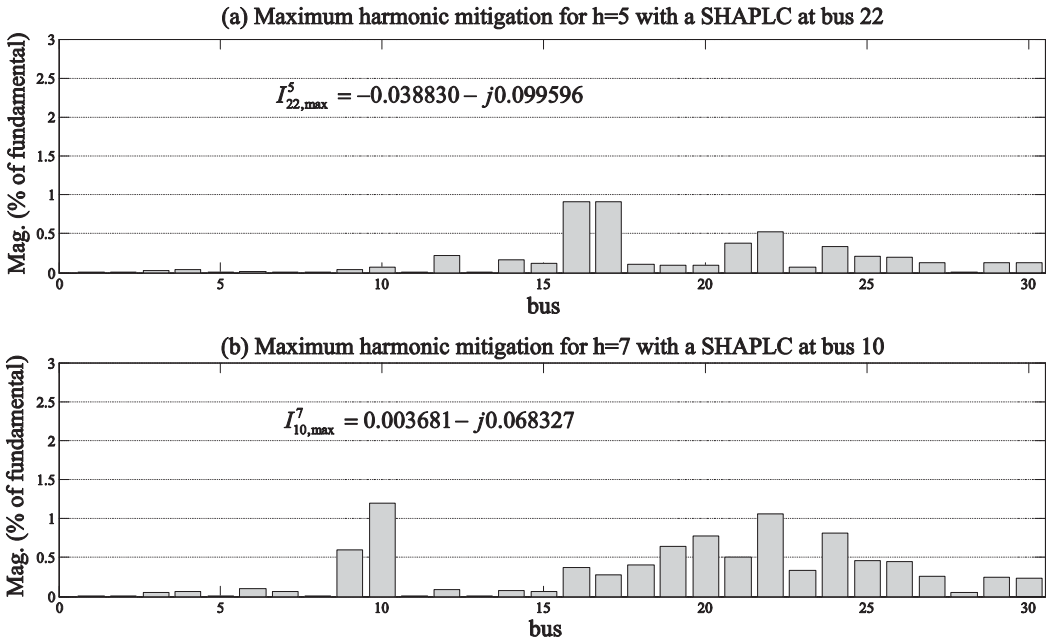

Figure 5.9 Maximum harmonic mitigation. (a) For harmonic h = 5 with a SHAPLC at bus 22. (b) For harmonic h = 7 with a SHAPLC at bus 10.

7. Now that we know the number and location of the SHAPLCs needed to achieve the goal, it is required to determine the optimal injection currents that will reduce the harmonic content in the power system under desirable distortion limits. The nonlinear optimization problem to be solved according to (5.37) is,

$$\begin{aligned} \text{Min} \quad & I_{22}^{(5,r)2} + I_{22}^{(5,i)2} + I_{10}^{(7,r)2} + I_{10}^{(7,i)2} \\ \text{s.t.} \quad & IHD_n^h \le \alpha \qquad h \in [5,7], \;\; n = 1,2,....,n,..N \\ & THD_n \le \beta \qquad n = 1,2,....,n,..N \end{aligned}$$

The optimal injection currents for the SHPALCs are,

$$I_{22}^{5,r} = -0.020301 \qquad I_{22}^{5,i} = -0.062812\, j$$

$$I_{10}^{7,r} = 0.002951 \qquad I_{10}^{7,i} = -0.045696\, j$$

The information about the harmonic distortion contamination in the electric system after compensation is illustrated in Figure 5.10 and Figure 5.11. Figure 5.10 illustrates that the IHD index in all buses meets the recommendation limit. The active inequality restrictions, e.g. with a IHD=3%, associated with this harmonic index are; at bus 17 for the harmonic 5, and at bus 22 for the harmonic 7.

On the other hand, for the case of the THD index, as illustrated in Figure 5.11, the only active inequality condition, e.g. with a THD=5%, is at bus 10.

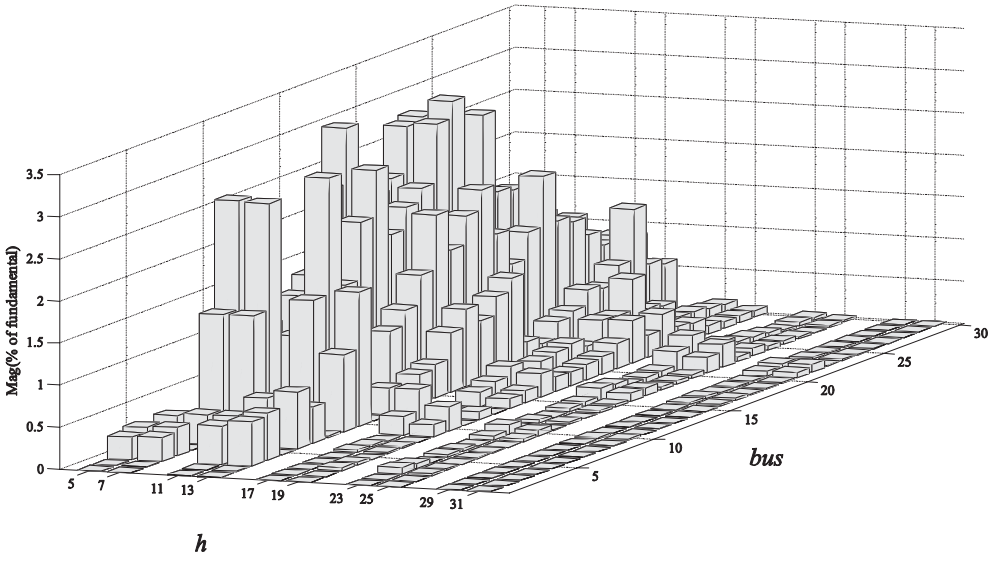

Figure 5.10 IHD in the 30-bus distribution system after SHAPLC harmonic mitigation.

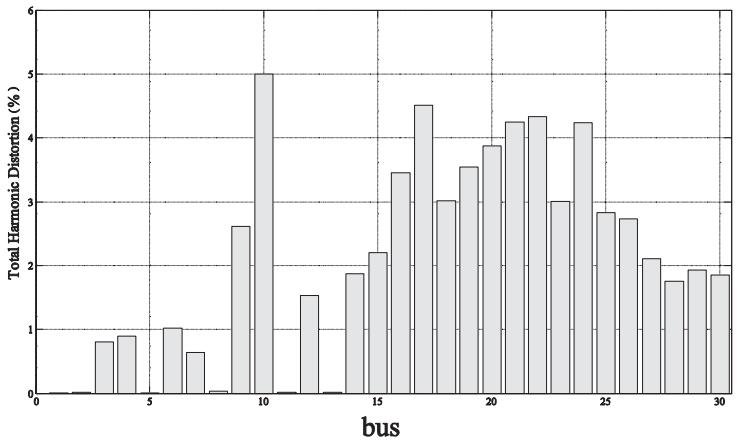

Figure 5.11 THD in the 30-bus distribution system after SHAPLC harmonic mitigation.

5.4 Conclusions

In this chapter a novel alternative in the Active Power Line Conditioner (APLC) planning field for harmonic voltage mitigation in power systems has been presented. It is based on the Single Harmonic Active Power Line Conditioner (SHAPLC) concept, which basically injects only a single harmonic current. The number of SHAPLCs to mitigate the harmonic distortion in the power system, and follow the recommended guidelines by the Standard IEEE-519, is directly associated to the severity of harmonic distortion present in the power system. The location is selected using a sensitivity analysis. The sensitivity analysis allow us to compensate the harmonic distortion for each harmonic h from the bus that is more convenient for this purpose, and not from different buses as for the case of APLC planning.

Finally, the injection currents are determined by solving a nonlinear problem which finds the minimum injections currents to achieve the goal.

The SHAPLC planning presented here has the advantage over other computational procedures in that a significant reduction on the computational effort is achieved to compensate the harmonic distortion in the power system. This is clear since to meet the IHD index guideline, the control algorithm for each SHAPLC unit only requires a single harmonic frequency. And a combination of the SHAPLCs can also ensure that the harmonic index THD is satisfied at all buses.

The analysis and formulation have been developed in detail, providing mathematical justification/validation and closed formulae that allow the control algorithm to be completely programmed and solved by a computer and/or using a commercial software package.

Chapter 6. General Conclusions and Future Research Work

6.1 General Conclusions

This section provides some conclusions on the work presented in this thesis, as well as it shares to the reader a particular point of view about the contributions of the research work.

- The shunt active power filter is a powerful device for compensating harmonic current and reactive power. Its performance will be always tied to the control strategy selected to compute the reference filtering currents, and there is a continuous research in this direction. The proposed algorithm for determining the reference filtering current has been developed to perform state-state and dynamic compensation in three-phase power systems. In order to handle non ideal supply voltage, the algorithm has been designed including a post-process over the measured data, still having an affordable computational effort needed to perform the calculations in real-time applications.
- When the shunt APF is used for dynamic compensation, the room for improving the control strategy to derive the reference filtering currents can be found in the application of other methodologies and algorithms to obtain the reference signals and/or parameters used by the control strategy. In particular, Neural Nets and Fuzzy Logic approaches have shown promising preliminary results for obtaining P_T and $v_k^*(t)$ in less than a half-cycle of the fundamental frequency when the complete harmonic spectrum is considered. Nevertheless, there are still some limitations in the methodology if the complete harmonic spectrum is not considered.
- In the shunt hybrid filter compensation scheme presented in Chapter 4, the commutation frequency of the designed LQR switching current controller should be properly identified and possibly fixed at a desired frequency of commutation. This consideration is important to take into account the commutation frequency limits of the actual converter switching-devices in order to make feasible the physical implementation under this compensation scheme. Nevertheless, the designed LQR switching current controller has shown a remarkable performance in the solution of the resonance associated problems.

- This compensation scheme, e.g. SHF, or any other including high-pass filtering alternative, is necessary to avoid parallel resonance problems and harmonic ripple current contamination to the source voltages. Another important advantage of the SHF compensation scheme is the reduction of the necessary KVA rating of the active power filter, and this situation should not be ignored.
- The Single-Harmonic Active Power Line Conditioner planning proposed in Chapter 5, has been developed to fully control the IHD and THD indices in all buses of a distribution power system. The closed formulation developed in Chapter 5 allows the optimization-based algorithm to be programmed using a commercial package or an open source code.
- At this research stage very good results have been obtained with the proposed SHAPLC planning methodology. It is still necessary to extent the methodology if we want to account for the coupling between harmonics and be able to provide a more realistic representation of the harmonic pollution into the distribution power system and the optimization based algorithm. In a similar way, the consideration of taking into account unbalanced three-phase systems is also an opportunity to improve the methodology.
- Other considerations can be made for the application of this SHAPLC planning procedure. For example, if the SHAPLC planning procedure is applied in electric networks considerable larger than that presented in Chapter 5 (increasing the complexity in the harmonic control) and there are no feasible buses to locate the SHAPLC, at its associated harmonic h, that ensure that the harmonic indices meet the guidelines. Then, the SHAPLC planning procedure no longer works as a proper solution. In this sense, the SHAPLC planning procedure may be found a better application in smaller scale electric systems with varying nonlinear load conditions or in industrial installations of a considerable size where the harmonic pollution control plays an important role in the production process reliability.
- The Shunt APF has not been tested under disturbances, such as fault conditions. The operation and performance under such conditions had not been considered since the APF is not capable of supplying average power to the load. If a fault condition takes presence in the electric system at the PCC and the shunt APF is maintained in operation, during the transient the dc capacitor would be rapidly discharged and the shunt APF would be no longer in conditions to continue in operation.

6.1.1 Contributions

A complete digital model of the shunt APF in *abc* coordinates for harmonic mitigation and reactive power compensation has been developed. The control strategy used to calculate the reference filtering currents of the shunt APF model is able to perform steady state and dynamic compensation of non linear loads. In addition, the algorithm for computing the reference filtering currents has been tested in real-time simulations for both steady state and dynamic compensation.

Practical considerations for a future physical implementation of the device has been given by extending the compensation scheme to a shunt hybrid filter scheme of compensation. In particular, for the shunt hybrid filter structure presented in this thesis, a Linear Quadratic Regulator switching controller has been designed and incorporated in the Matlab/Simulink® digital model. The goals achieved with this shunt scheme of compensation and its LQR switching controller design are: First; the reduction of the shunt APF rating by reducing the necessary rms injection current during compensation, thus, making the compensation device less expensive, and Second; a solution to the associated resonance problems, which has shown very good results.

A novel alternative in the APLC planning has been developed to determine optimal size and location of APLCs in distribution power systems. The computational effort demand for its solution algorithm is low and the harmonic distortion indices, IHD and THD, are properly met.

6.2 Future Research Work

As a result of the research work realized, the following directions have been identified to continue with this research field,

- Shunt Active Power Filter compensation using Hardware-in-the-Loop simulations. The aim is to test the control strategy in a commercial digital signal processor before the incorporation of the hardware switching devices. The entire process is to be completed with a physical implementation of the shunt Active Power Filter.
- It is necessary to determine, and if possible to assign, the commutation frequency of the LQR switching current controller for SHF compensation scheme as an important part of the switching control design.

- Dynamic compensation of the shunt active power filter in industrial power systems for maintaining acceptable/desired levels of harmonic distortion at those recommended by the harmonic Standards.
- Sensitivity analysis on the proposed optimization based methodology for Active Power Line Conditioner planning. The idea is to investigate how sensitive is the proposed optimization based method to error in the data inputs.
- Extent the optimization based methodology for Active Power Lines Conditioner planning to be able to handle unbalanced networks. As well as to develop of a new method for Active Power Line Conditioner planning that takes into account the coupling between harmonics.

After you create a Simulink® model, you can enter simulation parameters for use by Real-Time Workshop code generation software for creating C code and building a real-time application.

This procedure will use APF_rtwt.mdl as an example, and is assuming that the model has been already loaded.

1. In the Simulink® window, and from the **Simulation** menu, click **Configuration Parameters**.
2. Click the **Hardware Implementation** Node.
3. From the **Device type** list, choose 32-bit Real-Time Windows Target.
4. Under **Emulation hardware**, select None.
5. Click the **Real-Time Workshop** node. The **Real-Time Workshop** pane opens.
6. In the **Target selection** section, click the **Browse** button at the **RTW system target file** list. The **System Target File Browser** opens.
7. Select the system target file for building a Real-Time Windows Target application, and click **OK**.

The system target file rtwin.tlc, the template makefile rtwin.tmf, and the make command make_rtw are automatically entered into the **Real-Time Workshop** pane. Although not visible in the **Real-Time Workshop** pane, the external target interface MEX file rtwinext is also configured when you click **OK**. This allows external mode to pass new parameters to the real-time application and to return signal data from the real-time application. The data is displayed in Scope blocks or saved with signal logging.

The Real-Time Workshop pane looks similar to the Figure A.1

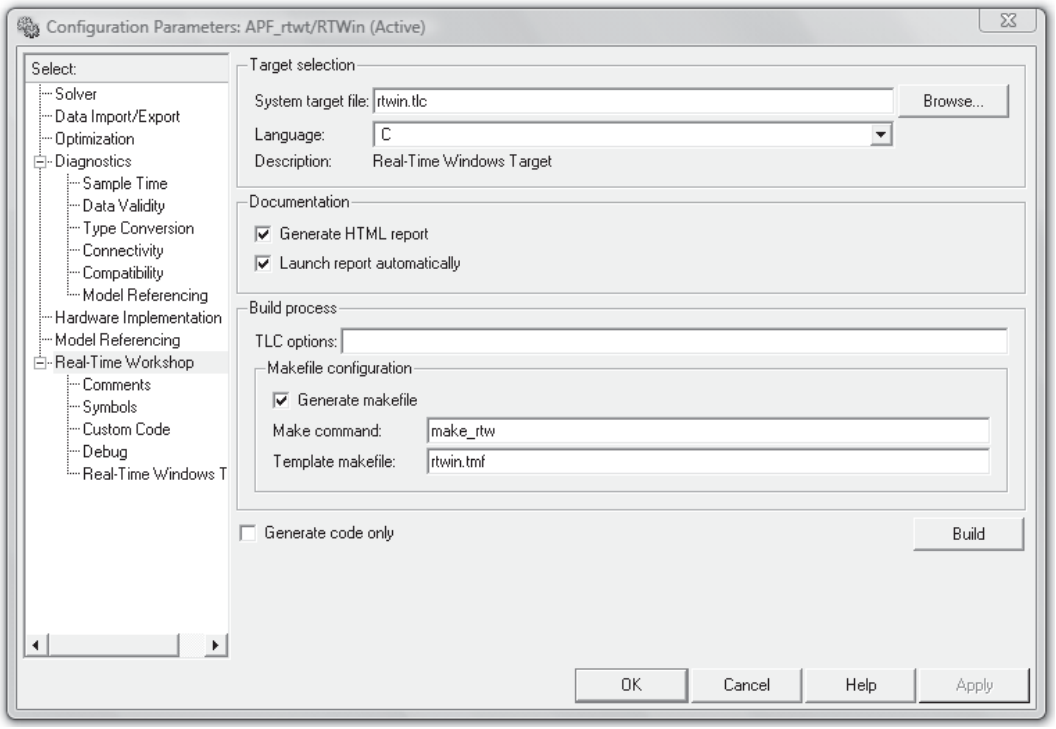

Figure A.1 Configuration parameters in the Real-Time Workshop pane.

The Real-Time Workshop code generation software creates C code from your Simulink model, then the Open Watcom C/C++ compiler compiles and links that C code into a real-time application. After you enter parameters into the Configuration Parameters dialog box for use by the Real-Time Workshop code generation software, you can build a real-time application.

a. In the Simulink window, from the **Tools** menu, point the **Real-Time Workshop**, and then click **Build Model**.
   The build process does the following:
   - The Real-Time Workshop code generation software creates the C code source files APF_rtwt.c and APF_rtwt.h
   - The make utility make_rtw.exe creates the make file APF_rtwt.mk from the template make file rtwin.tmf.
   - The make utility make_rtw.exe builds the real-time application example.rwd using the make file APF_rtwt.mk created above. The file example.rwd is a

binary file that we refer to as your real-time application. You can run the real-time application with the Real-Time Windows Target Kernel.

b. Connect your Simulink model to your real-time application. After you create a real-time application, you can exit the Matlab environment, start the Matlab environment again, and then connect and run the executable without having to rebuild. Once you have built the real-time application, you can run your model in real time.
    - From the Simulation menu:
      Select External mode simulation.
      Choose Connect To Target. The Matlab Command Window displays the message "Model APF_rtwt loaded"
    - From the Simulation menu, choose Start Real-Time Code.

Transfer of data is less critical than calculating the signal outputs at the selected sample interval. Therefore, data transfer runs at a lower priority in the remaining CPU time after real-time application computations are performed while waiting for another interrupt to trigger the next real-time application update.

To perform further analysis of the real-time application results you can save data to a variable in the Matlab Workspace. This allows you to use Matlab functions for data analysis and Matlab plotting functions for visualization.

According with Equation (5.12), the equality condition for the IHD index at bus *n* for the harmonic *h*, expressed as the exterior circle HDC of Figure 5.1, is given by,

B.1
$$\left(Z_{np}^{(h,r)2}+Z_{np}^{(h,i)2}\right)\left(I_p^{(h,r)2}+2I_p^{h,r}\left(\frac{Z_{np}^{h,r}V_{n,old}^{h,r}+Z_{np}^{h,i}V_{n,old}^{h,i}}{Z_{np}^{(h,r)2}+Z_{np}^{(h,i)2}}\right)\right)+$$
$$\left(Z_{np}^{(h,r)2}+Z_{np}^{(h,i)2}\right)\left(I_p^{(h,i)2}+2I_p^{h,i}\left(\frac{\left(Z_{np}^{h,r}V_{n,old}^{h,i}-Z_{np}^{h,i}V_{n,old}^{h,r}\right)}{Z_{np}^{(h,r)2}+Z_{np}^{(h,i)2}}\right)\right)=-\left(V_{n,old}^{(h,r)2}+V_{n,old}^{(h,i)2}\right)+\left(\alpha\left|V_n^1\right|\right)^2$$

Deriving B.1 with respect to the rectangular components of the SHAPLC injection currents we get,

B.2
$$\frac{\partial(\text{B.1})}{\partial I_p^{h,r}}=2I_p^{h,r}\left(Z_{np}^{(h,r)2}+Z_{np}^{(h,i)2}\right)+2\left(Z_{np}^{h,r}V_{n,old}^{h,r}+Z_{np}^{h,i}V_{n,old}^{h,i}\right)$$

B.3
$$\frac{\partial(\text{B.1})}{\partial I_p^{h,i}}=2I_p^{h,i}\left(Z_{np}^{(h,r)2}+Z_{np}^{(h,i)2}\right)+2\left(Z_{np}^{h,r}V_{n,old}^{h,i}-Z_{np}^{h,i}V_{n,old}^{h,r}\right)$$

Setting B.2 and B.3 to zero and solving for $I^{h,r}{}_p$ and $I^{h,i}{}_p$, respectively, we obtain

B.4
$$I_p^{h,r}=-\left(\frac{Z_{np}^{h,r}V_{n,old}^{h,r}+Z_{np}^{h,i}V_{n,old}^{h,i}}{Z_{np}^{(h,r)2}+Z_{np}^{(h,i)2}}\right)$$

B.5
$$I_p^{h,i}=-\left(\frac{Z_{np}^{h,r}V_{n,old}^{h,i}-Z_{np}^{h,i}V_{n,old}^{h,r}}{Z_{np}^{(h,r)2}+Z_{np}^{(h,i)2}}\right)$$

Please notice that the values of the injections currents in B.4 and B.5 correspond to the values of the center of the circle HDC as given in Equation (5.15). From the second derivatives of B.1 we have the Hessian in B.6, and its determinant given in B.7. Since the determinant in B.7 will always be positive, the Hessian in B.6 is positive definite, and the injections currents in B.4 and B.5 are the minimum of B.1. The determinant in B.7 also establishes the function B.1 as strictly convex [Nocedal and Wright 1999].

B.6
$$H_{B.1} = \begin{bmatrix} 2\left(Z_{np}^{(h,r)2} + Z_{np}^{(h,i)2}\right) & 0 \\ 0 & 2\left(Z_{np}^{(h,r)2} + Z_{np}^{(h,i)2}\right) \end{bmatrix}$$

B.7
$$\mathrm{Det}\left(H_{B.1}\right) = 4\left(Z_{np}^{(h,r)2} + Z_{np}^{(h,i)2}\right)^2$$

For the case of the harmonic voltage in all buses, for the harmonic *h*, as expressed in Equation (5.30); the second derivatives of (5.30) with respect to the injection currents will give us the Hessian as in B.8 and its determinant in B.9 will also be always positive, hence the injection currents in Equations (5.34)-(5.35) are a minimum of (5.30).

B.8
$$H_{Eq5.30} = \begin{vmatrix} 2\sum_{n=1}^{N}\left(Z_{np}^{(h,r)2} + Z_{np}^{(h,i)2}\right) & 0 \\ 0 & 2\sum_{n=1}^{N}\left(Z_{np}^{(h,r)2} + Z_{np}^{(h,i)2}\right) \end{vmatrix}$$

B.9
$$Det\left(H_{Eq5.30}\right) = 4\sum_{n=1}^{N}\left(Z_{np}^{(h,r)2} + Z_{np}^{(h,i)2}\right)^2$$

About the nonlinear optimization problem (5.37), the proof for convexity of the objective function and the inequality constraints is given next.

From the second derivatives of the objective function (5.36), the Hessian matrix is formed as in B.10.

B.10

$$H_{Eq.36} = \begin{vmatrix} \frac{\partial^2 f_{obj}}{\partial I_{p1}^{(h,r)2}} & \frac{\partial^2 f_{obj}}{\partial I_{p1}^{h,r}\partial I_{p1}^{h,i}} & \cdots & \frac{\partial^2 f_{obj}}{\partial I_{p1}^{h,r}\partial I_{pt}^{h,r}} & \frac{\partial^2 f_{obj}}{\partial I_{p1}^{h,r}\partial I_{pt}^{h,i}} & \cdots & \frac{\partial^2 f_{obj}}{\partial I_{p1}^{h,r}\partial I_{pT}^{h,r}} & \frac{\partial^2 f_{obj}}{\partial I_{p1}^{h,r}\partial I_{pT}^{h,i}} \\ \frac{\partial^2 f_{obj}}{\partial I_{p1}^{h,i}\partial I_{p1}^{h,r}} & \frac{\partial^2 f_{obj}}{\partial I_{p1}^{(h,i)2}} & \cdots & \frac{\partial^2 f_{obj}}{\partial I_{p1}^{h,i}\partial I_{pt}^{h,r}} & \frac{\partial^2 f_{obj}}{\partial I_{p1}^{h,i}\partial I_{pt}^{h,i}} & \cdots & \frac{\partial^2 f_{obj}}{\partial I_{p1}^{h,i}\partial I_{pT}^{h,r}} & \frac{\partial^2 f_{obj}}{\partial I_{p1}^{h,i}\partial I_{pT}^{h,i}} \\ \vdots & \vdots & & \vdots & \vdots & & \vdots & \vdots \\ \frac{\partial^2 f_{obj}}{\partial I_{pt}^{h,r}\partial I_{p1}^{h,r}} & \frac{\partial^2 f_{obj}}{\partial I_{pt}^{h,r}\partial I_{p1}^{h,i}} & \cdots & \frac{\partial^2 f_{obj}}{\partial I_{pt}^{(h,r)2}} & \frac{\partial^2 f_{obj}}{\partial I_{pt}^{h,r}\partial I_{pt}^{h,i}} & \cdots & \frac{\partial^2 f_{obj}}{\partial I_{pt}^{h,r}\partial I_{pT}^{h,r}} & \frac{\partial^2 f_{obj}}{\partial I_{pt}^{h,r}\partial I_{pT}^{h,i}} \\ \frac{\partial^2 f_{obj}}{\partial I_{pt}^{h,i}\partial I_{p1}^{h,r}} & \frac{\partial^2 f_{obj}}{\partial I_{pt}^{h,i}\partial I_{p1}^{h,i}} & \cdots & \frac{\partial^2 f_{obj}}{\partial I_{pt}^{h,i}\partial I_{pt}^{h,r}} & \frac{\partial^2 f_{obj}}{\partial I_{pt}^{(h,i)2}} & \cdots & \frac{\partial^2 f_{obj}}{\partial I_{pt}^{h,i}\partial I_{pT}^{h,r}} & \frac{\partial^2 f_{obj}}{\partial I_{pt}^{h,i}\partial I_{pT}^{h,i}} \\ \vdots & \vdots & & \vdots & \vdots & & \vdots & \vdots \\ \frac{\partial^2 f_{obj}}{\partial I_{pT}^{h,r}\partial I_{p1}^{h,r}} & \frac{\partial^2 f_{obj}}{\partial I_{pT}^{h,r}\partial I_{p1}^{h,i}} & \cdots & \frac{\partial^2 f_{obj}}{\partial I_{pT}^{h,r}\partial I_{pt}^{h,r}} & \frac{\partial^2 f_{obj}}{\partial I_{pT}^{h,r}\partial I_{pt}^{h,i}} & \cdots & \frac{\partial^2 f_{obj}}{\partial I_{pT}^{(h,r)2}} & \frac{\partial^2 f_{obj}}{\partial I_{pT}^{h,r}\partial I_{pT}^{h,i}} \\ \frac{\partial^2 f_{obj}}{\partial I_{pT}^{h,i}\partial I_{p1}^{h,r}} & \frac{\partial^2 f_{obj}}{\partial I_{pT}^{h,i}\partial I_{p1}^{h,i}} & \cdots & \frac{\partial^2 f_{obj}}{\partial I_{pT}^{h,i}\partial I_{pt}^{h,r}} & \frac{\partial^2 f_{obj}}{\partial I_{pT}^{h,i}\partial I_{pt}^{h,i}} & \cdots & \frac{\partial^2 f_{obj}}{\partial I_{pT}^{h,i}\partial I_{pT}^{h,r}} & \frac{\partial^2 f_{obj}}{\partial I_{pT}^{(h,i)2}} \end{vmatrix}$$

As well as, from (5.36) it can be founded that the elements off the main diagonal are zero, and the elements in the main diagonal are equal 2. Then,

B.11

$$H_{Eq5.36} = 2\left|\mathrm{I}_{(2*T)\mathrm{X}(2*T)}\right|$$

Where, I is the identity matrix and T is the total number of SHAPLCs. Hence the determinant in B.11 is always positive as given in B.12, thus, identifying the objective function in (5.36) as strictly convex.

B.12

$$\mathrm{Det}\left(H_{B.11}\right) = 2^{(2*T)}$$

The inequality constrains in (5.37), which are referred to the IHD index at bus n for the harmonic h, are convex. Since the Equation (5.10) associated to that constrain is given in B.1, after some algebraic manipulation, and to avoid redundancy, we have omitted to

rewrite the equations which would lead to B.6 and B.7. On the other hand, the inequality constraints in (5.37), which are referred to the THD index at bus *n*, are associated to Equation (5.31).

B.13

$$H_{Eq5.31} = \begin{vmatrix} \frac{\partial^2(31)}{\partial I_{p1}^{(h,r)2}} & \frac{\partial^2(31)}{\partial I_{p1}^{h,r}\partial I_{p1}^{h,i}} & \cdots & \frac{\partial^2(31)}{\partial I_{p1}^{h,r}\partial I_{pt}^{h,r}} & \frac{\partial^2(31)}{\partial I_{p1}^{h,r}\partial I_{pt}^{h,i}} & \cdots & \frac{\partial^2(31)}{\partial I_{p1}^{h,r}\partial I_{pT}^{h,r}} & \frac{\partial^2(31)}{\partial I_{p1}^{h,r}\partial I_{pT}^{h,i}} \\ \frac{\partial^2(31)}{\partial I_{p1}^{h,i}\partial I_{p1}^{h,r}} & \frac{\partial^2(31)}{\partial I_{p1}^{(h,i)2}} & \cdots & \frac{\partial^2(31)}{\partial I_{p1}^{h,i}\partial I_{pt}^{h,r}} & \frac{\partial^2(31)}{\partial I_{p1}^{h,i}\partial I_{pt}^{h,i}} & \cdots & \frac{\partial^2(31)}{\partial I_{p1}^{h,i}\partial I_{pT}^{h,r}} & \frac{\partial^2(31)}{\partial I_{p1}^{h,i}\partial I_{pT}^{h,i}} \\ \vdots & \vdots & & \vdots & \vdots & & \vdots & \vdots \\ \frac{\partial^2(31)}{\partial I_{pt}^{h,r}\partial I_{p1}^{h,r}} & \frac{\partial^2(31)}{\partial I_{pt}^{h,r}\partial I_{p1}^{h,i}} & \cdots & \frac{\partial^2(31)}{\partial I_{pt}^{(h,r)2}} & \frac{\partial^2(31)}{\partial I_{pt}^{h,r}\partial I_{pt}^{h,i}} & \cdots & \frac{\partial^2(31)}{\partial I_{pt}^{h,r}\partial I_{pT}^{h,r}} & \frac{\partial^2(31)}{\partial I_{pt}^{h,r}\partial I_{pT}^{h,i}} \\ \frac{\partial^2(31)}{\partial I_{pt}^{h,i}\partial I_{p1}^{h,r}} & \frac{\partial^2(31)}{\partial I_{pt}^{h,i}\partial I_{p1}^{h,i}} & \cdots & \frac{\partial^2(31)}{\partial I_{pt}^{h,i}\partial I_{pt}^{h,r}} & \frac{\partial^2(31)}{\partial I_{pt}^{(h,i)2}} & \cdots & \frac{\partial^2(31)}{\partial I_{pt}^{h,i}\partial I_{pT}^{h,r}} & \frac{\partial^2(31)}{\partial I_{pt}^{h,i}\partial I_{pT}^{h,i}} \\ \vdots & \vdots & & \vdots & \vdots & & \vdots & \vdots \\ \frac{\partial^2(31)}{\partial I_{pT}^{h,r}\partial I_{p1}^{h,r}} & \frac{\partial^2(31)}{\partial I_{pT}^{h,r}\partial I_{p1}^{h,i}} & \cdots & \frac{\partial^2(31)}{\partial I_{pT}^{h,r}\partial I_{pt}^{h,r}} & \frac{\partial^2(31)}{\partial I_{pT}^{h,r}\partial I_{pt}^{h,i}} & \cdots & \frac{\partial^2(31)}{\partial I_{pT}^{(h,r)2}} & \frac{\partial^2(31)}{\partial I_{pT}^{h,r}\partial I_{pT}^{h,i}} \\ \frac{\partial^2(31)}{\partial I_{pT}^{h,i}\partial I_{p1}^{h,r}} & \frac{\partial^2(31)}{\partial I_{pT}^{h,i}\partial I_{p1}^{h,i}} & \cdots & \frac{\partial^2(31)}{\partial I_{pT}^{h,i}\partial I_{pt}^{h,r}} & \frac{\partial^2(31)}{\partial I_{pT}^{h,i}\partial I_{pt}^{h,i}} & \cdots & \frac{\partial^2(31)}{\partial I_{pT}^{h,i}\partial I_{pT}^{h,r}} & \frac{\partial^2(31)}{\partial I_{pT}^{(h,i)2}} \end{vmatrix}$$

Again, the elements off the main diagonal are zero, and we can express the Hessian of B.13 in terms of an identity matrix as given in B.14, whose determinant will always be positive as indicated in B.15. Therefore, the inequality constraints referred to the THD index at bus *n*, are strictly convex. Similar demonstrations are given in [Chang *et al*. 1994], [Hong and Chang 1996]. The convexity of the objective function and the inequality constraints of the nonlinear optimization problem (5.36), allow us to determine that a local minimum that satisfies the first order KKT conditions, is also a global minimum [Nocedal and Wright 1999].

B.14

$$H_{Eq5.31} = 2.\left(Z_{np}^{(h,r)2} + Z_{np}^{(h,i)2}\right).\left|\mathrm{I}_{(2*T)\mathrm{x}(2*T)}\right|$$

B.15

$$\mathrm{Det}\left(H_{Eq5.31}\right) = \left(2.\left(Z_{np}^{(h,r)2} + Z_{np}^{(h,i)2}\right)\right)^{(2+T)}$$

Appendix C Identification of feasible points

Here, the main purpose is to select the point F that belongs to the feasible region, if this feasible region actually exits, such that condition (5.20) can be evaluated in the proper manner and be satisfied.

According with section 5.2.2.2, if condition (5.19) is satisfied, any HDC do share a feasible region with each other of the remaining HDCs in the set NC1, e.g., the circles intersect with each other, see Figure 5.3. On the other hand, from Figure 5.4 it can be observed that the feasible region is formed from the intersection points of the circles. Hereby, it is necessary to find the intersection points which are forming the feasible region in common, and then evaluate them in condition (5.20). If condition (5.20) holds, the feasible region in common for all the HDCs does actually exist.

The intersection points of two circles can be determined by solving the following system of equations,

C.1 $$I_p^{(h,r)2} + I_p^{(h,i)2} + A_n I_p^{h,r} + B_n I_p^{h,i} + C_n = 0$$

C.2 $$I_p^{(h,r)2} + I_p^{(h,i)2} + A_m I_p^{h,r} + B_m I_p^{h,i} + C_m = 0$$

Where, the circles, for buses n and m, are expressed in the general form. From Equation (5.12); the values for A_n, B_n and C_n can be obtained as,

C.3 $$A_n = \frac{Z_{np}^{h,r} V_{n,old}^{h,r} + Z_{np}^{h,i} V_{n,old}^{h,i}}{Z_{np}^{(h,r)2} + Z_{np}^{(h,i)2}} \quad B_n = \frac{Z_{np}^{h,r} V_{n,old}^{h,i} - Z_{np}^{h,i} V_{n,old}^{h,r}}{Z_{np}^{(h,r)2} + Z_{np}^{(h,i)2}} \quad C_n = \frac{V_{n,old}^{(h,r)2} + V_{n,old}^{(h,i)2} + \left(\alpha \left|V_n^1\right|\right)^2}{Z_{np}^{(h,r)2} + Z_{np}^{(h,i)2}}$$

In similar manner, the values for A_m, B_m and C_m can be obtained by substituting m instead of n in C.3. The system of equations C.1 and C.2 is equivalent to the system of equations C.4 and C.5; which results from replacing equation C.2 by a linear combination of C.1 and C.2. The equation C.5, is a straight-line equation, and is obtained by subtracting C.2 of C.1.

C.4 $$I_p^{(h,r)2} + I_p^{(h,i)2} + A_n I_p^{h,r} + B_n I_p^{h,i} + C_n = 0$$

C.5 $$I_p^{h,r}\left(A_n - A_m\right) + I_p^{h,i}\left(B_n - B_m\right) + \left(C_n - C_m\right) = 0$$

In this way, the intersection of two circles becomes the intersection of a circle, Equation C.4, with a straight-line, Equation C.5. See Figure C1.

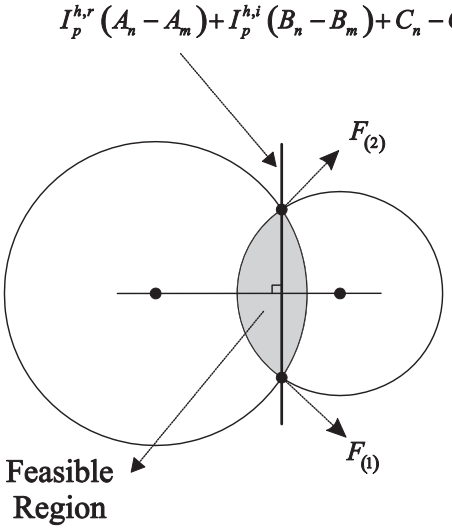

Figure C1. Straight-line formed by the intersection of two circles.

The straight-line of C.5 is perpendicular to the axis that connects the centers of both circles. Given two circles, if they are secant, the straight-line of C.5 is the line that joints the intersection points as shown in Figure C.2(a); if they are tangent, the straight-line of B.5 is the line tangent to both circles in their point of contact as shown in Figure C.2(b).

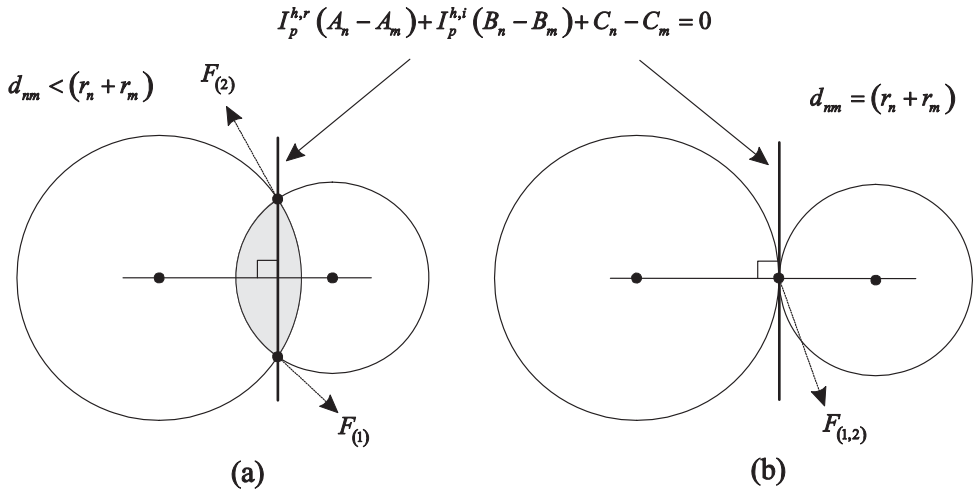

Figure C2 Intersection point of two circles. (a) Two different intersection points when they are secant. (b) A single intersection point when they are tangent.

To solve the system of equations C.4 and C.5, first from C.5:

C.6
$$I_p^{h,r} = \frac{I_p^{h,i}\left(B_m - B_n\right) + \left(C_m - C_n\right)}{\left(A_n - A_m\right)}$$

Substituting C.6 into C.4,

C.7
$$\left(\frac{I_p^{h,i}\left(B_m - B_n\right) + \left(C_m - C_n\right)}{\left(A_n - A_m\right)}\right)^2 + I_p^{(h,i)2} + A_n\left(\frac{I_p^{h,i}\left(B_m - B_n\right) + \left(C_m - C_n\right)}{\left(A_n - A_m\right)}\right) + I_p^{h,i}B_n + C_n = 0$$

Rearranging common terms,

C.8
$$I_p^{(h,i)2}\left(1 + \frac{\left(B_m - B_n\right)^2}{\left(A_n - A_m\right)^2}\right) + I_p^{h,i}\left(\frac{2\left(B_m - B_n\right)\left(C_m - C_n\right)}{\left(A_n - A_m\right)^2} + \frac{A_n\left(B_m - B_n\right)}{\left(A_n - A_m\right)} + B_n\right) + \frac{\left(C_m - C_n\right)^2}{\left(A_n - A_m\right)^2} + \frac{A_n\left(C_m - C_n\right)}{\left(A_n - A_m\right)} + C_n = 0$$

This is a quadratic equation, and can be solved using the quadratic formula.

C.9
$$I_{p\,(1,2)}^{h,i} = \frac{-b \pm \sqrt{b^2 - 4ac}}{2a}$$

Where

C.10

$$a = \left(1 + \frac{\left(B_m - B_n\right)^2}{\left(A_n - A_m\right)^2} \right)$$

$$b = \left(\frac{2\left(B_m - B_n\right)\left(C_m - C_n\right)}{\left(A_n - A_m\right)^2} + \frac{A_n\left(B_m - B_n\right)}{\left(A_n - A_m\right)} + B_n \right)$$

$$c = \left(\frac{\left(C_m - C_n\right)^2}{\left(A_n - A_m\right)^2} + \frac{A_n\left(C_m - C_n\right)}{\left(A_n - A_m\right)} + C_n \right)$$

The solutions of C.9 will be substituted into C.6 to find the real component of the injection current, e.g.,

C.11

$$I^{h,r}_{p\,(1,2)} = \frac{I^{h,i}_{p\,(1,2)}\left(B_m - B_n\right) + \left(C_m - C_n\right)}{\left(A_n - A_m\right)}$$

Then, the interception points will be given as,

C.12

$$F_{(1)} = \left(I^{h,r}_{p(1)}, I^{h,i}_{p(1)}\right) \quad ; \quad F_{(2)} = \left(I^{h,r}_{p(2)}, I^{h,i}_{p(2)}\right)$$

It is important to notice that if the circles *n* and *m* are secant, e.g. $d_{nm} < (r_n + r_m)$, like those shown in Figure C2(a), the two solutions of C.9 will be real and different, and consequently there will be two different points of intersection,

C.13

$$F_{(1)} \neq F_{(2)}$$

On the other hand, if the circles *n* and *m* are tangent, e.g. $d_{nm} = (r_n + r_m)$, like those shown in Figure C2(b), the two solutions of C.9 will be the same, and consequently there will be just the point of contact as the solution, e.g.,

C.14 $$F_{(1)} = F_{(2)}$$

Please notice that the solutions of C.9 can not be complex, real and imaginary components, since this condition on the solution of C.9 is only present when the circle *n* is involving the circle *m*, or vice versa. As stated in section 5.2.2.2 this is not the case for the remaining circles that integrate the set NC1.

Once we have the points of interception $F_{(1,2)}$; the distance between the center of a HDC and the points $F_{(1,2)}$, to be used in (5.20), can be determined as,

C.15 $$d_{nF_{(1,2)}} = \sqrt{\left(-\left(\frac{Z_{np}^{h,r} V_{n,old}^{h,r} + Z_{np}^{h,i} V_{n,old}^{h,i}}{Z_{np}^{(h,r)2} + Z_{np}^{(h,i)2}} \right) - I_{p(1,2)}^{h,r} \right)^2 + \left(-\left(\frac{Z_{np}^{h,r} V_{n,old}^{h,i} - Z_{np}^{h,i} V_{n,old}^{h,r}}{Z_{np}^{(h,r)2} + Z_{np}^{(h,i)2}} \right) - I_{p(1,2)}^{h,i} \right)^2}$$

As observed in Figure 5.4, from the two points of interception of any two circles, usually, only one interception point belongs to the feasible region as a vertex. We suggest picking the HDC, among the remaining circles in the set NC1, with the smallest radius, and then to obtain the intersection points, using C.9 and C.11, of this circle with all others circles in the set NC1. The total number of interception points will be 2*(NC1-1).

According with section 5.2.2.2, in order to identify the bus *p* as a feasible bus, at least one of the obtained interception points must satisfy condition (5.20).

Appendix D IEEE 30-bus Test System Data

Bus Data

Base MVA=100 MW; Bus Code: Load →0, Slack → 1, Voltage-controlled →2

Bus No.	Bus Code	Volt. Mag.	Angle Deg.	Generation		Load		Injected MVAR
				P_{gen} MW	Q_{gen} MVAR	P_{load} MW	Q_{load} MVAR	
1	1	1.06	0	0.0	0.0	0.0	0	0
2	2	1.043	0	21.7	12.7	40	0	0
3	0	1.0	0	2.4	1.2	0	0	0
4	0	1.06	0	7.6	1.6	0	0	0
5	2	1.01	0	94.2	19.0	0	0	0
6	0	1.0	0	0.0	0.0	0	0	0
7	0	1.0	0	22.8	10.9	0	0	0
8	2	1.01	0	30.0	30.0	0	0	0
9	0	1.0	0	0.0	0.0	0	0	0
10	0	1.0	0	5.8	2.0	0	0	19
11	2	1.082	0	0.0	0.0	0	0	0
12	0	1.0	0	11.2	7.5	0	0	0
13	2	1.071	0	0.0	0.0	0	0	0
14	0	1.0	0	6.2	1.6	0	0	0
15	0	1.0	0	8.2	2.5	0	0	0
16	0	1.0	0	3.5	1.8	0	0	0
17	0	1.0	0	9.0	5.8	0	0	0
18	0	1.0	0	3.2	0.9	0	0	0
19	0	1.0	0	9.5	3.4	0	0	0
20	0	1.0	0	2.2	0.7	0	0	0
21	0	1.0	0	17.5	11.2	0	0	0
22	0	1.0	0	35.0	25.0	0	0	0
23	0	1.0	0	3.2	1.6	0	0	0
24	0	1.0	0	8.7	6.7	0	0	4.3
25	0	1.0	0	0.0	0.0	0	0	0
26	0	1.0	0	3.5	2.3	0	0	0
27	0	1.0	0	0.0	0.0	0	0	0
28	0	1.0	0	0.0	0.0	0	0	0
29	0	1.0	0	2.4	0.9	0	0	0
30	0	1.0	0	10.6	1.9	0	0	0

Line Data

Bus Send	Bus Rec.	*R* pu	*X* pu	*B*/2	Trans. Tap Setting (1 for Line code)
1	2	0.0192	0.0575	0.02640	1
1	3	0.0452	0.1852	0.02040	1
2	4	0.0570	0.1737	0.01840	1
3	4	0.0132	0.0379	0.00420	1
2	5	0.0472	0.1983	0.02090	1
2	6	0.0581	0.1763	0.01870	1
4	6	0.0119	0.0414	0.00450	1
5	7	0.0460	0.1160	0.01020	1
6	7	0.0267	0.0820	0.00850	1
6	8	0.0120	0.0420	0.00450	1
6	9	0.0	0.2080	0.0	0.978
6	10	0.0	0.5560	0.0	0.969
9	11	0.0	0.2080	0.0	1
9	10	0.0	0.1100	0.0	1
4	12	0.0	0.2560	0.0	0.932
12	13	0.0	0.1400	0.0	1
12	14	0.1231	0.2559	0.0	1
12	15	0.0662	0.1304	0.0	1
12	16	0.0945	0.1987	0.0	1
14	15	0.2210	0.1997	0.0	1
16	17	0.0824	0.1923	0.0	1
15	18	0.1073	0.2185	0.0	1
18	19	0.0639	0.1292	0.0	1
19	20	0.0340	0.0680	0.0	1
10	20	0.0936	0.2090	0.0	1
10	17	0.0324	0.0845	0.0	1
10	21	0.0348	0.0749	0.0	1
10	22	0.0727	0.1499	0.0	1
21	22	0.0116	0.0236	0.0	1
15	23	0.1000	0.2020	0.0	1
22	24	0.1150	0.1790	0.0	11
23	24	0.1320	0.2700	0.0	1
24	25	0.1885	0.3292	0.0	1
25	26	0.2544	0.3800	0.0	1
26	27	0.1093	0.2087	0.0	1
28	27	0.0	0.3960	0.0	0.968

27	29	0.2198	0.4153	0.0	1
27	30	0.3202	0.6027	0.0	1
29	30	0.2399	0.4533	0.0	1
8	28	0.0636	0.2000	0.0214	1
6	28	0.0169	0.0599	0.0650	1

Appendix E Proof-check of the sensitivity analysis

In section 5.3.1, among the feasible buses, the best candidate buses for placing the SHAPLCs are, for *h*=5 and *h*=7 the buses 22 and 10, respectively. In this appendix we provide the proof-check that justifies and proves the selection of such buses, by solving individually for *h*=5, 7, at each feasible bus, the nonlinear programming problem in E.1.

E.1

$$\begin{aligned} &\text{Min} \quad I_p^{(h,r)2} + I_p^{(h,i)2} && P^h = [10 \quad 17 \quad 21 \quad 22] \\ &\text{s.t.} \quad IHD_n^h \le \alpha && h \in [5,7], \;\; n = 1,2,....,n,..N \end{aligned}$$

In E.1 we only take into account one harmonic *h* of interest at a time. Therefore, the nonlinear problem in E.1 had to be solved for the harmonic *h* as many times as the number of feasible buses. The results of the simulations are shown in Figure E1 and Figure E2. Figure E1, illustrates that as established previously in Section 5.3.1 the SHAPLC is able to mitigate the harmonic distortion for harmonic *h*=5 in each one of the buses identified as feasible buses. Also, the magnitude of the injection current needed to achieve the goal at each bus is given and it can be observed how the bus 22 represents the minimum value, in magnitude, of the injection current.

The same situation is presented for the SHAPLC for the harmonic *h* = 7. Although the SHAPLC placed at each one of the feasible buses achieves the goal, mitigating the harmonic content as indicated by the Standard IEEE-519, the best bus candidate to place the SHAPLC results to be the bus 10, see Figure E2, which is the bus with the smallest injection current, in magnitude, needed to achieve the goal. Recalling the sensitivity analysis results, both buses, 22 and 10, are the buses with the higher sensitivity value, among the feasible buses, for the harmonics 5 and 7 respectively.

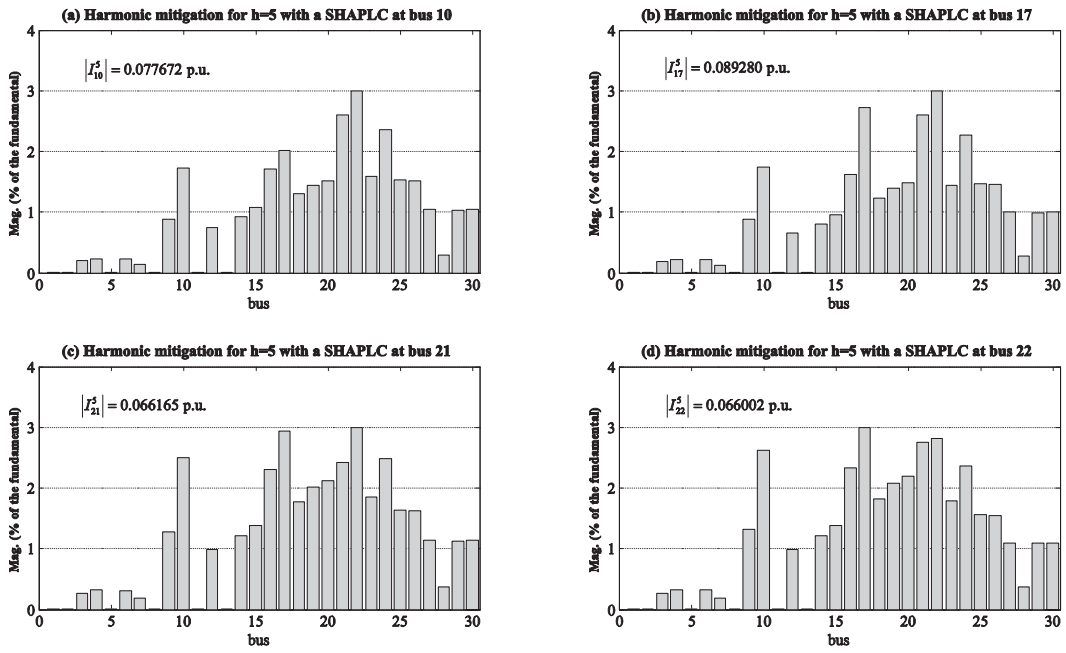

Figure E1. SHAPLC performance at feasible buses for the harmonic $h = 5$. (a) At bus 10. (b) At bus 17. (c) At bus 21. (d) At bus 22.

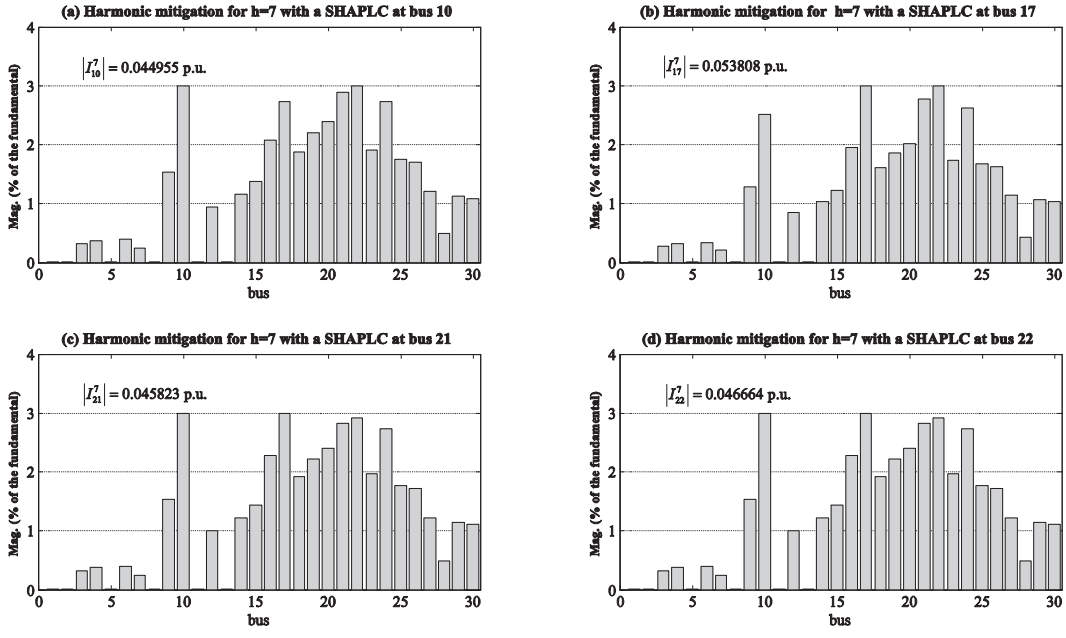

Figure E2. SHAPLC performance at feasible buses for the harmonic $h = 7$. (a) At bus 10. (b) At bus 17. (c) At bus 21. (d) At bus 22.

[ABB 2010]

www.abb.com

[Akagi *et al*. 1984]

H. Akagi, Y. Kanazawa, and A. Nabae, "Instantaneaous reactive power compensators comprising switching devices without energy storage components", IEEE Trans. Ind. Applications, Vol. IA-20, pp. 625-630, May/June 1984.

[Akagi 1994]

H. Akagi, "Trends in Active Power Line Conditioners", IEEE Transactions on Power Electronics, Vol. 9, p.p. 263-268, May 1994.

[Akagi *et al*. 2003]

H. Akagi, S. Srianthumrog, Y. Tamayi, "Comparisons in circuit configuration and filtering performance between hybrid and pure shunt active filters", *IAS Annual Meeting*, vol. 2, pp. 1195-2002, Oct. 2003.

[Akagi 1995]

H. Akagi, "New Trends in Active Filters", in Proc. Eur. Conf. Power Electron. and Applications, (EPE'95), Vol. 0, p.p. 17-26, 1995.

[Acha and Madrigal 2001]

E. Acha, M. Madrigal, "*Power system Harmonics, Computer Modelling and Analysis*", John Wiley & Sons, 2001.

[Anderson and Moore 1971]

B. D. O. Anderson, J. B. Moore, "*Linear Optimal Control*", Englewood Cliffs, NJ: New Jersey: Prentice Hall, 1971.

[Aredes *et al*. 1997]

M. Aredes, J. Hafner, K. Heunman, "Three-phase Four-wire Shunt Active Filter Control Strategies", IEEE Transactions on Power Electronics, Vol. 12, p.p. 311-318, 1997.

[Arrillaga and Watson 2003]

J. Arrillaga, N. R. Watson, "*Power System Harmonics*", Second Edition, John Wiley & Sons, 2003.

[Arrillaga *et al*. 2001]

J. Arrillaga, N. R: Watson, S. Chen, "*Power System Quality Assessment*", John Wiley & Sons, 2001.

[Bollen and Gu 2006]

M. H. J. Bollen, I. Y. H. Gu, "*Signal Processing of Power Quality Disturbances*", John Wiley & Sons, 2006.

[Buso *et al*. 1998]

S. Buso, L. Malesani, P. Mattavelli, "Comparison of Current Control Techniques for Active Filter Applications", IEEE Transactions on Industrial Electronics, Vol. 45, No. 5, pp. 722-729, October 1998.

[Chang *et al*. 1994]

G. W. Chang, W. M. Grady, M. J. Samotyj, "Meeting IEEE-519 Harmonic Voltage and Voltage Harmonic Constraints with an Active Power Line Conditioner", IEEE Transactions on Power Delivery, Vol. 9, pp. 1531-1537, 1994.

[Chang *et al*. 2004]

G. W. Chang, H.L. Wang, S. Y. Chu, "Strategic Placement and Sizing of Passive Filters in a Power System for Controlling Voltage Distortion", IEEE Transactions on Power Delivery, Vol. 19, No. 3, pp. 1204-1211, July 2004.

[Chang *et al*. 2006]

G. W. Chang, S. Y. Chu, H. L. Wang, "A New Method of Passive Harmonic Filter Planning for Controlling Voltage Distortion in a Power System", IEEE Transactions on Power Delivery, Vol. 21, No. 1, pp. 305-312, January 2006.

[Chang and Shee 2002]

G. W. Chang, T.C. Shee, "A Comparative Study of Active Power Filter Reference Compensation Approaches", IEEE Power Eng. Soc. Summer Meeting, Vol. 2, p.p. 1017-1021, 2002.

[Chang and Shee 2004]

G. W. Chang, T.C. Shee, "A Novel Reference Compensation Current Strategy for shunt active power filter control", IEEE Transactions on Power Delivery, Vol. 19, p.p. 1751-1758, 2004.

[Chen *et al*. 1993]

C. L. Chen, C. E. Lin, C. L. Huang, "Reactive and harmonic current compensation for unbalanced three-phase systems using the synchronous detection method", Elect. Power Syst. Res., Vol. 26, pp. 163-170, 1993.

[Chiarelli *et al*. 1993]

C. Chiarelli, L. Malesani, S. Pirondini, and P. Tomasin, "Single-phase, three-level, constant frequency current hysteresis control for UPS applications", in Proc. European Conf. Power Electronics and Applications, Brighton U.K., pp. 180-185, Sept. 1993.

[Chiasson *et al*. 2003]

J. N. Chiasson, L. M. Tolbert, K. J. McKenzie, and Z. Du, "Control of multilevel converter using resultant theory", IEEE Transactions Cont. Syst. Tech., Vol. 11, p.p. 345-354, 2003.

[Choi and Jang 2004]

S. Choi, M. Jang, "A reduced-rating hybrid filter to suppress neutral current harmonics in three-phase four-wire systems" IEEE Trans. Industrial Electronics, vol. 51, pp. 927-930, August 2004.

[Corasaniti *et al*. 2009]

V. F. Corasaniti, M. B. Barbieri, P. L. Arnera, M. I. Valla, "Hibrid active filter for reactive and harmonics compensation in a distribution network" IEEE Trans. Industrial Electronics, vol. 56, pp 670-677, March 2009.

[Czarnecki 1998]

L. S. Czarnecki, "Orthogonal Decomposition of the Current in a 3-phase Nonlinear Asymmetrical Circuit with a Nonsinusoidal Voltage Source", IEEE Trans. Intrumentation and Measurement, Vol. 35, pp. 30-34, 1998.

[Fuchs and Mosoum 2008]

E. F. Fuchs, M. A. S. Mosoum, "*Power Quality in Power Systems and Electrical Machines*", Elsevier Academic Press, 2008.

[Fukuda and Endoh 1995]

S. Fukuda, T. Endoh, "Control Method for a Combined Active Filter System Employing a Current Source Inverter and a High Pass Filter", IEEE Transactions on Industry Applications, Vol. 31, p.p. 590-595, May/June 1995.

[Gosh and Ledwich 2002]

A. Gosh, G. Ledwich, Power Quality Enhancement Using Custom Power Devices, Kluwer Academic Publishers, 2002.

[Gosh and Ledwich 2003]

A. Ghosh, G. Ledwich, "Load compensating DSTATCOM in weak AC systems", IEEE Trans. Power Delivery, Vol. 18, pp. 1302-1309, October 2003.

[Grady *et al*. 1990]

W. M. Grady, M. J. Samotyj, A. H. Noyola, "Survey of Active Power Line Conditioning Methodologies", IEEE Trans. on Power Delivery, Vol. 5 pp. 1536-1542, 1990.

[Grady *et al*. 1992][1]

W. M. Grady, M. J. Samotyj, A. H. Noyola, "The Application of Network Functions for Actively Minimizing the Impact of Voltage Harmonics in Power Systems", IEEE Transactions on Power Delivery, Vol. 7, p.p. 1379-1386, 1992.

[Grady *et al*. 1992][2]

W. M. Grady, M. J. Samotyj, A. H. Noyola, "Survey of Active Power Line Conditioning Methologies", IEEE Transactions on Power Delivery, Vol. 5, p.p. 1536-1542, 1992.

[Grady *et al*. 1991]

W. M. Grady, M. J. Samotyj, A. H. Noyola, "Minimizing network harmonic voltage distortion with an active power line conditioner", IEEE-PES Winter Meeting, 1991.

[Hayashi *et al*. 1991]

Y. Hayashi, N. Sato, K. Takahashi, "A novel control of a current-source active filter for ac power system harmonic compensation", IEEE Trans. Ind. Applications, Vol. 27, pp.380-385, March/April 1991.

[Hong and Chang 1996]

Y. Y. Hong, and Y. K. Chang, "Determination of location and sizes for active power line conditioners to reduce harmonics in power systems", Vol. 11, pp. 1610-1617, 1996.

[IEEE-18 1992]

IEEE Std. 18-1992, IEEE for Shunt Capacitor, IEEE Press, 1993.

[IEEE-519 1992]

IEEE Std. 519-1992, Recommended Practices and Requirements for Harmonic Control in Electric Power Systems. IEEE Press. 1993.

[Kawamura and Hoft 1984]

A. Kawamura and R. G. Hoft, "Instantaneous feedback controlled PWM inverters with adaptive hysteresis", IEEE Transactions Ind. Applications, Vol. IA-20, pp. 769-775, July/Aug. 1984.

[Lai *et al*. 1999]

L. L. Lai, W. L. Chang, C. T. Tse, A. T. P. So, "Real-Time Frequency and Harmonic Evaluation Using Artifitial Neural Networks", IEEE Trans. Power Delivery, Vol. 14,pp. 52-59, 1999.

[Lin 2004]

H. C. Lin, "Intelligent neural-network-based adaptive power line conditioner for real-time harmonics filtering", IEE Proc.-Gener. Transm. Distrib., Vol. 151, pp. 561-567, 2004.

[Malesani and Tenti 1990]

L. Malesani and P. Tenti, "A novel hysteresis control method for current controlled VSI PWM inverters with constant modulation frequency", IEEE. Trans. Ind. Applications, Vol. 26, pp. 88-92, January/February 1990.

[Malesani *et al*. 1996]

L. Malesani, P. Mattavelli, P. Tomasin, "High-performance hysteresis modulation technique for active filters", in Proc. IEEE APEC'96, pp. 939-946, 1996.

[Mattavelli 2002]

P. Mattavelli, "A close-loop selective harmonic compensation for active filters", IEEE Trans. Power Electronics, Vol. 17, pp. 273-278, March 2002.

[Medina-Rios and Ramos-Carranza 2007]

A. Medina-Rios and H. A. Ramos-Carranza, "An active power filter in phase coordinates for harmonic mitigation", IEEE Transactions on Power Delivery, Vol. 22, No. 3, pp.1991-1993. July 2007.

[MGEUPS 2010]

www.mgeups.com

[Nocedal and Wright 1999]

J. Nocedal, S. J. Wright, *Numerical Optimization*, Springer USA, 1999.

[Nuñez-Zuñiga and Pomillo 2001]

T. E. Nuñez-Zuñiga, and J. A. Pomillo, "Shunt active power filters synthetizing resistive loads", IEEE Trans. Ind. Applications, Vol. 37, pp. 81-89, Jan/Feb 2001.

[Pak *et al*. 2007]

L. Pak, V. Dinavahi, G. Chang, M Steurer, P. F. Ribeiro, "Real-Time digital time-varying harmonic modeling and simulation techniques", IEEE Trans. Power Delivery, Vol. 22, pp.1218-1227, 2007.

[Qiao *et al*. 2004]

C. Qiao, T. Jin, and K. M. Smedley, "One-cycle control of three-phase active power filter with vector operation", IEEE Trans. Ind. Electronics, Vol. 51, pp. 455-463, April 2004.

[Ramos-Carranza and Medina 2010]

H. Ramos-Carranza, A. Medina, "Optimization based method for shunt hybrid compensation in non-stiff systems" International Journal of Circuit Theory and Applications. (Accepted)

[Ramos-Carranza *et. al.* 2008]

Hugo A. Ramos-Carranza, Aurelio Medina, Gary W. Chang, "Real-Time Shunt Active Power Compensation", IEEE Transactions on Power Delivery, Vol. 23, No. 4, pp. 2623-2625, October 2008.

[Rodríguez *et al*. 2002]

J. Rodríguez, J. S. Lai, F. Z. Peng, "Multilevel inverters: a survey of topologie, controls, and applications", IEEE Trans. Ind. Electronics., Vol. 49, pp. 724-738, August 2002.

[Rastogi *et al*. 1995]

Rastogi M, Mohan N, Edris A, "Hybrid-active filtering of harmonic currents in power systems", IEEE Trans Power Delivery. Vol. 10, pp. 1994-2000, 1995.

[RTWT 2007]

Real-Time Windows Target User's Guide, The Mathworks Inc., 2007.

[RTW 2007]

Real Real-Time Workshop, The Mathworks Inc., 2007.

[Singh *et al*. 1999]

B. Singh, K. Al-Haddad, A. Chandra "A review of active filters for power quality improvement", IEEE Trans. Industrial Electronics, vol. 46, pp. 960–971, October 1999.

[Singh *et al*. 2005]

B. Singh, V. Verma, A. Chandra, K. Al-Haddad, "Hybrid filters for quality improvement" in Proc. IEE Gener. Trans. Distrib., vol. 152, pp. 365-378, May 2005.

[Yao and Holmes 1993]

Q. Yao and D. G. Holmes, "A simple, novel method for variable-hysteresis-band current control of a three-phase inverter with constant switching frequency", in Conf. Rec. IEEE-IAS Annu. Meeting, Toronto, Ont., Canada, pp. 1122-1129, Oct. 1993.